PHOTOACTIVATED FLUORESCENCE OF SMALL SILVER NANOCLUSTERS AND THEIR RELATION TO RAMAN SPECTROSCOPY

A Thesis
Presented to
The Academic Faculty

by

Lynn Anne Capadona

In Partial Fulfillment
of the Requirements for the Degree
Doctor of Philosophy in Chemistry

Georgia Institute of Technology
July, 2004

PHOTOACTIVATED FLUORESCENCE OF SMALL SILVER NANOCLUSTERS AND THEIR RELATION TO RAMAN SPECTROSCOPY

Approved:

Professor Robert M. Dickson, Chairman

Professor Mostafa A. El-Sayed

Professor L. Andrew Lyon

Professor Mohan Srinivasarao

Professor Robert Whetten

July 12, 2004

For my parents

Linda Alves

and

Lawrence Peyser

Who always believed this was possible, and for being my support network

“Have fun, be curious, and everything will be all right”

-M.S.

ACKNOWLEDGMENTS

I would like to thank my advisor, Professor Robert Dickson for giving me the opportunity to work in his lab. His years of guidance have well prepared me for the rest of my scientific career and to face the challenges that lie ahead. Additional acknowledgement is extended to the members of my thesis committee who all provided insight and helpful conversation in each of their areas of expertise during this thesis research. The members of the Dickson group both past and present are also given thanks for their insights on difficult issues and for their friendship. To the “Studio 54” cluster….thanks for never letting there be a dull moment! Thanks especially to Jie Zheng who, without his excellent synthetic skills, the results in this thesis may not have been discovered. I would also like to thank Professor John Fourkas and the members of his laboratory in 1998-1999 for providing me a vehicle of exploration to develop my scientific interests.

Finally, at the end of this list but always first in my heart, my deepest gratitude is for my best friend and wonderful husband, Jeffrey Royce. Without his unconditional love, understanding and constant support every day, this thesis would not have been possible. At my best and at my worst you are always my biggest advocate. I began this degree for me, and I am finishing it for us. Without you, I am incomplete. You are my lobster.

TABLE OF CONTENTS

LIST OF TABLES

LIST OF ILLUSTRATIONS

SUMMARY

This thesis investigates the relationship between photoactivated fluorescence of small silver nanoclusters and surface-enhanced Raman spectroscopy. Silver nanoclusters were formed by many methods including excitation of thermally and chemically deposited AgO thin-films and synthesis within water soluble dendrimer and peptide scaffolds* . Single molecule level observation was employed to then efficiently study the optical properties of these reduced dimension nanoclusters. The silver nanoclusters formed by any of the methods show strong, wavelength-dependent, multicolored emission at room temperature, and show robust read/write properties potentially enabling their future use in higher density optical storage. Displaying a superlinear value of the fluorescence emission with respect to incident intensity, photoactivation of the surface bound $Ag_{n= 2-8}$ atom nanoclusters results from continuous stabilizing and de-stabilizing interactions present on the surface which direct atomic level changes in both geometry and size of each activated nanocluster and subsequent final distribution of nanoclusters. A light-dependent equilibrium based on the forward and reverse reaction rates was established using typical excitation energies far exceed gas-phase dissociation energies for small nanoclusters. The small nanoclusters were found to be useful as true single molecule Raman-enhancing agents without the assistance or need for a large, plasmon supporting nanoparticle. Sufficient in their own environments, the large

transition moment afforded by the short fluorescence lifetime and extremely high absorption cross sections is the vehicle to connecting this large effective polarizability with available electronic states in either the peptide or dendrimer scaffold. Allowing scaffold- specific Raman studies that are truly proven to be on the single molecule level, Raman emission on the higher energy (antistokes) side becomes observable, and is modeled largely as a thermal distribution of excited state populations. This may also enable background-free biological imaging. Time averaging of Raman spectra can effectively minimize complicated on-off behavior of nanocluster fluorescence that may otherwise obscure interesting results. The reproducible scaffold specific results from these nanoclusters can be useful as extremely efficient in –vivo biological labels that do not suffer from any of the current technology's toxicity, spectral limitation, and general utility. This scientifically rich system (photoactivated fluorescence from atomic level silver nanoclusters giving rise to scaffold specific Raman scattering at room temperature) has many interesting properties as investigated in this thesis research. Most importantly, this system produced the first ever observation of single molecule Raman spectra from a truly non-classical system as confirmed in finality by antibunching of the underlying emission from these samples. Revealed by this research, various enhancement factors once thought to be unequivocal contributors to observed SERS signals now may be open for further study and discussion.

---

[*] The synthesis of water-based dendrimer and peptide nanocluster solutions was performed exclusively by Jie Zheng.

CHAPTER 1

INTRODUCTION

1.1 Small silver nanoclusters and the photographic process

The photographic process is well known [1-3] and hence a tremendous wealth of literature exists regarding the formation and reduction of silver clusters, mostly by the chemical development process. Briefly, the well established silver photochemistry involves the formation of very poor black and white latent images on emulsive (gelatinous) surfaces when light is incident on them [2, 3]. The emulsion is a mixture containing both a silver nitrate solution and an alkali halide solution which via a double decomposition reaction [4] , various Ag-halide crystal grain sizes can be obtained.

$$Ag^{+} + NO_3^{-} + K^{+} + Br^{-} \rightarrow AgBr + K^{+} + NO_3^{-} \qquad (1.1.1)$$

Commonly performed with low granularity silver halide crystals such as AgBr in the reaction above [1, 5, 6], the mechanism is fairly simple. Light hits the complex and photo-reduces it by ejecting an electron from the bromine which is pulled toward the now positively charged silver. Emulsions are used in this process for a number of

reasons, primarily to keep the silver halide crystals well dispersed and to prevent recombination of the metal and halide. When this rather simple light-driven process occurs time and again very quickly, and throughout all layers of the film, what remains are small silver clusters on the film surface known to range in size from 2-8 atoms [1, 2, 5]. The lower the granularity, the higher the final image contrast will be. Chemical sensitization in blue, red, and green are responsible for the actual development and amplification of the latent image [7], generating your favorite snapshot. Both Ag_n and AgBr are extremely photosensitive hence the need for darkrooms. However of interest in this thesis are the small silver clusters which in the photographic process are the image storage elements.

1.2 Silver cluster fluorescence

Noble metal nanocluster fluorescence and high polarizibilties

Neutral and charged small silver clusters of 2-8 atoms show strong size-dependent visible fluorescence [3, 8, 9]. They have been heavily studied at low temperature in matrix isolated conditions, and in the gas phase demonstrating similar optical properties to those on silver halide crystals [8-20], even fluorescence [6, 17]. Various assignments have been proposed regarding the optical absorption and emission of small sized clusters (from one atom to as large as ~40 atoms [11]) in these environments, not all of which are in agreement. The uncertainty in assignment can be slightly better controlled when certain size clusters are mass-selected and deposited in a low temperature matrix environment such as Argon or Krypton and deposited. The clusters are neutralized during deposition in order to prevent

Couloumb repulsion effects in the matrix allowing the individual study of a certain size-selected species. Though many spectroscopic studies of this nature have focused on the absorption and emission of the very small clusters, Ag_2 [6, 9, 12-14, 17] and Ag_3 [6, 8, 13-16, 18, 19, 21, 22] both in neutral and cationic form, results continue to range from dimer absorption /emission at 440/520nm, to stronger trimer absorption/emission from 310-510nm /381-545nm. Additionally, matrix-isolated absorptions of Ag_4 and Ag_6 have been assigned at 535nm and 557nm with corresponding fluorescence emission at 640nm [8, 16, 19]. Assignments for clusters larger than three atoms (~4 – 6) also disagree on the specific peak center depending on the particular matrix used, but are generally recognized to be responsible for observed longer wavelength red and near infra-red emission [6, 8, 10-13, 15-17, 19, 23]. Clearly there are discrepancies in the exact wavelengths for cluster absorption and emission based on the low temperature experimental evidence. For example, experiments in Krypton matrices support emission from small silver clusters at 545nm and 625nm from excitation at 510nm, values previously assigned to Ag_3 and Ag_{4-6} [8, 12, 13, 15-19]. Though the transitions for the small clusters do not always correlate from report to report, the take away message lies in that reduced-dimension silver nanoclusters exhibit size-dependent absorption for two to eight atom clusters at low temperature, and the various emission lines span the visible region of the spectrum. Of notable importance however, the low temperature fluorescence that appears from nanocluster agglomeration during deposition in a noble gas matrix disappears as soon as the temperature is raised [6, 24]. The so called cage effect refers to any matrix that prevents clusters from dissociating and can be indicated by the lack of signal

decrease over time in measurement of Ag clusters up to 39 atoms [11]. The cage effect works at low temperature for fluorescence and other measurements such as electron affinities, however, when the stabilizing matrix collapses (melts) with temperature, it causes destabilization of the clusters, and the lack of measurable emission. The low temperature studies are very helpful in the general understanding of reduced-dimension silver clusters. The visible matrix-isolated peaks [16, 18, 19] together with the observed low temperature "cage" effect aid in interpretation and design of room temperature studies as will be shown by this research.

The cage effect and cluster stabilization are necessary to measure lifetimes of fluorescence lines for metal clusters at low temperatures. With increasing cluster size, competition between different relaxation pathways (vibrations, fluorescence, fragmentation) increases, and due to their characteristic time scales, radiationless relaxation processes can be expected to quench any fluorescence [25-27]. For example, experiments attempting to measure a radiative transition for K_3 are foiled because the fragmentation of such clusters occurs at a few hundred femtoseconds – much shorter than the average time needed for a dipole transition and subsequent fluorescence. Cage effects stabilize clusters such that the excited state is long-lived enough for a radiative transition to take place, and is the reason that fluorescence has been measured from small silver clusters.

Interestingly and also directly connected to the research results presented in this thesis, the silver trimer and tetramer, Ag_3 and Ag_4, change their shape under continuous excitation. The tetramer even shifts in its reported absorption and emission lines due to a geometrical modification[9, 28]. At low temperature, this can be

attributed either to changes in lattice sites within the matrix, or a geometrical change in structure because the energy needed to dissociate the gas phase cluster (for Ag_2, this is about 1.68 eV) is less than the absorption energy in the visible [9, 17-19] . The similarity to photoelectron spectroscopy work done on sodium clusters [25] is extremely suggestive that the d interband transitions have an increased structural effect as the cluster size increases [13]. As the interband transitions for copper and gold are in the visible, and the low UV for Silver, strong couplings with surface plasmons are expected and govern large shifts in frequency for larger particles, and consequently can account for large metal nanocluster polarizabilities. Recent theoretical investigations on the d-electron contribution also propose structures to go along with the experimental work on silver, and concur that the strongly localized d electron effects cause similarities in structural properties among silver and the alkali metals [29]. Since the d-electrons are localized, they are therefore not directly involved in strong bonding and their effect on the optical response of small Ag clusters remains an important issue to resolve. de Heer summarizes that the interband transitions do not effect the small silver clusters as much as the larger ones, and proposes that the cluster transitions from the d-level to the Fermi level are suppressed or shifted [25].

Small metal nanoclusters possess extremely high polarizabilities, especially when considering the transition from the atomic to bulk levels in metals [30-32]. As quantum mechanics dictates, materials behave very differently when reduced to a size comparable to the wavelength of light. With respect to metals, the optical properties are markedly changed when their size is comparable to about half a

nanometer (or, the Fermi wavelength of an electron) making discrete energy levels accessible. When the metallic density of states is not sizable enough to be continuous as in a bulk metal, such tens of atoms nanoclusters can exhibit molecule-like transitions [32-36]. Especially when the excitation energy is shifted lower than the metallic plasmon absorption wavelength (~390nm for Ag, and ~520nm for Au), the strength of optical and electronic transitions are greatly enhanced due to the collective effect of electron oscillation. Nanoscale silver and gold clusters at this size level are able to possess strong oscillator strengths and extremely high quantum yields, but at a much smaller size than other comparable nanomaterials [33, 34, 36, 37].

The optical properties of the noble-metal clusters have been studied, theorized, and argued for over one hundred years, but only recently have further advances in examination of optical and electronic properties been made possible by molecular beams. The optical spectra reported in such experiments demonstrate that only a few atoms are needed to establish the above referenced massive resonance and subsequent polariziblitly. For example, Tiggsbaumker et. al. [38] were further able to measure the resonance of small clusters by depletion spectroscopy, and observed peaks correspond nicely with those for n<15 mass-selected clusters of Harbich et. al.[10] indicaticing the same collective electron osciallation is responsible for the ”giant resonances” seen in the photofragmentation spectra.

Ag cluster fluorescence on silver halide surfaces

Of importance to the photographic process, chemical and optical sensitization of silver halide crystals such as AgBr produces small, 2-6 atom silver

clusters [1, 2, 5]. Fluorescence from such crystals has recently been reported [6], and the optical properties found to be similar to those in the matrix-isolated studies. Though again, there is a lack of general agreement on size assignments, there is a consensus that increased cluster size exhibits red-shifted emission due to surface interactions manifesting red-shifted electronic transitions. On AgBr crystals, as much as a 1600 cm^{-1} shift has been estimated [6] which has enabled absorption wavelength predictions of Ag_3 (>470nm) and Ag_4 (>527nm) and all cluster sizes up to seven atoms [6]. Corresponding with absorption wavelengths increasing as the cluster grows larger, cluster emission also follows this pattern as is revealed by the many matrix-isolated emission peaks. Photophysical properties from industrially produced photographic emulsions for example, have also benefited from the correlations between matrix-isolated clusters and those on solid supports. In one demonstration, low temperature dimer studies on AgBr crystals characterized the absorption/emission maxima [6] but at room temperature, the absorption was found to be red-shifted [24], and emission completely quenched.

In light of all the work done on silver dimmers and trimers, it shouldn't be overlooked than equal work (and discontinuity) also exists for larger clusters such as Ag_4 and Ag_5, even Ag_8 fluorescence in an Argon matrix [39].

Photogenerated clusters from silver oxide

Small surface bound silver clusters on silver oxide surfaces can also be produced when excited with visible irradiation above its bandgap of about 2.25 eV [40-43]. Silver oxide can take several forms depending on preparation (AgO, a

combination of silver (I) and silver (III)), along with silver metal and oxygen) and is commonly reported with respect to large colloidal systems [40, 42, 44, 45]. Because both silver oxides (AgO and Ag_2O) have visibly accessible bandgaps, photoreduction to produce metallic Ag clusters is allowed and is responsible for numerous effects to be discussed further in section 1.6 [40, 42, 44, 46-50]. A wide range of fluorescence has clearly been reported as arising from small silver nanoclusters from blue – near IR. Smaller cluster emission is predominantly in the green spectral region while larger clusters show more red-shifted emission. However, incredible modification of the observed absorption and emission properties can occur as a function of different cluster geometries being stabilized by the silver oxide support. Producing small silver clusters from the oxide, visible excitation should simultaneously provide enough energy to dissociate the gas phase cluster, and is likely to continuously modify the cluster size and geometry. Controversy exists over matrix-isolated and solid support emission peaks, but the important fundamental understanding is clear. Small silver clusters produce very strong visible fluorescence, and their absorption and emission lines shift to longer wavelength as their size increases. Cluster size and geometry can be easily modified by optical excitation.

Until the research presented in this thesis began, small silver nanoclusters produced from various silver oxides were never studied by fluorescence microscopy at room temperature, let alone on the single-molecule level. Revealed by this research, nanosized metal clusters photolytically produced from the oxides of silver are found to be photoactive and tremendously fluorescent due to modified size and geometry at *room temperature*. In the last five years, other authors have begun to

explore further connections between this newly discovered type of nanoparticle fluorescence and other applications [51, 52] such as Raman spectroscopy and fluorescence quenching effects due to the addition of Lewis bases. Primarily, since a number of earlier referenced papers on silver colloid Raman spectroscopy were published, close connection with this type of fluorescence was also examined in that light. The fluorescence associated with our fluorescent photoproduced, photoactive nanoclusters on the AgO surface has been linked to the ever-present non-resonant fluorescent background in surface-enhanced Raman studies [41, 53-61], as well as a link to a potential chemical enhancement factors in SERS signals [47, 49] further discussed in sections 1.5 and 1.6.

1.3 Quantum mechanical consideration of resonance Raman scattering

Raman scattering occurs when monochromatic radiation interacts with a molecule and causes it to vibrate. Scattered frequencies of light (ω_s) occur due to the interaction, the spectrum of which contains elastic and inelastic components. The elastic portion of ω_s retains the same frequency as the incident frequency, ω (Rayleigh scattering) while the inelastically scattered frequency is changed. The inelastically scattered components are divided according to whether or not the atom makes a transition from a final state that differs from its initial state before the scattering process occurs [62]. Fluorescence results because the atom reradiates by ordinary emission after initial excitation with frequencyω, while Raman scattering results when an atom remains in an excited state of energy $\hbar\omega_f$ after the scattering process occurs. The component of the purely inelastic scattering that satisfies

conservation of energy with ω-ω_f is the Raman scattered frequency which is given off with either a lower (Stokes) energy, or a higher (antistokes) energy. When excitation gets close to an electronic transition of a molecule, both resonance Raman scattering and fluorescence can occur, and must be independently considered. The basic difference between the two is the time scales on which they occur and the nature of the intermediate states resulting from interactions with the laser field. Fluorescence results from the emission of a photon from the lowest vibrational level of an excited electronic state requiring typically around a nanosecond. Because the interaction of the photon with the molecule and re-emission of a Raman scattered photon occur essentially simultaneously, virtual states always exist. Resonance Raman becomes important when the excitation frequency approaches that of a molecular electronic transition. Under such conditions, intensities of Raman bands may be selectively enhanced anywhere from three to five orders of magnitude [63]. This selectivity is not only important in identifying particular molecular vibrations, but more relevant for locating specific electronic transitions within the molecule's absorption spectrum, even when the direct electronic spectra are totally vibrationally unresolved.

The classical interpretation of the Raman effect can be thought of in terms of the connection of the electric field produced by the laser (E) and the induced dipole (μ) through a polarizability tensor (α).

$$\tilde{\mu} = \alpha \cdot \tilde{E} \qquad (1.3.1)$$

If the molecule were rigid, the molecular polarizability could be considered effectively constant with respect to nuclear motion. But since a vibrating molecule is considered, the polarizability tensor is clearly a function of the vibration of the normal coordinate of the vibration. For a full consideration of resonance Raman scattering, a quantum mechanical treatment should be examined with the Kramers-Heisenberg-Dirac formula (below). Originally derived from time-dependent perturbation theory, the total power resulting from a Raman transition from an initial state to final state must be integrated over all directions and all polarizations of scattered light and assumed to be a randomly oriented sample. This is generally given by [64, 65]:

$$P_{I\to F} = H\sigma_{I\to F}(E_L) \tag{1.3.2}$$

where

$$\sigma_{I\to F}(E_L) = \frac{8\pi e^4 E_s^3 E_L}{9\hbar^4 c^4} \sum_{\rho,\lambda} \left|(\alpha_{\rho\lambda})_{I\to F}\right|^2 \tag{1.3.3}$$

and

$$(\alpha_{\rho\lambda})_{I\to F} = \sum_V \frac{\langle F|m_\rho|V\rangle\langle V|m_\lambda|I\rangle}{E_V - E_I - E_L - i\Gamma} + \frac{\langle F|m_\lambda|V\rangle\langle V|m_\rho|I\rangle}{E_V - E_F + E_L - i\Gamma} \tag{1.3.4}$$

and $|I\rangle$ and $|F\rangle$ represent the final and initial states, respectively. In the above equations, E_L and E_S signify the incident and scattered photon energies and $|I\rangle, |V\rangle$, and $|F\rangle$ are the initial, virtual (intermediate) and final vibronic states with energies E_L, E_V, and E_F. Γ is the homogeneous linewidth of the transition, m_ρ is a vector component of the transition dipole operator and λ is the wavelength of the exciting laser. The representation $P_{I\to F}$ quantifies radiated power (photons/sec) with respect to an incident photon flux, H, (photons/area/sec) where σ is a cross section with units of area. In equations 1.3.3 and 1.3.4, the Raman scattering is interpreted as a two photon process involving the virtual states described briefly above. Absorption occurs from the initial state to all available excited states, followed by emission from the virtual states to the final state. The physical size of the contribution from each state depends on both the length of the transition, and the energy difference in the denominator. Clearly, as the denominator approaches resonance due to the similarity of the excitation frequency and that of an allowed transition, the vibrational levels of that particular state begin to dominate the sum.

In the particularly common case when the exciting laser wavelength overlaps well with a single strongly allowed absorption band, two approximations can be made in order to simplify the interpretation of the above equations. The Born-Oppenheimer (B-O) approximation may be used to factor the vibronic states into products of their respective electronic/vibrational states as dictated in equation 1.3.5

$$\langle F|m_\rho|V\rangle = \langle f|\langle g|m_\rho|e\rangle|\nu\rangle = \langle f|M_\rho(Q)|\nu\rangle \qquad (1.3.5)$$

where $|g\rangle$ and $|e\rangle$ are the ground and excited electronic states with vibrational levels $|f\rangle$ and $|\nu\rangle$. The electronic transition length matrix element, $M_\rho(Q)$ is defined as a function of the nuclear coordinates, Q, as the B-O approximation depends on this. It should be noted that since the B-O electronic states heavily depend on the system's nuclear coordinates that this approximation is only valid for a static system where no nuclear motion exists. Although the B-O parameters are connected to the nuclear coordinates, they are generally ignored when on resonance with a strongly allowed electronic transition [64]. When on resonance, $M_\rho(Q)$ is replaced with $M_\rho(Q_0)$ where this is the ground state equilibrium geometry allowing only the vibrational levels of the resonant electronic state to be considered. Secondly, invocation of the Franck-Condon approximation neglects the implicit dependence of the electronic transition moment on the nuclear coordinate, thereby forcing the numerator in (1.3.4) to consist purely of a product of vibrational overlap; dropping the non resonant terms as well as the sum over the ρ and λ indices. In the Condon approximation, each excited state vibrational level contributes to the absorption weighted by a certain factor, which, in the approximation, is simply the Franck-Condon factor, $|\langle f|i\rangle|^2$. With these approximations accounted for, the expression for resonance Raman polarizability within the sum-over-states framework now becomes:

$$\alpha_{i\to f}(E_L) = M^2 \sum_{v} \frac{\langle f|v\rangle\langle v|i\rangle}{\varepsilon_v - \varepsilon_i + E_0 - E_L - i\Gamma} \qquad (1.3.6)$$

where E_0 is the energy separation between the lowest vibrational levels of the ground and excited electronic states and ε_v and ε_i are the energies of vibrational states v and i relative to their respective excited state potential wells. M is the length of the electronic transition in Angstroms.

1.4 SERS background and history

Background and introduction to Raman scattering

As previously mentioned, the Raman scattering process occurs when a laser photon interacts with a molecule and loses a certain amount of energy to a molecular vibration. The resulting associated emission is detected at lower (or higher) energy (stokes / antistokes process). Since this inelastic process can occur many times within a material, various frequency shifts associated with different vibrations give rise to a continuous spectrum. As a result, Raman spectroscopy can provide detailed structural information about a molecule. Though comparable to IR spectroscopy, Raman experiments have some advantages in sensitivity over IR (which is commonly used for examination of molecules with polar bonds). Water and glass result in little inelastic scattering, for example, making imaging in aqueous solution possible without the need to purge. Raman is also a convenient solution when direct contact with the material may not be possible. Over the years, many

different systems have benefited from the study of Raman spectroscopy from advanced metallic structures to biological materials [63, 66, 67]. Unfortunately, Raman transitions are typically extremely weak ($\sigma \sim 10^{-29}$ cm^2), requiring intense laser excitation and high concentrations to yield sufficient signals that are not obscured by noise.

Early observations that Raman scattering was an interesting and complex physical process were discovered in the 1970's when Fleischmann and colleagues saw six orders of magnitude enhanced Raman signal when pyridine was adsorbed on a roughened silver electrode [68, 69]. Attributed to the increased surface area on the roughened electrode, the enhancement of the Raman signal was only seen after the electrode underwent an oxidation-reduction cycle and not simply on the smooth-surface, flat electrode. As experiments progressed in the seventies, other work presented different interpretations of the same observation. For example, a similar experiment was carried out, but the electrodes were only roughened enough such that the increase in surface area did not exceed a factor of ten. Even with the minimally roughened electrodes, similar enhancement factors were seen. These papers independently demonstrated that in fact the measured 10^6 enhancement was not due to the increased surface area of roughened electrodes, but it was due to the interaction with the metal surface [70-72]. From this observation relating to the metal surface, much more work was done moving away from electrodes and toward colloidal solutions of nanoparticles to further explore the mechanism by which these signals were observed. However, as experiments continued, reported enhancements of near 10^{15} grew so large that they were unable to be explained

simply by an interaction of a molecule with a metal surface [73]. Clearly the mechanism causing the reported enhancements was not simply attributable to one effect, but may also include effects from the metal interacting with the molecule at specific sites. Before various theories (presented below) were produced attempting to directly ascertain the answer to these mechanistic questions, the surface-enhanced Raman effect continued to be responsible for a large body of literature across chemistry, biology, and material science [54, 74]. Some twenty years and ~2500 publications later, it still remains unclear exactly what mechanisms and structural factors are responsible for incredible SERS enhancements. Historically postulated to be broken up into mechanisms containing both an electromagnetic and a chemical enhancement component, no clear agreement has yet been reached on either the relative contributions of each or the importance. The next section will present the theories and discuss the mechanisms.

1.5 SERS theory and advancements

The electromagnetic enhancement

This type of enhancement is based on enhanced electric field generation at roughened metal surfaces due to electron excitation in the conduction band of a metal known as a plasmon [54, 75]. The electromagnetic enhancement has been modeled extensively on spheres of both gold and silver and predicts enhancements ranging from six to seven orders of magnitude which agree very well with experimental results [76-81]. Upon excitation, the surface plasmon generates a secondary field by which the adsorbed molecule feels the radiation from both the

incident and the scattered fields. Since the width of the resonance is particularly broad [82], the Raman scattered field by the molecule is generally resonant with the surface plasmon, and similarly enhanced. Noble metals work particularly well to this effect since their resonances are supported in the visible region of the spectrum and the field intensity scales as the second power of the excitation frequency $((E_s/E_0)^2$ where E_0 is the field produced by the incident laser and E_s is the magnitude of the field at the surface of the metal). With the above information, a logical explanation is provided to explain why the EM enhancement is much more effective on roughened surfaces as opposed to smooth, flat surfaces.

Generally, a flat surface of a good conductor has a surface electromagnetic resonance (plasmon) whose frequency and parallel momentum obey the dispersion relation [54, 75]

$$k_{//}^2 = (\omega / c)^2 \,\mathrm{Re}\left[\varepsilon_0 \varepsilon (\varepsilon_0 + \varepsilon)^{-1}\right] \qquad (1.5.1)$$

where $\varepsilon(\omega)$ is the dielectric function of the conductor, and ε is that of the surrounding adjacent medium. The plasmon is a surface wave with the electric field as the variable - the plasmon oscillates along the surface. The only kinematic parameters are the parallel momentum and the frequency. In order for the plasmon to be excited, the frequency and parallel momentum of the incident plane wave must be conserved, which cannot be achieved in conditions with air or vacuum as the ambient medium from which the incident plane wave originates (except at zero

frequency). If $\varepsilon_0 = 1$, the constraints forbid plasmon excitation by the incident field since the dispersion equations for both the plasmon ($k_{||}^{pl}$) and the photon ($k_{||}^{ph}$) cannot be satisfied simultaneously [75]. The emission intensity and the dipole lifetime are affected by the interaction of the emitting dipole and the plasmon. The emitting dipole is not forbidden to transfer its energy to the plasmon since no conservation requirement exists for transfer from such a point source to a 2-D wave. However, the excited plasmon is prevented by momentum conservation from emitting this energy as a photon. For this reason, such a surface plasmon on a flat surface does not radiate, it is confined to the surface although its amplitude decays exponentially with distance away from the metal surface which eventually dissipates the energy as heat [75].

When surface roughness or curvature is introduced, the wave vector requirement becomes relaxed, and the surface plasmon is then allowed to radiate. A good example of the role of kinematic restriction in the dipole-plasmon interaction is presented by the following [83, 84]: A very thin frozen layer of N_2 molecules on a flat silver surface is considered. Excited N atoms that emit green light can be formed by bombarding the N_2 surface with electrons – no emission is observed on the flat surface as the excited atoms preferentially transfer their energy to the non-radiative plasmon. This flat-surface can be tested by the introduction of a ruled grating (wavelength L, chosen to allow plasmon radiation) on the surface. The momentum condition then becomes

$$k_{||}^{ph} = k_{||}^{pl} + 2\pi n/L \quad \text{with } n = 0,1,2\ldots \qquad (1.5.2)$$

making the plasmon able to radiate. As a consequence of $k_{||}^{ph} = (\omega/c)\sin\theta$, there is a length *L* and an integer *n* which satisfies equation 1.5.2. The emission angle θ with respect to the surface normal is fixed, and the photons are emitted at fixed angle giving rise to sharp, experimentally observed "angular resonances"[83]. The introduction of the grating allows the otherwise dissipated plasmon on the flat surface to be recovered as radiation because of a partial transfer of molecular energy.

The chemical enhancement mechanism

Many describe the commonly referred classical effect rather unspecifically with the general idea that the molecule "feels" the effect of the metal both before and after a scattering event, though the metal is unchanged [85]. Since extremely high SERS enhancements are not being completely explained simply by classical electromagnetic means, interactions of the metal with the molecule have been considered. In the literature, classical mechanisms are so heavily portrayed that the mention of "SERS-active" surface only implies that the occurrence of SERS is solely governed by the properties of the surface and not by the adsorbate. This section with the growing number of experiments (presented below) being done which point to a chemical mechanism, (or perhaps simply the lack of a purely classical EM explanation sufficing) the origin is still unclear.

A wealth of scientific evidence exists promoting "SERS-active" sites in general. In 1984, Hildebrandt and Stockberger [73] demonstrated SERS from very low

concentrations of Rhodamine 6G adsorbed at two different sites on silver colloids solutions. Characterized by both dye concentration and absorption strength, the signal from the first site saturated with the addition of nanomolar concentration of dye (64.9 kJ/mol adsorption strength). The concentration of R6G was added linearly to the second site, with which the SERS signal increased linearly and appeared saturated at only millimolar dye concentration (35.8 kJ/mol adsorption strength, still a fairly high value when compared to van der Walls type interactions). This type did not require specific structural factors at the surface, while the more tightly bound first site was found only to be formed in the presence of anions and only covered an extremely small fraction of the surface. Other completely different experiments show the same type of chemically specific behavior but measured on a different system where the addition of sub-monolayer amounts of certain ions in low concentration at the surface can irreversibly quench the SERS from pyridine on a silver electrode [86]. Attributed to the apparent vanishing of "SERS-active" sites, the roughness on the silver electrode did not change during the experiment indicating the cooperation of both local and non-local effects

Considering the prediction of the electromagnetic enhancement mechanism (EM) that all molecular species should be identically enhanced regardless of their structure, this does not provide a route to chemical specificity, usually, the exact purpose for these experiments. For example, CO in comparison to N_2 shows a near 50 times greater SERS enhancement, but it has an almost identical free-space Raman scattering cross section [87]. There is another strange aspect in SERS in which no enhancement is seen from any solvent. Many of the early SERS experiments

were done in solution and were conducted using Ag electrodes, but only the Raman signal from the molecule of interest (pyridine, for example) was observed. Present in much higher quantities, water did not display any evidence of enhancement [54]. Additionally, CO that is chemisorbed shows a higher SERS enhancement over that which is physisorbed [74] on the same surface indicating even further that the observed signal may be structure-dependent (versus totally EM). Many other examples exist including benzene and ethylene showing 100 times stronger enhancements than methane and ethane while all four species demonstrate similar intensity of their signals in ordinary Raman scattering (un-enhanced) [54].

The evident chemical specificity of SM-SERS in a chemical enhancement manner is also displayed from DC-resistivity measurements on thick, cold-deposited silver films. When adsorbed to the surface, the only molecules that produce any SERS signals are the ones that produce a change in resistance, ΔR across the metal [74] which occurs due to adsorbates acting as centers of electron scattering as similarly occurs in bulk. It must be noted that, in order for a change on this level to be detected in ΔR, the adsorbates must have a significant interaction with the metallic electrons in the Fermi level indicating the potential connection of DC resistivity changes with chemically-enhanced SERS.

In conjunction with a chemical enhancement mechanism, Otto et al demonstrated what is referred as the "single layer effect" [74]. Following classical EM theory, certainly the molecules closest to the surface should feel the greatest enhancement. However, since the electromagnetic field decays exponentially with distance away from the sample, even layers greater than one (for example, two

monolayers sit angstroms from the surface) should also be enhanced. In reality, experiments do not occur quite this way as was nicely dempnstrated on Ag island films with isotopic forms of pyridine on the surface (hydrogenated and deuterated)[88]. One layer of one molecule was put down followed by a multilayer of the other and the SERS signal at 30 K was only observed from the monolayer of molecules adsorbed directly to the surface. Upon heating to 100 K, signals from both were observed, most likely from a mixing of the monolayers due to heating causing a distribution of both closest to the surface, which indicates a short-range effect not obtainable with classical EM theory.

To explain these puzzling results within the context of a chemical mechanism of enhancement, several formalisms have been presented over the years [85, 89-91]. Unfortunately, the following theories have been extremely difficult to model, but the predicted enhancements for both range from a factor of 10 to a factor of 100 to the overall contribution to SERS enhancement. As this section will demonstrate, each one is different, and potentially even controversial; however, the common link between them holds the potential to explain the aforementioned results in light of the fact that the results strongly indicate a necessary interaction between the SERS metal and the molecule. Based primarily on early calculations from Lombardi, et. al [89] and later followed up by complementary experiments, the first mechanism depicts the similarities present between a resonance Raman process and a chemical enhancement situation. The early work had proposed that the (then unknown) chemical enhancement mechanism occurred as resonance Raman scattering from a charge transfer intermediate state [89]. Since then, a large body of literature exists

citing resonance Raman as the precursor to the chemical enhancement mechanism [91-98], most of which treat the system as interacting bodies rather than one unified system. Thus the problem is simplified by the consideration of only bulk metallic densities of states [89, 91-98] and surface defect sites [98] rather than bonding orbitals at the surface which would provide more surface specificity. Induced by an absorption event, the resonant excitation may involve either a transfer from the occupied states of the molecule to the unoccupied states above the Fermi level in the metal, or vice versa, a transfer from the filled states of the metal to the LUMO of the molecule [89, 90] as represented in (Figure 1.5.1 [89, 90]). The second mechanism attests more to dynamic charge transfer between the metal and the molecule which could also potentially explain the chemical effect [85, 91]. To summarize, a photon excites an electron-hole pair in the metal generating a "hot" electron which goes to the LUMO of the adsorbed molecule. It then returns to the metal with the energy difference resulting from the vibration of the molecule. Subsequent recombination with the hole then emits the Stokes-shifted photon which is chemically specific to the vibrational mode of the molecule (Figure 1.5.2 [99]). Alternatively, a new low lying electronic state can be created involving charge transfer between the molecule and metal. These types of electronic states are able to provide an optically accessible resonant transition with a very high oscillator strength, potentially yielding additional resonance enhancement. Both mechanisms remain somewhat controversial but the main points of both dictate a necessary interaction between the molecule and the metal to explain the results presented in the above sections, and potentially those in the future.

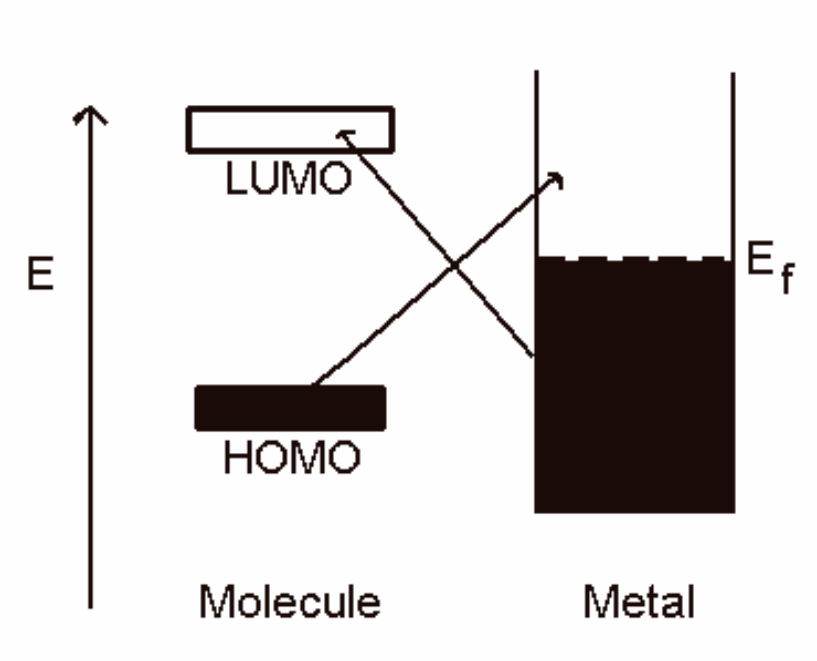

Figure 1.5.1 Potential scheme to model a chemical enhancement mechanism of SERS. Complementary to a resonance Raman transition, this example can involve a transition between the molecular HOMO and the metal or the metal to the molecular LUMO.

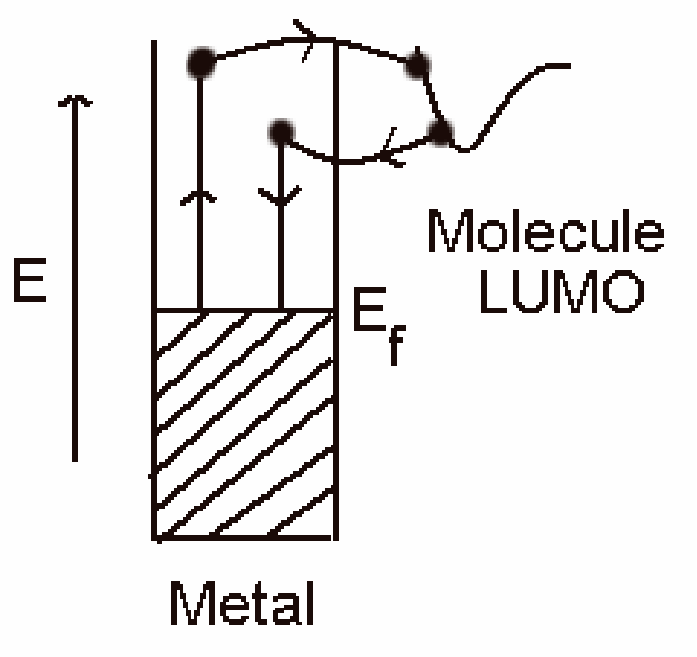

Figure 1.5.2. Schematic of a secondary chemical enhancement mechanism involving dynamic transfer of a created “hot” electron which crosses to the excited state LUMO of the molecule. It then returns to the metal with an energy differeng from that of the vibrational energy of the molecule. A stokes photon is then emissed with energy corresponding to the molecular vibration after recombination with the hole.

1.6 Single Molecule SERS

Briefly, by using the strong electromagnetic enhancement present in the optical near field of small metal nanoparticles such as silver and gold and charge-transfer chemical interactions, sensitivity of the SERS technique can be increased by ~15 orders of magnitude. With such degrees of enhancement, SERS enables the detection of individual molecules with sensitivities that surpass those obtainable with fluorescence-based methods [55, 100, 101] by coupling single molecules to nanoparticles. Through coupling, the nanometer sized features can amplify the spectroscopic molecular signatures, and the size-dependent nanostructure properties may be examined at the single molecule level. With the exceptions of low temperature solids [102, 103], detailed molecular information is not provided by fluorescence measurements, as they are often limited by photobleaching. The use of Raman spectroscopy in theory is capable of providing highly detailed, vibrationaly resolved information, and does not succumb to photobleaching, but the extreme weakness of the unassisted Raman cross section (~10^{-29} cm^2 per molecule) is ~ 13 orders of magnitude short of what is obtainable by fluorescent dyes (~10^{16} cm^2 per molecule) [100]. In order to achieve the needed sensitivity to detect on the single molecule level, the efficiency of normal Raman scattering must be at least thirteen orders of magnitude higher.

Given that SERS is a very powerful technique, and in fact, the only technique to date that can truly combine chemical information with single molecule sensitivity, much attention has been focused on the both the role that the silver nanoparticle

plays in enhancement, and the mechanism by which it occurs. For a molecule adsorbed on a small metal particle, the combined EM and chemical enhancement mechanisms provide an explanation for at most seven or eight orders of magnitude. Though the EM and chemical arguments presented above have elucidated a wealth of information, the theories still fundamentally conflict, and neither can provide a suitable explanation for the fairly recent detection of single –molecule SERS.

In that light, the early results of both Kneipp et. al. [55] and Nie and Emory [100] were seminal in the single-molecule SERS field due to their reporting of unprecedented SERS enhancements of 10^{15} from near infrared excitation of crystal violet on a colloidal silver solution, and from Rhodamine 6G, respectively. By exploiting the properties of the SERS and the resonance enhancement effects, these incredible enhancements were attributed to a very small number of nanoparticles. Since only a few nanoparticles demonstrated the unusually high enhancement, they were deemed “hot particles” or “hot spots”, a description that is still under consideration today for its role in surface enhancement. Following their work, Nie and co-workers also observed similar results on both gold colloids for molecules such as 4-mercaptopyridine [57]. The common link in these early results shows an extremely small percentage (~1%) of the adsorbed molecules being capable of generating the observed very large SERS signals with no common singularly defining factor among them. This made it impossible to distinguish which molecules are generating the enhancement, and which are not. Since current single-molecule spectroscopic techniques rely primarily on fluorescence [104, 105], if control were able to be gained over the enhanced Raman signals, an extremely

powerful analytical technique may be spawned exploiting the experimental benefits of both techniques. Not suffering from the sometimes unstable properties of fluorescence such as photobleaching and signal saturation at long times, Raman spectroscopy is still a very highly spectroscopically detailed tool, however it remains application limited by its inherent weakness. If its weak signals were able to be amplified or enhanced as the ones reported above, one could imagine SERS being an extremely useful and sensitive probe of ultra-fine chemical structure in many arenas [106].

Researchers at Columbia have made great strides in this effort to elucidate the two separate enhancement mechanism of SERS on the single molecule level such that other useful applications may be identified. Their early results study the relationship of SERS occurrences to the electromagnetic properties of small silver colloids. In essence, their reported signals show zero dependence on the Rayleigh scattering spectrum of an individual molecule on its' SERS enhancement [101] which not only deviates from the traditional EM prediction, but indicates that an EM enhancement cannot be solely responsible for the effect. Further study from this group concentrated heavily on both electron microscopy and atomic force microscopy studies on the colloidal particles responsible for SERS. Combined topographic imaging and optical analysis suggested that a minimum two-particle colloidal aggregate structure is necessary for SERS enhancements to be generated on the single-molecule level [101, 107, 108] instead of direct correlation to a plasmon resonance in the colloid. These results further suggests the likelihood of a chemical interaction that is independent from a purely electromagnetic enhancement. A

comparable theoretical study suggests a limit to the maximum enhancement allowed by an EM route of 10^{11} and can only be achieved at either extremely rough surfaces or at interstitial sites between two particles [109], which also helps support the need for a chemical or other mechanism besides EM to explain such interesting results.

Given the discrepancies in the nature of the enhancement effect with respect to bulk and single-molecule level investigations, consideration of silver itself and its effects relating to the scattering properties of the metal remain important. As shown in Brus's work, a junction of two nanoparticles may be necessary for colloidal SERS, but not specifically for the electromagnetic contributions. The reports of strong photoactivated fluorescence from individual silver nanoclusters presented in this thesis[35, 36, 110] are also though to interact with analytes in a charge-transfer type mechanism further enhancing SERS signals. In a complementary study detailing the interplay of the same Ag_n fluorescence [35], with SERS of analytes bound to partially cationic Ag_n nanoclusters [52, 111], substantial scientific evidence exists to study the small metal Ag_n nanoclusters themselves.

1.7 Antibunching from single photon/single quantum systems

All of the Raman work presented in this thesis is based on the concept of small silver nanoclusters behaving as single molecules, thus conclusive proof of the single-quantum nature of the system is needed to support claims that such strongly enhanced Raman signals arise from interactions with such nanoclusters [112]. Strong indicators and very suggestive of single particle behavior, we have shown fluorescence intermittency and observation of unique dipole emission patterns [35], but

these lack the completeness in characterization that fluorescence intensity correlation techniques can provide. Intensity correlation techniques such as photon antibunching offer extremely powerful methods for investigating the single versus multiple emitter uncertainty in single –molecule systems. Because an individual quantum mechanical system must relax before emitting another photon, photons are spaced in time by at least the fluorescence lifetime. Consequently, measurements of photon statistics from a single molecule exhibit distinctly non-classical emission that is manifested as a dip toward zero in the second order fluorescence correlation function, $g^2(\tau) = \langle I(\tau_0)I(\tau_0 +\tau)\rangle/\langle I\rangle^2$ [113] at zero delay where $I(\tau_0)$ is the photon emission rate at τ_0.

In theory, the measurement of such a system is straightforward, experimentally, it proves much more challenging. Fluorescence of single quantum systems must be split such that two photon counting devices see roughly equal intensity from the same fluorescent entity. After dividing the luminescence, the distribution of time intervals τ, between detection events is measured as a histogram correlation of start-stop pairs. On short times scales, the histogram distribution nicely approximates the correlation function $g^2(\tau)$ and can be approximated [114] by

$$g^2(\tau) = 1 - (1/N)\exp(-(W_p + \Gamma_f)\tau) \qquad (1.7.1)$$

where N is the number of emissive sites within the nanostructure [113, 114], W_p is the pumping rate, and Γ_f is the fluorescence decay rate. For a large number of emissive sites (large N), the correlation function approaches unity and the emitted histogram

appears as would a classical system. For a single quantum emitter, (N=1), the correlation function approaches zero, a phenomenon known as photon antibunching [115] that was first demonstrated in dilute atomic beams, and later for single molecules in cryogenic host crystals [116]. The spectral feature indicative of photon antibunching shows a characteristic minimum (dip) near zero whose physical interpretation represents the inability of a single quantum system to emit two photons at exactly the same time. The experiment can be performed with a number of different experimental setups, the most common being a Hanbury- Brown and Twiss configuration [117]. However, the particulars of the system very much dictate the excitation source and detection to be used. For example, antibunching can be observed with the use of a pulsed laser provided the pulse width is extremely short relative to the fluorescence lifetime. The probability of detecting two photons at time delay zero approaches zero preventing the observation of a peak at zero delay. The other peaks in the histogram will appear spaced at 1/f, or the inverse of the laser repetition rate (1/84.1 MHz for out system = spacing of ~12ns) (Figure 1.7.1)[118]. However, most systems under investigation to date have a lifetime that is sufficiently long to measure with continuous wave (CW) excitation in which the limitation lies in the time-response of the detectors. Typically, photomultiplier tubes are used in our CW experiments due to their faster time resolution, but photon counting sensitivity is sacrificed. Avalanche photodiodes are also sufficient, and are much more sensitive detectors, though they suffer from poorer time resolution. With continuous excitation, the dip follows the inverse of the exponential decay of the fluorescence lifetime, and can be used to extrapolate the excited state lifetime (Figure 1.7.1).

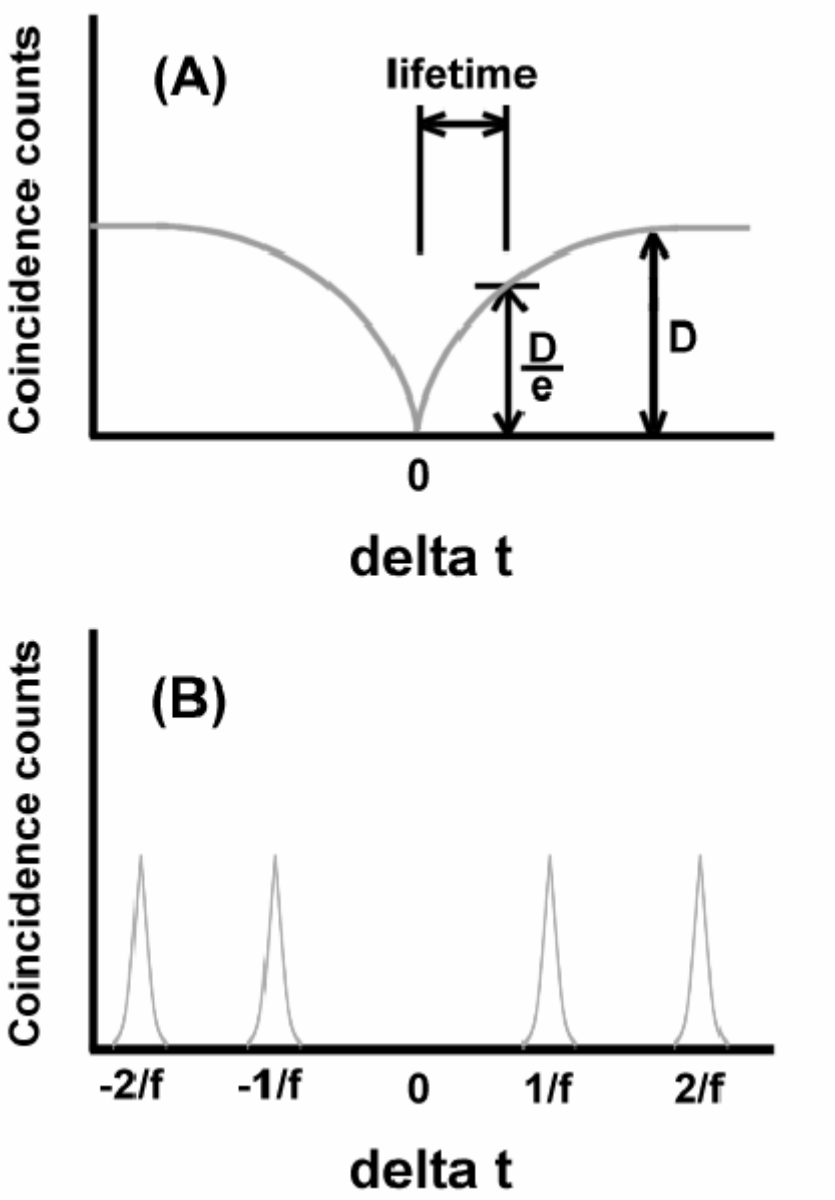

Figure 1.7.1 Ideal antibunching signatures in a Hanbury-Brown and Twiss configuration. All correlates start-stop pairs are measured and displayed on a histogram with the x-axis representing the difference in time between the two detection events. The CW case follows the inverse of the fluorescence lifetime while the pulsed case indicates the one-photon-in / one-photon out theory as both approach zero time delay.

Additionally, when choosing detection, quantum efficiency and spectral sensitivity are two very important factors in collecting statistically significant $g_2(\tau)$ data.

Even if the sample has a sufficient fluorescence lifetime to allow facile detection, many of these experiments suffer from the tremendous lack in photostability of the organic emitters. A severely reduced number of fluorescence photons results from the poor photostability, generally foiling the experiment as does any discernable level of background fluorescence. To avoid this general instability, researchers have been able to generate fluorescence correlations resulting from hundreds or thousands of individual emitters taken together [114].

Photon antibunching experiments are capable not only of proving the existence of single quantum systems, but further of using this information as a molecular-level reporting scheme. The most known examples to date build on quantum encryption schemes that historically have proposed electrons as a communication source by modifying such properties as their spin [119]. However, since the use of many electrons is plagued by capacitance problems, the use of photons for this purpose alleviates practical problems while adding more functionality in the ability to manipulate a photon by polarization. Controlled polarization states of photons for this purpose have been shown to provide a form of quantum mechanical security by preventing signal interception by an unwanted third party [120]. There is large amount of literature surrounding quantum dot type experiments, but a very limited number of quantum optical experiments using fluorescence intensity correlation techniques [121, 122]. Recent work on conjugated polymer systems however, has shown an optical output that is highly dependent on

the polymeric chain configuration [114, 123]. Conjugated polymer systems such as MEH-PPV (modified poly(phenelyne- vinylene) have been proposed next-generation flexible light-emitting diodes (LED's), all-organic integrated circuits, and optoelectronic components due to their superb photoluminescent properties [124]. However, chain configuration has an effect on the nature of the sites generating such emission. For example, MEH-PPV shows and antibunching signatures in the collapsed-chain confirmation, but behaves completely classically in an unfolded confirmation [114]. In systems such as optoelectronic devices where precise control is needed, these types of experiments are the only conclusive indicators of the nature of the individual quantum system.

References

(1) Eachus, R.S., A.P. Marchetti, and A.A. Muenter, *The Photophysics of Silver Halide Imaging Materials.* Ann. Rev. Phys. Chem. 1999. **50**: p. 117.

(2) Mitchell, J.W., *The Formation of the Latent Image in Photographic Emulsion Grains.* Photogr. Sci. Eng. 1981. **25**: p. 170.

(3) Tani, T. and M. Murofushi, *Silver Microclusters on Silver Halide Grains as Latent Image and Reduction Sensitization Centers.* J. Imag. Sci. Technol. 1994. **98**: p. 1.

(4) Bjelkhagen, H.J., *Silver Halide Recording Materials for Holography and their processing*. 1995, New York: Springer-Verlag.

(5) Ehrlich, S.H., *Spectroscopic Studies of AgBr With Quantum-Sized Clusters of Iodide, Silver, and Silver Sulfides.* J. Imaging Sci. Technol. 1993. **37**(1): p. 73.

(6) Marchetti, A.P., et al., *Formation and spectroscopic manifestation of silver clusters on silver bromide surfaces.* J. Phys. Chem. B 1998. **102**(27): p. 5287.

(7) Sahyun, M.R., D.K. Sharma, and N. Serpone, *Mechanisms of spectral sensitiztion of silver halides: role of sensitizing dye complexation.* J. Img. Sci. Tech. 1995. **39**(5): p. 377.

(8) Harbich, W., et al., *Deposition of mass selected silver clusters in rare gas matrices.* J. Chem. Phys. 1990. **93**: p. 8535.

(9) Rabin, I., W. Schulze, and G. Ertl, *Light emission during the agglomeration of silver clusters in noble gas matrices.* J. Chem. Phys. 1998. **108**(12): p. 5137.

(10) Harbich, W., S. Fedrigo, and J. Buttet, *The Optical-Absorption Spectra of Small Silver Clusters (N = 5- 11) Embedded in Argon Matrices.* Chem. Phys. Lett. 1992. **195**(5-6): p. 613.

(11) Harbich, W., S. Fedrigo, and J. Buttet, *The Optical-Absorption Spectra of Small Silver Clusters (N=8- 39) Embedded in Rare-Gas Matrices.* Z. Phys. D-Atoms Mol. Clusters 1993. **26**(1-4): p. 138.

(12) Harbich, W., et al., *Optical spectroscopy of size-selected silver clusters embedded in solid neon: A cluster-support interaction study.* Surf. Rev. Lett. 1996. **3**(1): p. 1147.

(13) Fedrigo, S., et al., *Evidence For Electronic Shell Structure of Small Silver Clusters in the Optical-Absorption Spectra.* Chem. Phys. Lett. 1993. **211**(2-3): p. 166.

(14) Fedrigo, S., W. Harbich, and J. Buttet, *Optical-Response of Ag2, Ag3, Au2, and Au3 in Argon Matrices.* J. Chem. Phys. 1993. **99**(8): p. 5712.

(15) Fedrigo, S., W. Harbich, and J. Buttet, *Collective Dipole Oscillations in Small Silver Clusters Embedded in Rare-Gas Matrices.* Phys. Rev. B-Condens Matter 1993. **47**(16): p. 10706.

(16) Felix, C., et al., *Fluorescence and excitation spectra of Ag-4 in an argon matrix.* Chem. Phys. Lett. 1999. **313**(1-2): p. 105.

(17) Konig, L., et al., *Chemiluminescence in the agglomeration of metal clusters.* Science 1996. **274**(5291): p. 1353.

(18) Rabin, I., et al., *Absorption and fluorescence spectra of Ar-matrix-isolated Ag-3 clusters.* Chem. Phys. Lett. 2000. **320**(1-2): p. 59.

(19) Rabin, I., W. Schulze, and G. Ertl, *Absorption spectra of small silver clusters Ag-n (n >= 3).* Chem. Phys. Lett. 1999. **312**(5-6): p. 394.

(20) Rabin, I., W. Schulze, and G. Ertl, *Light emission in matrix assisted cluster-cluster reactions.* Cryst. Res. Technol. 1998. **33**(7-8): p. 1075.

(21) Boo, D.W., et al., *Femtosecond dynamics of linear Ag-3.* J. Phys. Chem. A 1997. **101**(36): p. 6688.

(22) Ellis, A.M., E.S.J. Robles, and T.A. Miller, *Dispersed Fluorescence Spectroscopic Study of the Ground Electronic State of Silver Trimer.* Chem. Phys. Lett. 1993. **201**(1-4): p. 132.

(23) Willey, K.F., et al., *Electronic Spectroscopy of Silver Dimer Rare-Gas Complexes.* J. Chem. Phys. 1991. **95**(9): p. 6249.

(24) Oku, Y. and M. Kawasaki, *Diffuse Transmittance Spectroscopy of Diatomic Ag Nuclei on AgBr Microcrystals.* J. Phys. Chem. B 1998. **102**: p. 9061.

(25) de Heer, W.A., *The physics of small metal clusters.* Rev. Mod. Phys. 1993. **65**(3): p. 611.

(26) Brucat, P.J., et al., *Metal cluster ion photofragmentation.* J. Chem. Phys. 1986. **84**(6): p. 3078.

(27) Menezes, W.J.C. and M.B. Knickelbein, *Photodissociation spectroscopy of niobium-argon (NbnArm) complexes.* J. Chem. Phys. 1993. **98**(3): p. 1856.

(28) Bechthold, P.S., et al., *Guest-Host Interaction and Photochemical Transformation of Silver Particles Isolated in Rare Gas Matrices.* Z. Phys. D - Atoms, Molec. Clust. 1986. **3**: p. 263.

(29) Bonacic-Koutecky, V., V. Veyret, and R. Mitric, *Ab initio study of the absorption spectra of Agn (n=5-8) clusters.* J. Chem. Phys. 2001. **115**(22): p. 10450.

(30) El-Sayed, M., *Some interesting properties of metals confined in time and nanometer space of different shapes.* Acc. Chem. Res. 2001. **34**: p. 257.

(31) Empedocles, S. and M. Bawendi, *Spectroscopy of Single CdSe Nanocrystallites.* Acc. Chem. Res. 1999. **32**: p. 389.

(32) Wilcoxon, J.P., et al., *Photoluminescence from nanosize gold clusters.* J. Chem. Phys. 1998. **108**: p. 9137.

(33) Link, S., et al., *Transition from nanoparticle to molecular behavior: a femtosecond transient absorption study of a size-selected 28 atom gold cluster.* Chem. Phys. Lett. 2002. **356**: p. 240.

(34) Huang, T. and R.W. Murray, *Visible luminescence of water-soluble monolayer protected gold clusters.* J. Phys. Chem. B. 2001. **105**: p. 12498.

(35) Peyser, L.A., et al., *Photoactivated fluorescence from individual silver nanoclusters.* Science 2001. **291**: p. 103.

(36) Zheng, J. and R.M. Dickson, *Individual Water-Soluble Dendrimer-Encapsulated Silver Nanodot Fluorescence.* JACS 2002. **124**(47): p. 13982.

(37) Zheng, Z., J. Petty, and R.M. Dickson, *High Quantum Yield Blue Emission from Water-Soluble Au8 Nanodots.* JACS Commun 2003. **125**(26): p. 7780.

(38) Tiggesbaumker, J., et al., *Giant Resonances in Silver-Cluster Photofragmentation.* Chem. Phys. Lett. 1992. **190**(1,2): p. 42.

(39) Felix, C., et al., *Ag8 fluorescnece in Argon.* Phys. Rev. Lett. 2001. **86**(14): p. 2992.

(40) Kotz, R. and E. Yeager, *Raman studies of the silver/silver oxide electrode.* J. Electroanal. Chem. 1980. **111**: p. 105.

(41) Pettinger, B., et al., *Thermal-Decomposition of Silver-Oxide Monitored By Raman- Spectroscopy - From Ago Units to Oxygen-Atoms Chemisorbed On the Silver Surface.* Angew. Chem.-Int. Edit. Engl. 1994. **33**(1): p. 85.

(42) Wang, X., et al., *Enhancement mechanism of SERS from cyanine dyes adsorbed on Ag2O colloids.* Spectroc. Acta Pt. A-Molec. Biomolec. Spectr. 1997. **53**(14): p. 2495.

(43) Weaver, J.F. and G.B. Hoflund, *Surface Characterization Study of the Thermal-Decomposition of AgO.* J. Phys. Chem. 1994. **98**(34): p. 8519.

(44) Brandt, E.S., *Selective Enhanced Raman Scattering from an Oxacarbocyanine Dye and 1-Phenyl-5-Mercaptotetrazole Adsorbed to Silver and Silver Halide Surfaces in Photographic Films.* Appl. Spectrosc. 1993. **47**: p. 85.

(45) Watanabe, T., et al., *Evidence for surface Ag+ complexes as the SERS-active sites on Ag electrodes.* Chem. Phys. Lett. 1983. **102**: p. 565.

(46) Wang, X.Q., et al., *Surface-enhanced Raman scattering from citrate, azobenzene, pyridine and cyanine dyes adsorbed on Ag2O colloids.* Spectroc. Acta Pt. A-Molec. Biomolec. Spectr. 1997. **53**(9): p. 1411.

(47) Wang, X.Q., et al., *Enhancement mechanism of SERS from cyanine dyes adsorbed on Ag2O colloids.* Spectrochim. Acta A 1997. **53**: p. 2495.

(48) Temperini, M.L.A., G.I. Lacconi, and O. Sala, *Raman-Spectroscopy Investigation of the Silver-Oxide Silver Electrode - Influence of Experimental Conditions.* J. Electroanal. Chem. 1987. **227**(1-2): p. 21.

(49) Li, Y.S., *Surface-Enhanced Raman-Scattering At Colloidal Silver-Oxide Surfaces.* J. Raman Spectrosc. 1994. **25**(10): p. 795.

(50) Gui, J. and T.M. Devine, *Influence of Hydroxide On the Sers of Water and Chloride.* Surf. Sci. 1989. **224**(1-3): p. 525.

(51) Mihalcea, C., et al., *Intrinsic fluorescence and quenching effects in photoactivated reactively sputtered silver oxide layers.* J. Am. Chem. Soc. 2001. **123**(29): p. 7172.

(52) Buchel, D., et al., *Sputtered silver oxide layers for surface-enhanced Raman spectroscopy.* Appl. Phys. Lett. 2001. **79**(5): p. 620.

(53) King, F.W., R.P. Van Duyne, and G.C. Schatz, *Theory of Raman scattering by molecules adsorbed on electrode surfaces.* J. Chem. Phys. 1978. **69**: p. 4472.

(54) Moskovits, M., *Surface-enhanced spectroscopy.* Rev. Mod. Phys. 1985. **47**: p. 783.

(55) Kneipp, K., et al., *Single molecule detection using surface-enhanced Raman scattering (SERS).* Phys. Rev. Lett. 1997. **78**: p. 1667.

(56) Emory, S.R. and S.M. Nie, *Near-field surface-enhanced Raman spectroscopy on single silver nanoparticles.* Anal. Chem. 1997. **69**(14): p. 2631.

(57) Krug, J.T., et al., *Efficient Raman enhancement and intermittent light emission observed in single gold nanocrystals.* J. Am. Chem. Soc. 1999. **121**(39): p. 9208.

(58) Garrell, R.L. and J.E. Pemberton, eds. *Fundamentals and Applications of Surface Raman Spectroscopy*. 1994, VCH Publishers: Deerfield Beach, FL.

(59) Chang, R.K. and T.E. Furtak, eds. *Surface-Enhanced Raman Scattering*. 1981, Plenum Press: New York.

(60) Baibarac, M., et al., *Interfacial chemical effect evidenced on SERS spectra of polyaniline thin films deposited on rough metallic supports.* J. Raman Spectrosc. 1999. **30**(12): p. 1105.

(61) Nandra, S.S., J. Bandekar, and A.L. Cholli, *Detection of Silver-Oxide Film Sandwiched in a Multilayer Dielectric Stack By Raman-Spectrometry.* Appl. Spectrosc. 1991. **45**(7): p. 1183.

(62) Loudon, R., *The Quantum Theory of Light*. 2nd ed. 2000, New York: Oxford University Press.

(63) Ferraro, J.R., *Introductory Raman Spectroscopy*. 1994, Boston: Academic Press.

(64) Myers, A.B. and R.A. Mathies, *Resonance raman intensities: a probe of excited -state structure and dynamics*, in *Biological applications of Raman spectroscopy*, T.G. Spiro, Editor. 1987, Wiley and Sons: New York. p. 1.

(65) Myers, A.B., *Excited electronic state properties from ground state resonance Raman*, in *Laser techniques in chemistry*, A.B. Myers and T.R. Rizzo, Editors. 1995, Wiley and Sons: New York. p. 325.

(66) Long, D.A., *The Raman Effect: A Unified Treatment of the theory of Raman scattering by molecules*. 2002, New Yoru: Wiley.

(67) Long, D.A., *Raman Spectroscopy*. 1977, New York: McGraw-Hill.

(68) Fleischmann, M., P.J. Hendra, and A.J. McQuilan, *Raman spectra from electrode surfaces.* J. Chem. Soc. Chem. Comm. 1973: p. 80.

(69) Fleischmann, M., P.J. Hendra, and A.J. McQuilan, *Raman spectra of pyridine at a silver electrode.* Chem. Phys. Lett. 1974. **26**: p. 163.

(70) Jeanmaire, D.L. and R.P. Van Duyne, *Surface-enhance spectroelectrochemistry part 1: Heterycyclic, aromatic, and aliphatic aminesadsorbed on the anodized silver electrode.* J. Electroanal. Chem. 1977. **84**: p. 1.

(71) Albrecht, M.G. and J.A. Creigton, *Anomalously intenst Raman spectra of pyridine at a silver electrode.* J. Am. Chem. Soc. 1977. **99**(15): p. 5215.

(72) Albrecht, M.G., J.F. Evans, and J.A. Creighton, *The nature of an electrochemically roughened silver surface and its role in promoting anomalous Raman scattering intensity.* Surf. Sci. 1978. **75**: p. 777.

(73) Hildebrandt, P. and M. Stockburger, *Surface enhanced Raman Spectroscopy of Rhodamine 6G adsorbed on colloidal silver.* J. Phys. Chem. 1984. **88**: p. 5935.

(74) Otto, A., et al., *Surface -enhanced Raman scattering.* J. Phys. Condens. Mater. 1992. **4**(5): p. 1143.

(75) Metiu, H. and P. Das, *The electromagnetic theory of surface ehanced raman scattering.* Ann. Rev. Phys. Chem 1984. **35**: p. 507.

(76) Barber, P.W., R.K. Chang, and H. Massoudi, *Electrodynamic calculations of the surface-enhanced electric intensities on large Ag spheroids.* Phys. Rev. B. 1983. **27**: p. 7251.

(77) Creigton, J.A., *Metal Colloids*, in *Surface-enhanced Raman scattering*, R.K. Chang and T.E. Furtak, Editors. 1982, Plenum Press: New York. p. 243.

(78) Garcia-Vidal, F.J. and J.B. Pendry, *Collective theory for surface enhanced Raman scattering.* Phys. Rev. Lett. 1996. **77**(6): p. 1163.

(79) Gersten, J. and A. Nitzan, *Electromagnetic theory of enhanced Raman scattering by molecules adsorbed on rough surfaces.* J. Chem. Phys. 1980. **73**: p. 3023.

(80) Gersten, J. and A. Nitzan, *Radiative Properties of Solvated Molecules in Dielectric Clusters and Small Particles.* J. Chem. Phys. 1991. **95**(1): p. 686.

(81) Kerker, M., D. Wang, and H. Chew, *Surface-enhanced Raman scattering (SERS) by molecules adsorbed at spherical particles.* Appl. Opt. 1980. **19**: p. 3373.

(82) Link, S. and M. El-Sayed, *Size and temperature dependence of the plasmon absorption of colloidal gold nanoparticles.* J. Phys. Chem. B. 1999. **103**: p. 4212.

(83) Aravind, P.K., E. Hood, and H. Metiu, *Angular resonances in the emission from a dipole located near a grating.* Surf. Sci. 1981. **109**: p. 95.

(84) Adams, A., J. Moreland, and P.K. Hansma, *Angular responses in the light emission fromatoms near a grating.* Surf. Sci. 1981. **111**: p. 351.

(85) Otto, A., *Surface enhanced Raman scattering: "Classical" and "Chemical" origins*, in *Light Scattering in Solids IV*, M. Cardona and G. Gundtherodt, Editors. 1984, Springer-Verlag: Berlin. p. 289.

(86) Pettinger, B. and L. Moerl, *Influence of foreign matal atoms deposited at electrodes on local and non local processes in surface enhanced Raman scattering.* J. Elec. Spec. Rel. Phenom. 1983. **29**: p. 383.

(87) Moskovits, M. and D.P. DiLella, *Vibrational spectroscopy of adsorbed molecules*, in *Surface Enhanced Raman Scattering*, R.K. Chang and T.E. Furtak, Editors. 1982, Plenum Press: New York. p. 243.

(88) Mrozek, I. and A. Otto, *Long-range and short-range effects in SERS from silver.* Europhys. Lett. 1990. **11**: p. 243.

(89) Lombardi, J.R., et al., *Charge-transfer theory of surface enhanced Raman spectroscopy: Herzeberg-Teller contributions.* J. Chem. Phys. 1986. **84**: p. 4174.

(90) Kambhampati, P., et al., *On the chemical mechanism of surface enhanced Raman scattering: experiment and theroy.* J. Chem. Phys. 1998. **108**(12): p. 5013.

(91) Persson, B.N.J., *On the theory of surface enhanced Raman scattering.* Chem. Phys. Lett. 1981. **82**(3): p. 561.

(92) Adrian, F.J., J. Chem. Phys. 1981. **77**: p. 5302.

(93) Arya, K. and R. Zeyher, *Theorty of surface enhanced Raman scattering fro molecules adsorbed at metal surfaces.* Phys. Rev. B. 1981. **24**: p. 1852.

(94) Arenas, J.F., et al., *Charge transfer processes in surface enhanced Raman scattering: Franck Condon active vibrations of pyridine.* J. Phys. Chem. 1996. **100**: p. 9254.

(95) Osawa, M., et al., *Charge transfer resonance Raman process in surface-enhanced Raman scattering from p-aminothiophenol adsorbed on silver.* J. Phys. Chem. 1994. **98**: p. 12702.

(96) Rubim, J.C., et al., *Contribution of resonance Raman scattering to the surface-enhanced Raman effect on electrode surfaces.* J. Phys. Chem. 1995. **99**: p. 15765.

(97) Ueba, H., *Theory of charge transfer excitation in surface enhanced Raman scattering.* Surf. Sci. 1983. **131**: p. 347.

(98) Ueba, H., *Role of defect induced charge transfer excitation in SERS.* Surf. Sci. 1983. **129**: p. L267.

(99) Michaels, A.M., *Surface enhanced Raman spectroscopy at the single molecule level.* Thesis 2000.

(100) Nie, S.M. and S.R. Emory, *Probing single molecules and single nanoparticles by surface-enhanced Raman scattering.* Science 1997. **275**: p. 1102.

(101) Michaels, A.M., M. Nirmal, and L.E. Brus, *Surface enhanced Raman spectroscopy of individual rhodamine 6G molecules on large Ag nanocrystals.* J. Am. Chem. Soc. 1999. **121**(43): p. 9932.

(102) Meyers, A.B., et al., *Vibronic spectroscopy of individual molecules in solids.* J. Phys. Chem. 1994. **98**(41): p. 10377.

(103) Fleury, J., et al., 1995. **236**: p. 87.

(104) Nie, S.M. and R.N. Zare, *Optical detection of single molecules.* Annu. Rev. Biophys. Biomolec. Struct. 1997. **26**: p. 567.

(105) Xie, X.S. and J.K. Trautman, Ann. Rev. Phys. Chem. 1988. **49**: p. 441.

(106) Kneipp, K., et al., *Ultrasensitive chemical analysis by Raman Spectroscopy.* Chem. Rev. 1999. **99**: p. 2957.

(107) Michaels, A.M., J. Jiang, and L.E. Brus, *Ag Nanocrystal Junctions as the Site for Surface-Enhanced Raman Scattering of Single Rhodamine 6G Molecules.* J. Phys. Chem. B 2000. **104**: p. 11965.

(108) Jiang, J., et al., *Single molecule raman spectroscopy at the junctions of large Ag nanocrystals.* J. Phys. Chem. B. 2003. **107**: p. 9964.

(109) Xu, H., et al., *Electromagnetic contributions to single-molecule sensitivity in surface-enhanced Raman scattering.* Phys. Rev. E 2000(62): p. 4318.

(110) Peyser, L.A., T.-H. Lee, and R.M. Dickson, *Mechanisn of Ag_n nanocluster photoproduction from silver oxide films.* J. Phys. Chem B. 2002. **106**: p. 7725.

(111) Mihalcea, C., et al., *Intrinsic Fluorescence and Quenching Effects in Photoactivated Reactively Sputtered Silver Oxide Layers.* J. Am. Chem. Soc. 2001. **123**(29): p. 7172.

(112) Capadona, L.P., J. Zheng, and R.M. Dickson, *Nanoparticle-Free Single Molecule Antistokes Raman Spectroscopy.* 2004. **submitted**.

(113) Walls, D.F. and G.J. Milburn, *Quantum Optics*. 1994, Berlin: Springer.

(114) Hollars, C.W., S.M. Lane, and T. Huser, *Controlled non-classical photon emission from single conjugated polymer molecules.* Chem. Phys. Lett. 2003. **370**: p. 393.

(115) Kimble, H.J., M. Dagenais, and L. Mandel, *Photon antibunching in resonance fluorescence.* Phys. Rev. Lett. 1977. **39**: p. 691.

(116) Paul, H., *Photon antibunching.* Rev. Mod. Phys. 1982. **54**(4): p. 1061.

(117) Hanbury Brown, R.H. and R.Q. Twiss, *Correlation between photons in coherent light rays.* Nature 1956. **178**: p. 1447.

(118) Lee, T.H., *Silver nanocluster single molecule optoelectronics and its applicatons.* Thesis 2004.

(119) *The international technology roadmap for semiconductors.* International Sematech 2001.

(120) Beveratos, A., et al., *Single photon quantum cryptography.* Phys. Rev. Lett. 2002. **89**: p. 187901.

(121) Brunel, C., et al., *Triggered source of single photons based on controlled single molecule fluorescence.* Phys. Rev. Lett. 1999. **83**(14): p. 2722.

(122) Lounis, B. and W.E. Moerner, *Single photons on demand from a single molecule at room temperature.* Nature 2000. **407**: p. 491.

(123) Kumar, P., et al., *Photon antibunching from oriented semiconducting ploymer nanostructures.* J. Am. Chem. Soc. 2004. **126**(11): p. 3376.

(124) Friend, R.H., et al., *Electroluminescence in conjugated polymers.* Nature 1999. **397**: p. 121.

CHAPTER 2

EXPERIMENTAL

Various types of experiments were performed throughout this thesis work all pointing toward a more complete investigation of the optical behavior and properties of reduced dimension silver nanoclusters at room temperature. Silver nanoclusters were formed by a number of different methods both on thin metal films and in solution all exhibiting similar optical behavior, some lending themselves more directly to certain experiments. For example from a materials perspective, initial applications of the photoactivation properties of thin silver films were investigated as potential optical storage elements by careful investigation and analysis of the contributing factors. Further experiments on the nanoclusters were directed at a mechanistic determination of photoactivation and creation dynamics of such intense, dynamic species. From a more fundamental perspective, the more recent solution based experiments focus more on application of the elucidated optical properties to the well-known but not well understood phenomenon of surfaced-enhanced Raman spectroscopy. The spectral dynamics common to the film work and solution based studies served as the connection between the two, and also assisted in determining which factors contribute to our quest for understanding of the atom to bulk transition of such a common, but extremely complex metal.

All samples were prepared on either glass cover slides (Fisher Scientific model # 12-548-B FisherFinest, 22x22mm) or quartz (Electron Microscopy Sciences, purchased through Fisher Scientific # 72256-02 25x22x0.2mm) coverslides. The coverslides were cleaned in a solution of concentrated sulfuric acid/NoChromix™ solution for about five hours. They were agitated slightly before removal to prevent to presence of salt formation on the glass followed by a triple rinse in de-ionized water, and a rinse in 99.99% purity spectrophotometric grade methanol. The slides were then blown dry under inert gas and subjected to ozonation treatment for two hours to further oxidize any fluorescent impurities. All slides were stored in a beaker cleaned in the same manner covered with parafilm to minimize outside contamination.

2.1 Silver oxide thin film preparation

Thin silver/silver oxide films were prepared in the following three manners. All three methods render similar films, however some methods offer more precise control over sample creation.

Thermal evaporation

A DV-502A Denton Vacuum Thermal Evaporator at a moderate vacuum pressure of < $2x10^{-6}$ torr was used. Evaporation was carried out using high purity silver wire with a hot filament inducing evaporation at a rate of ~ 1Å/sec. The rate of evaporation through the duration of the deposition must be carefully controlled as it

affects final film quality. Usually, the filament is heated until visual melting is observed through the observation window with the shutter to the samples on the "closed" position. Then the current is turned off after initial melting of deposition metal. The shutter to the samples is then opened, and current turned up slowly to reach a constant deposition rate. Otherwise, samples may end up with unwanted deposits (oxides) while the wire is first melted. When preparing samples it is always necessary to wear gloves as any oil from hands, etc may become volatile at under such moderate vacuum conditions. Once final sample thickness is set, deposition continues at a constant rate until about 5 Å short of the desired film thickness. The current is tuned off with the rotor continuing to move the samples around. Since the thickness is measured by a reflectance quartz crystal micro balance, there is a small (~0.5nm) error in its accuracy. Usually, the final thickness reading on the monitor will continue to rise after the current is turned off. By leaving the ~5 Å to still be deposited when the current is turned off, the increase in the thickness should end up reading what it was set at. For example, if the setting is on 180 Å (18nm), the current should be turned off when the monitor reads 175 Å, and it will creep up to a final thickness of 180 Å. Care should be taken to let samples cool for about fifteen minutes after deposition, and to protect films from light and organics as the films quickly oxidize.

Chemical bath deposition

While oxidized thin films yield good results, chemically prepared films offer greater ease of sample preparation and better reproducibility. Chemical films of

silver oxide (AgO) ranging from 50 – 80 nm in thickness were produced in a bath deposition medium by simultaneously mixing 5 mL of 0.1M NaOH and 0.1M $AgNO_3$ [1]. The AgOH precipitate is washed three times in de-ionized water, leaving behind ~ 10mL after the last wash to enable stirring. The precipitate is then completely dissolved to a clear solution by the drop-wise addition of triethanolamine (TEA). The resulting viscous mixture is transferred to a larger beaker and stirred while 100mL of water is added. The pH of this clear solution is then further increased by the addition of excess NaOH until slightly turbid. Although thought to produce pure AgO, the resulting mixture likely contains a mixture of oxides. We further oxidized these films with ozone treatment [2]. Both silver oxide thin film preparations (evaporation and chemical deposition) exhibited similar optical properties, but the chemically prepared films exhibit a higher density of nanoclusters, and are more homogeneous with respect to the surface quality.

Reactive RF sputtering

AgO and Ag_2O films were also prepared under more still more controllable atmospheric conditions in the reactive-RF sputterer [3, 4]. Films of pure AgO ranging in thickness from 50 to 125 nm were reproducibly prepared by reacting sputtered atoms from a pure metallic silver target with different partial pressures of oxygen in the plasma to form silver oxide. This method provides the best control over final film composition through the precise control over the RF-power and plasma gas mixture ratio (O_2: Ar). The additional benefit of RF sputtering is the control of sample thickness, and the added functionality of being able to run multiple thickness batches

fairly quickly. This method allowed us to easily study the effect of surface oxygen composition in a trial and error manner while examining which deposition conditions gave the most photoactive samples. At an O_2 to Argon ratio of three, and 250 W of RF power, the deposition rate was about 0.07 nm yielding final film thicknesses of about 25nm after twenty minutes.

2.2 Single-molecule fluorescence microscopy methods

Because of the great range of dynamics present in nanoscale systems, most single molecule experiments report on the combined properties of the probe and the surrounding matrix. Such experiments have the ability to discern information about a complex system otherwise studied by ensemble averaging of all available molecular behaviors. The development of single molecule imaging techniques truly opened new areas of research unable to be addressed by conventional bulk methodologies since their introduction over a decade ago [5-14]. The ability to detect and understand molecular behavior on the smallest observable level using single molecules as probes is in fact, a reporting limit. Still, the utilization of single molecules as reporters of the environment has been hindered by observables that are tremendously difficult to interpret. By using methods for true three-dimensional orientation determination developed in our lab [15, 16], we can directly probe geometry changes without interference from complex environmental interactions altering fluorescence behavior. These methods afford a relatively unobstructed view of molecular dynamics and their manifestations as reporters of nanoscale materials.

Total internal reflection

For the specific cases of experiments in our lab, individual quantum systems e.g. (single molecules) fluoresce with the unique signature of an individual dipole (the linear transition dipole connecting their specific ground and excited states). Though very suggestive of individual molecular behavior, the verification of polarized emission cannot be used alone to conclusively prove single molecule behavior. With the use of wide field excitation, simultaneous imaging of the emission dipoles can be performed giving information on the local environment to each specific molecule. Molecules with specific orientations are then represented and analyzed with respect to the emission pattern produced by them (see section 3.2 for a more detailed discussion). Fluorescence was studied under both Ar^+ laser and band-pass filtered mercury lamp excitation. Because of the nature of emission of single molecules, the optical setup allowing accurate collection of their emission dipoles is critical. For this, total internal reflection microscopy (TIR) is used (Figure 2.2.1). TIR conditions are met when light propagating in an area of high refractive index meets an interface possessing a lower index of refraction. Given by Snell's law, this occurs at all angles greater than the critical angle,

$$\theta_H = \theta_C = \sin^{-1}\left(\frac{n_l}{n_h}\right) \qquad (2.2.1)$$

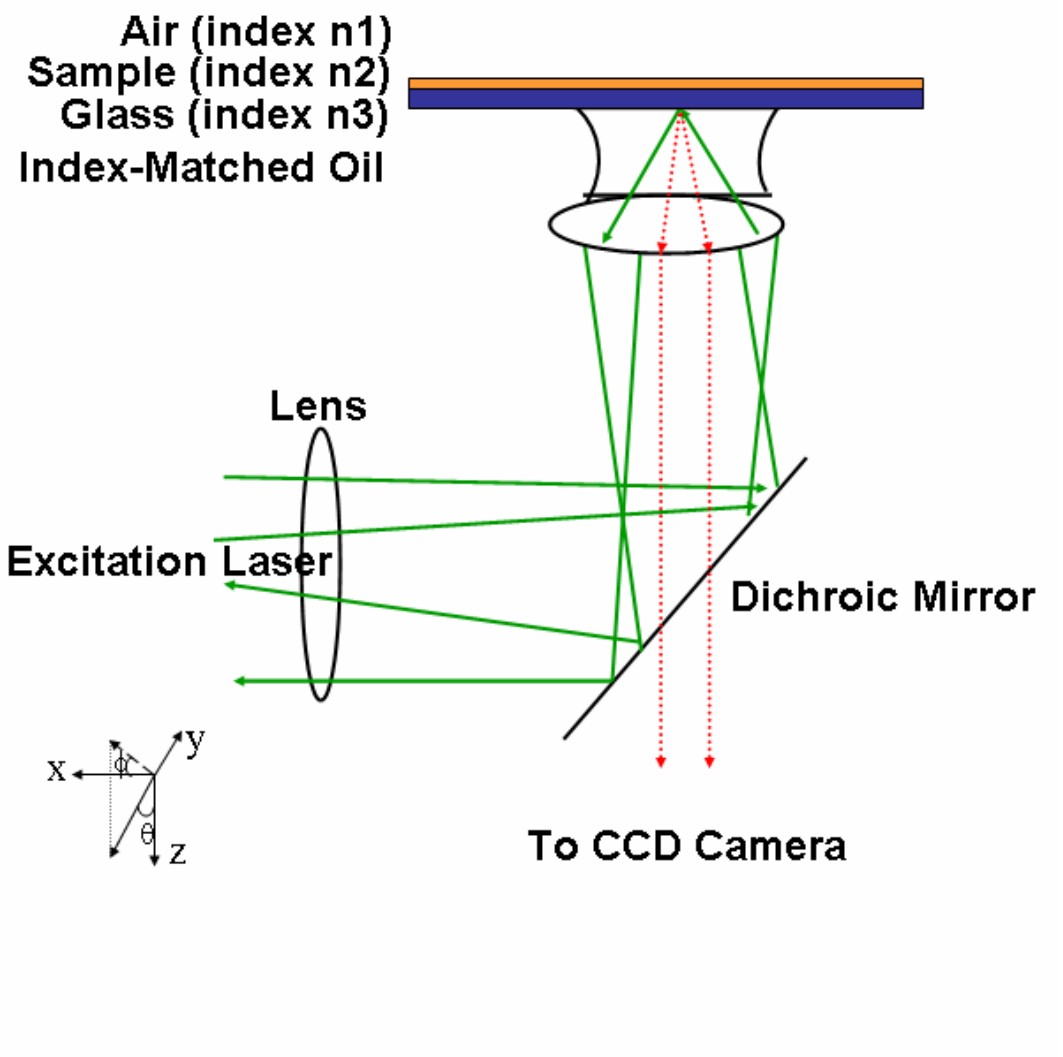

Figure 2.2.1. Total internal reflection through a microscope objective; illumination only at high incident angles. Excitation and image formation through the microscope objective simultaneously enables high-resolution optical imaging with single molecule orientational sensitivity.

with n_h (high) and n_l (low) refractive indices characteristic of the dielectric boundary. Light impinging on the boundary with angles greater than or equal to the critical angle, θ_c will be totally reflected into the more dense medium while conversely light at lower angles is transmitted through the interface. With respect to molecular excitation, an optical field intensity also exists within several hundred nanometers of the interface. This must be taken into consideration as it is capable of exciting molecules. Perpendicular to the surface, this evanescent field decays exponentially as a function of both the wavelength used, the polarization of the incident light and of course the respective refractive indices. The evanescent field intensities will vary for each direction with respect to the microscope stage, x, y, and z, with only p-polarized light incident on the boundary being able to generate a z-direction (normal to the sample surface) polarized evanescent field. This is useful for preferential excitation of a subpopulation of the sample allowing even more control on the single molecule level to probe local environmental dynamics.

The actual laser setup is rather simple once the optical conditions defined above for efficient TIR generation are met. For wide-field viewing, the Argon-Ion laser must be expanded before entering the microscope through its side port. It is then reflected from the coated surface of a dichroic mirror made to properly reflect the incident wavelength. For single molecule measurements, the light is then focused off- axis inside the body of a 1.4 NA oil immersion objective, and aligned such that refraction at the primary surface of the objective is at a high enough angle to produce total internal reflection at the coverglass / air interface. Light is totally reflected back down from the sample and collected through the same objective, and

the fluorescence filtered and collected generally by a CCD camera. This geometry enables efficient excitation with x, y and z-polarized light.

Epi-fluorescent illumination

Epi-fluorescent illumination with a Hg lamp allows facile switching between the three excitation wavelengths used for analysis (ultraviolet (340-360 nm), blue (460-490nm), and green (510-550 nm)). Additionally, epi-illumination allows observation of the entire field of view as well as the use of a limited illumination area through a tapered aperture. Intensity can be accurately attenuated by the use of sliding neutral density filters on the excitation side of the light path. The lamp also provides the flexibility of using selective excitation by using various filter combinations. Since the lamp emits light throughout the visible, combinations of long-and short-pass optical filters can be used to selectively excite the sample with narrow or wide band excitation of many different wavelengths. In all cases, samples were optically excited and observed from both sides of the silver film [15] to ensure that exciting or collecting emission through different thickness of silver oxide did not affect the results.

2.3 Preparation of encapsulated Ag_n nanoclusters

Encapsulation of silver nanoclusters was first done within PAMAM G4-OH and G2-OH (Fourth and second generation OH-terminated poly(amidoamine)) dendrimers by Jie Zheng. Dendrimers make excellent scaffold hosts because they

are three dimensional polymeric materials with very well defined structure (G4-OH formula weight 14279, diameter ~ 4.5 nm) (Figure 2.3.1). The same method of photoactivation that we used with the film-based experiments works extremely well with the dendrimer solution based chemistry, and it is a much better controlled system. In the literature, dendrimers are used to encapsulate much larger silver (and other) nanoparticles with the use of a reducing agent such as sodium borohydride ($NaBH_4$) [17-20]. This reproducibly yields larger particles in the <10nm range that do not exhibit any fluorescence and also display a characteristic plasmon absorption at 398nm. However, to produce the size nanoclusters of interest for this work, the need for a chemical reducing agent is unnecessary as light works to that end. The nanoclusters are prepared at room temperature by mixing 0.5μmol of the G4-OH dendrimer with 1.5 μmol of silver nitrate ($AgNO_3$). This is added to one mL of 18MΩ distilled water and adjusted to neutrality with acetic acid. When light is incident on an otherwise unactivated sample, the small silver nanoclusters photoactivate, whose size is characterized by electrospray-ionization (ESI) mass spectroscopy [21].

The same type of chemistry also works to encapsulate small silver nanoclusters in a short amine-rich peptide of sequence AHHAHHAAD (figure 2.3.1). This particular peptide is known to interact with larger metal nanoparticles after reduction [22] so was an excellent initial sequence. The basic preparation is the same in which the silver concentration is about 0.3 mg/mL and the silver/peptide ratio is about one peptide molecule per 6 atoms of silver. The same silver nitrate is used to generate the silver ions from the silver salt (about 0.04 g $AgNO_3$). About 4 g distilled

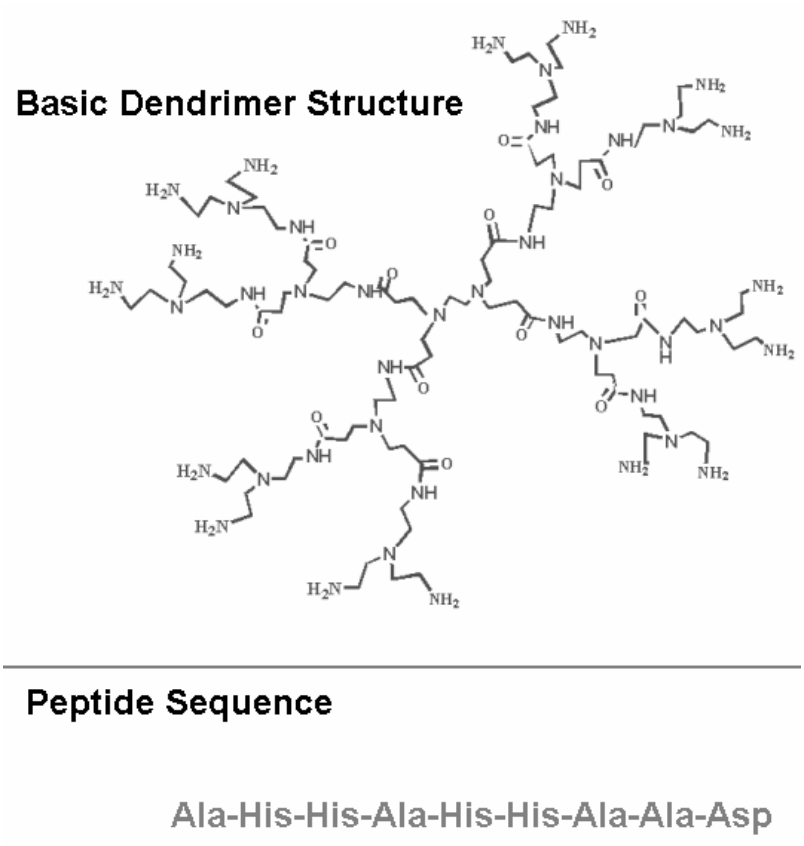

Figure 2.3.1. (Top) Basic organic structure of a Generation 4 NH_2 terminated dendrimer, for example. Well- defined structures, these polymeric materials act as hosts for our silver nanoclusters because of their 3-D structure and water-based solubility. (Bottom) Chosen sequence of amino acids making up the peptide also serving as an equally stable host for the Ag_n nanoclusters. Amino acid residues are non-fluorescent.

water is added such that the resulting concentration is in the range of 10mg/mL. Once this solution is prepared, in a separate vial, the peptide solution is prepared by adding a very small amount of peptide (0.0006g) and mixing it with water (density=1) until the total tared weight is one gram. 30 µL of the silver solution is then added directly into the vial with the peptide solution. Slight agitation is sometimes needed to break up any aggregation that may occur in solution. Solutions should always be kept in the refrigerator. Solutions are also checked to be certain that no large particles remain before proceeding with experiments. Using a small centrifuge (BioFuge *pico*, courtesy Dr. Lyon), samples are centrifuged at 13000 RPM for 30 minutes. All large particles are forced to the bottom and the supernatant liquid contains only the small nanoclusters of interest.

2.4 Single molecule spectroscopy setup

This setup is common for doing any spectroscopy requiring a monochromator. The Olympus IX-70 (71) was used for these experiments in which the laser was incident through the back port. Attached to the microscope on the side port is an Acton Spectra-Pro 300i imaging monochromator equipped with a mirror for imaging of zeroth order light, a 150l/mm (22.2 cm^{-1}/pixel) grating and a 600l/mm (3.39 cm^{-1} / pixel) grating. Resolution increases with the number of lines on a grating. The entrance slit is adjustable both in width and position (up = in the path, down = out). A Roper Scientific CCD is attached at the output of the monochromator which is parfocal with the eyepieces. The setup is seen in Figure 2.4.1. All Raman spectroscopy was carried out with a lens inserted into the excitation beam path just

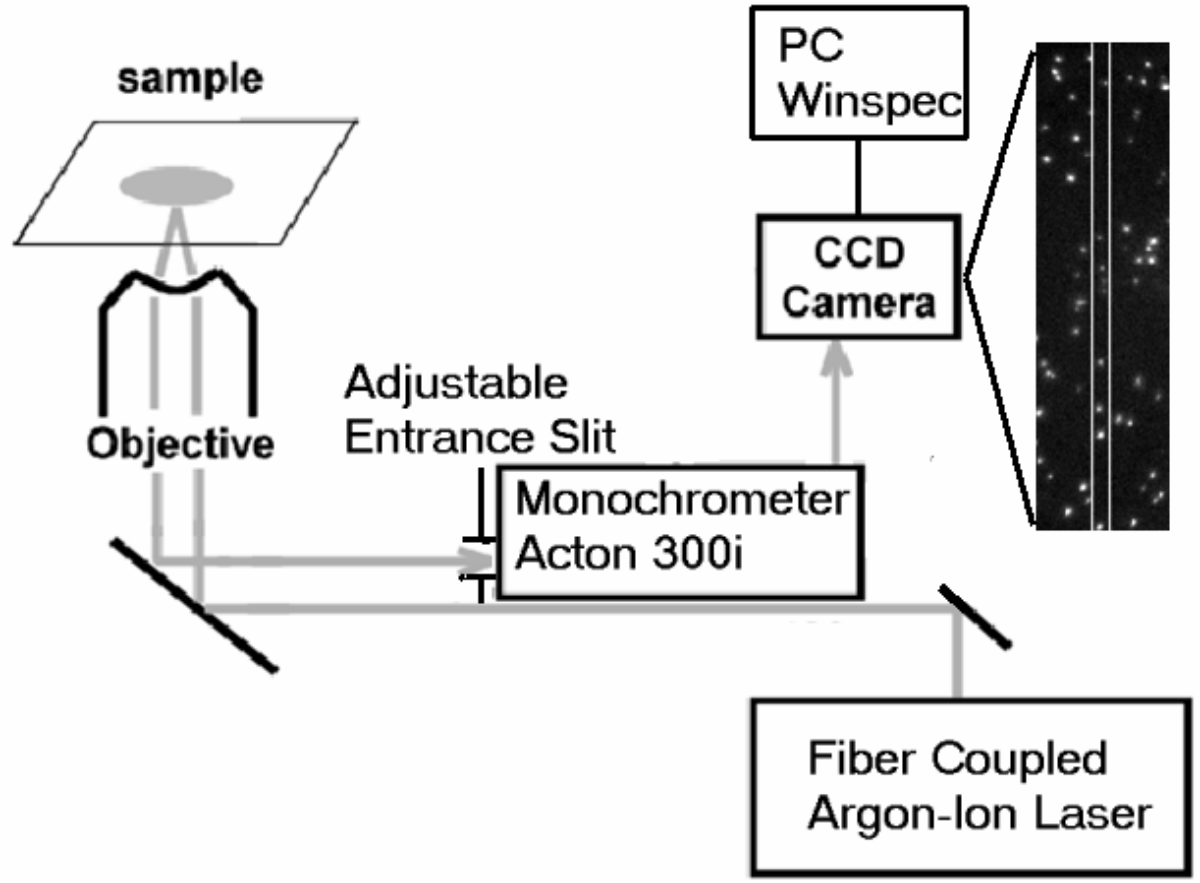

Figure 2.4.1. Experimental geometry for obtaining fluorescence or Raman spectra with laser excitation. Here, an adjustable entrance slit is used to allow only the spectrum from an individually selected molecule to be taken. Shown above, the white lines represent the area that will generate a spectrum, even though plenty of other fluorescence features are present. The slit can also be removed in order to take an image of the full field of view.

before it enters the microscope to yield an epi-fluorescent configuration. Allowing a wide-field view of the sample, individual molecules could then be positioned with either positioning by hand or by the Nanonics scanning stage through the entrance slit of the monochromator. With simultaneous imaging on the Roper Scientific spectroscopy TE-cooled CCD, fluorescence of those selected molecules was imaged, and when a grating was rotated into the path, a spectrum of those selected molecules was obtained. See the appendix for the spectrometer calibration procedure.

2.5 The Ti:Sapphire laser setup

A minimal assembly oscillator "kit" from KM-labs (www.kmlabs.com) was constructed to be a very useful diagnostic tool and later modified to add additional functionality in frequency doubling and tunability. The oscillator itself needs sufficient pump power (range 4.5W – 5.8W) currently provided by all lasing lines of a six watt Argon-Ion laser (Coherent, Innova 90C-6). A polarization switch tower is set up at the output of the Argon before entrance into the Ti:Sapphire cavity, since Argon lasers typical manifest a vertical beam polarization and the Ti:Sapphire crystal is cut such that a horizontal polarization is needed for efficient excitation along the crystal axis. The cavity is in a folded ("Z") configuration in which a fold mirror is employed. This is a convenient space-saving bench top technique as well as a user-friendly design for the operator. The general scheme of the cavity layout is presented in figure 2.5.1.

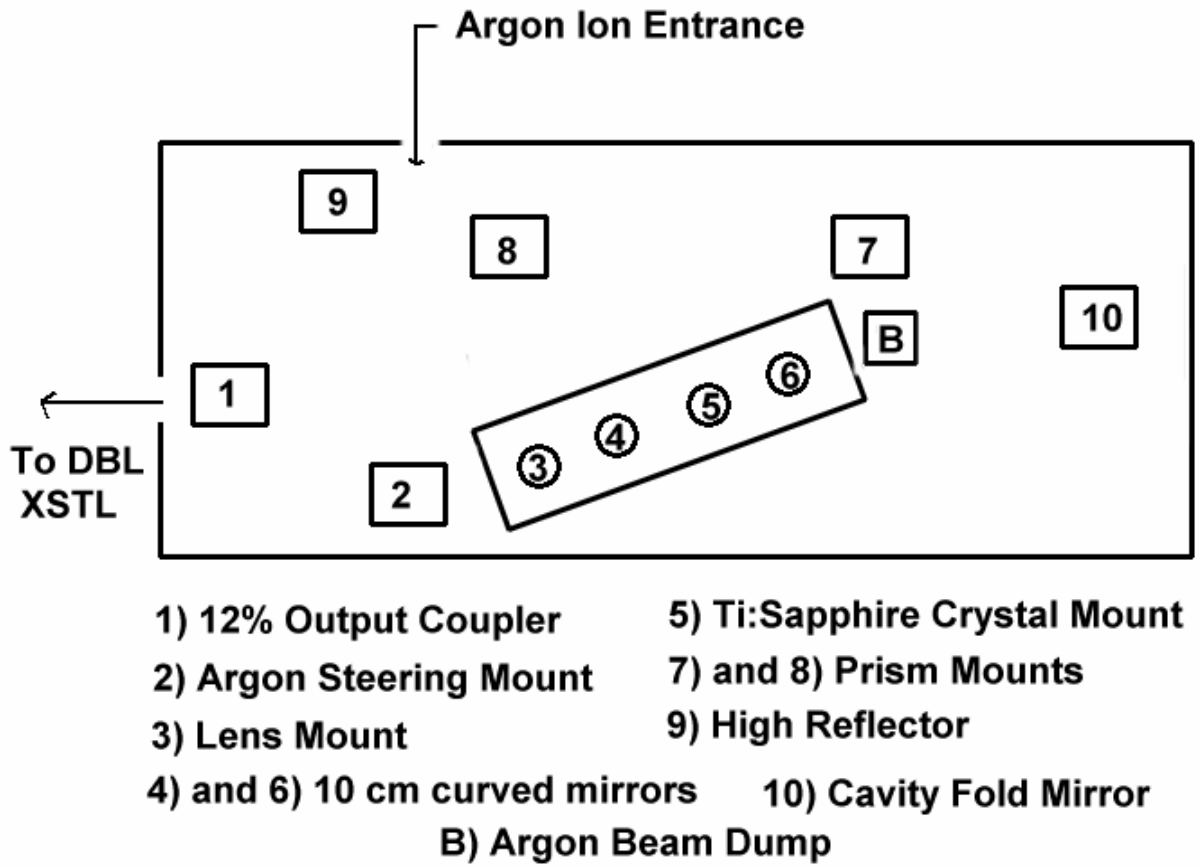

Figure 2.5.1. Schematic of the folded-cavity Ti:Sapphire laser layout. Prism eight is computer controlled. Additionally, a computer-controlled tuning slit may be placed between prism 7 and prism 8 to achieve greater utility. The crystal is angled in the mount at Brewster's angle for minimum deviation of pump light, as are both prisms for minimum deviation of cavity light. Beam height is crucial throughout and should be maintained to a precise level during alignment.

Initial alignment of the lasing cavity can be achieved by maintaining overlap of the fluorescence generated by the crystal (Sapphire, doped with Titanium) and achieving efficient gain through the cavity. (This explanation is extremely simplified - for a specific tutorial on the methods found most convenient, see the appendix). The mirror set supplied with the oscillator is designed for 800 nm central wavelength operation with a bandwidth of greater than 60nm achievable allowing ~10fs pulse output. In practive, laser pulses of ~200 fs were used. However, laser control of both a motorized slit and second prism is attainable by LabView control in a self-contained VI. Through control of the slit, limited tunability within the reflectivity ranges of the mirror set can be achieved. With this particular set, the laser could be stabilized out to ~840 nm. Since the experiments that pertain to our lab often require pulsed excitation, a type I (refers to the phase matching properties of the crystal: input polarization is orthogonal to output) BBO (Beta-BaB_2O_4) second harmonic generating (SHG) crystal (Quantum Technology) was placed in the laser path outside of the Ti:Sapphire cavity itself to generate the doubled frequency of whatever fundamental output the cavity produced. The crystal thickness (5x5x2 mm) was chosen in a very specific way such that minimum broadening of the ultra-fast pulse would occur while simultaneously retaining the best conversion efficiency (about 20%, minimal broadening).

Since the maximum attainable doubled frequency was centered at ~420nm with the current optic set, a number of experiments suffered from background fluorescence from the optics excited at these short wavelengths. While we could circumvent some of these issues by using lower average powers, or choosing

substrates with minimal absorption in these ranges (quartz, for one), we could not avoid the adverse effects from the internal optics of the microscope. An additional optics set was purchased whose coating was centered at ~875 nm. Frequency doubling with precise slit control and prism insertion allowed generation of stable modelocked excitation at ~450nm. At this wavelength, the bandwidth is significantly sacrificed, however, for the applications presented herein; this was inconsequential to the results. Efficient mode-lock can be easily achieved by introduction of cavity noise, most efficiently by "jogging" of the second prism in the cavity.

2.6 Fluorescence lifetime measurement

Using the in-house set-up (see section 2.5 and appendix) frequency doubled (~84MHz), modelocked Ti:Sapphire Laser (~400-450nm tunable, ~200fs pulse width), reliable fluorescence lifetimes of the excited state encapsulated silver nanoclusters were measured. The measured instrument response of the system was ~35ps, with which after deconvolution, reliable lifetimes down to 7ps could be measured. The laser was run through the microscope and the reflected fluorescence was dispersed through a monochromator with a movable mirror in the emission path. One could either reflect the emission to a CCD spectroscopy camera (1152x400), or rotate the mirror into position and collect a fluorescence lifetime with the use of a micro channel plate photomultiplier tube (MCP-PMT), Hammamatsu R3809) and computer based time-correlated single photon counting electronics (Becker-Hickl TCSPS-630), (Setup, Figure 2.6.1). The electronics consisted of an integrated discriminator/time to digital converter/ multi channel analyzer. A Thor-

Labs photodiode was used as a sync for the laser at the inverse of the repetition rate, or 12.2 ns. With such sensitive electronics, it was absolutely crucial to have set up the experiment properly so that the lifetime signal would be seen in the active area of the photon counting board. One could either employ a delay module such as the Ortec 425A which allowed adjustable delay of either signal line, but usually the sync, or add enough extra BNC cable lengths along the sync leg of the setup to account for the delay. A good estimate is one nanosecond of delay per one foot of cable. It was also necessary to use a pulse-inverter on the sync side since the photodiode puts out a positive pulse and the photon counting board only accepts negative pulses. The setup is shown in figure 2.6.1. Estimating where the signal will show up (correlate the arrival of the electrical signal to both the sync and CFD channels of the TCSPC board) was done with a highly fluorescent sample like a fluorescent bead or a very weakly attenuated laser. In a trial and error process, the Ortec delay module should be used at first to easily adjust the delay of the sync line with respect to the CFD line was adjusted until the signal is seen and is close to the center of the board such that longer lifetimes can still be measured without “running-off” the board. Once the delay is set with the Ortec, it is fine to take out the board and add enough cable to compensate for the delay. Using the same delays, accurate fluorescence lifetime measurements can be carried out.

In order to perform spectrally selected lifetime measurements, an adjustable exit slit can be used. It is a fairly straight-forward procedure to spectrally select the bandwidth incident on the PMT while “scanning” with the monochromator and WinSpec software. For example, if the sample emits everywhere from 500nm - 750

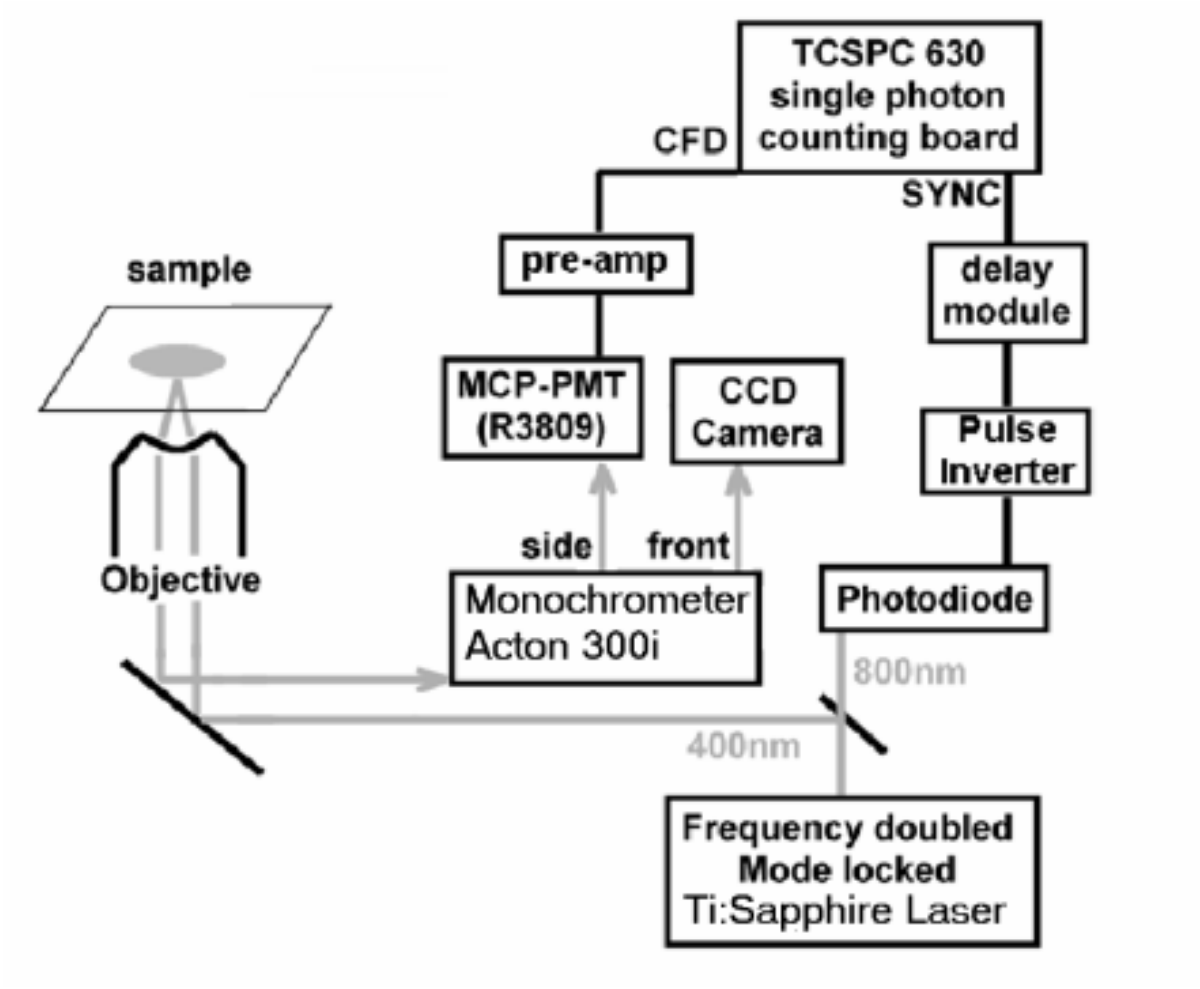

Figure 2.6.1. Schematic of the setup for measuring fluorescence lifetimes. A pulsed laser and a triggering photodiode must be used in conjunction with a PMT detector. Typically, wavelength selection from the controllable exit slit of the monochromator was used with this setup to allow more flexibility. Imaging of the dispersed, spectrally selected region was also possible with the use of the rotatable mirror on the exit side of the monochromator.

nm one can measure the lifetime of any selected region in between, the smallest accurate measurement being about a 10 nm region. The exit slit is micrometer-controlled and needs to be calibrated such that a certain width of the slit lets through a known amount of spectral width. See the appendix for a detailed calibration procedure and calibration curve for the instrument.

2.7 Dark field microscopy

Dark filed microscopy is an extremely useful technique to enhance contrast in samples otherwise not imaged well under bright field conditions. The basic technique involves zeroth order (direct) light being blocked by an opaque stop in the light path inside the condenser instead of letting it pass through and around the sample. This allows oblique rays from every azimuth to hit the sample. The spherically concave top lens of a condenser allows light rays emerging from the surface of the sample to form an inverted hollow light cone. Physically, if there is no specimen present, the field of view will appear dark if the numerical aperture of the condenser is higher than that of the objective (all light rays avoid entering the objective). With a sample in place, and the zeroth order light removed by the stop, the diffracted rays due to the sample morphology form a pattern at the rear focal plane of the objective retains an image formed only from higher order diffraction intensities scattered by the sample. Only light that is scattered at very high angles is collected by the microscope which forms a bright image superimposed on a dark background (Figure 2.7.1). Sometimes if the sample has a smooth surface, it is possible for the indices of refraction to vary significantly from the surrounding

medium, or maintain an index gradient. In these situations, light can be refracted from the sample producing a small angular change in the light direction causing it to couple in to the objective. In consequence, light is also diffracted when incident on the sample producing an arc of light which passes the numerical aperture range in its entirety. In this case, in order to maintain a satisfactory image with the optical resolving power of the objective, a specially designed iris may be used to lower the effective numerical aperture with a high N.A. immersion objective.

The scattering limits are somewhat ill-defined, but a lower limit can be measured (currently 1.8nm Au particles can be detected) for a given set of experimental conditions. Darkfield experiments were carried out primarily with a high-numerical aperture (N.A.) condenser, but can also be done with lower N.A. optics. Alignment works best when the aperture in the low NA condenser in is made in focus since it is considerable larger and easier to see than is the high-NA version When the aperture is in focus, the low NA condenser can be switched out with the high-NA one and alignment should be very close. Slight adjustments of the iris on the 1.35 NA 100x Olympus objective might be necessary.

2.8 Antibunching of silver nanocluster fluorescence

Many different setups were used for anti-bunching experiments however given the short lifetime of the silver nanoclusters, pulsed excitation from the Ti:Sapphire seemed to work most efficiently with two avalanche photodiodes set up in a Hanbury-Brown and Twiss arrangement [23] (Figure 2.8.1). The laser was tuned

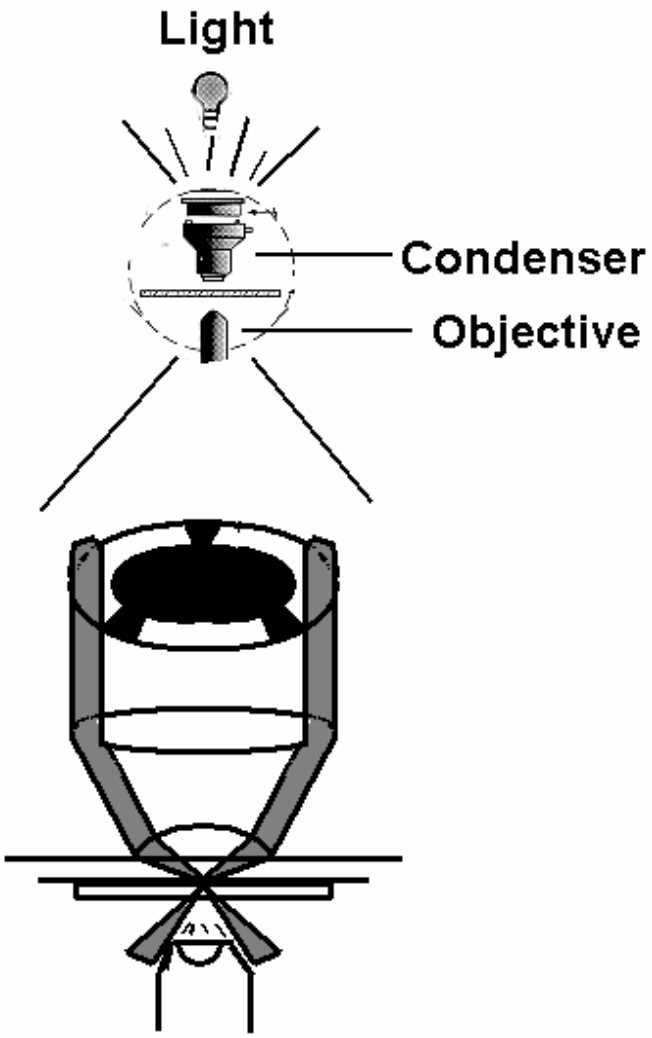

Figure 2.7.1. Schematic of the dark field setup on an inverted microscope with a Halogen light source on a pillar above the microscope. Light is blocked by the opaque stop placed inside the condenser to create a hollow cone of light which does not directly enter the objective lens. Only lights scattered by the sample (drawn as lines above) enters the objective and is seen as a dark field image.

to operate at ~450nm when frequency doubled as to minimize fluorescence from microscope optics. With the tightest focus possible, (minimizing the probability of two molecules being simultaneously excited in the laser focus, and also to generate a non-zero z component at the focus) the fluorescence was clipped with a 590nm emission filter to be certain that no Raman was able to pass. The electronic setup includes a “coincidence” measurement in which the pulses put out by each of the APDs were used as “start” and “stop” triggers, respectively. The histogram of detector coincidences was separated in time by using a computer based time-to – amplitude-converter converter (TAC) and a pulse-height analysis system (Time-Harp 100, Picoquant GMbH). Again as with the fluorescence lifetime setup, care is taken to ensure that the proper zero delay between start and stop detection events is achieved within the observation window. To do this, adjust the delay of the sync signal from one of the detectors with the Ortec as described in section 2.5. The zero delay can also be estimated by splitting a +4V 84MHz pulse from the Datron pulse generator into two identical inverted +2V pulses connected to the board in sync and CFD. Adjusting the delay will give a delta function very close to zero delay. Typically with the TimeHarp, the delay needed is longer than the 74ns allowable with the delay box so additional cable is still needed. Antibunching data can be taken by using a well controlled sample concentration but first should be checked on a system with a lifetime much longer and more well defined than the measurable limit such as CdSe (~4 ns). The data can either be collected as a summation of the photon emission from an ensemble average of many different molecules (employing again the Nanonics scanning stage), or if one stable molecule is in the laser focus, this is

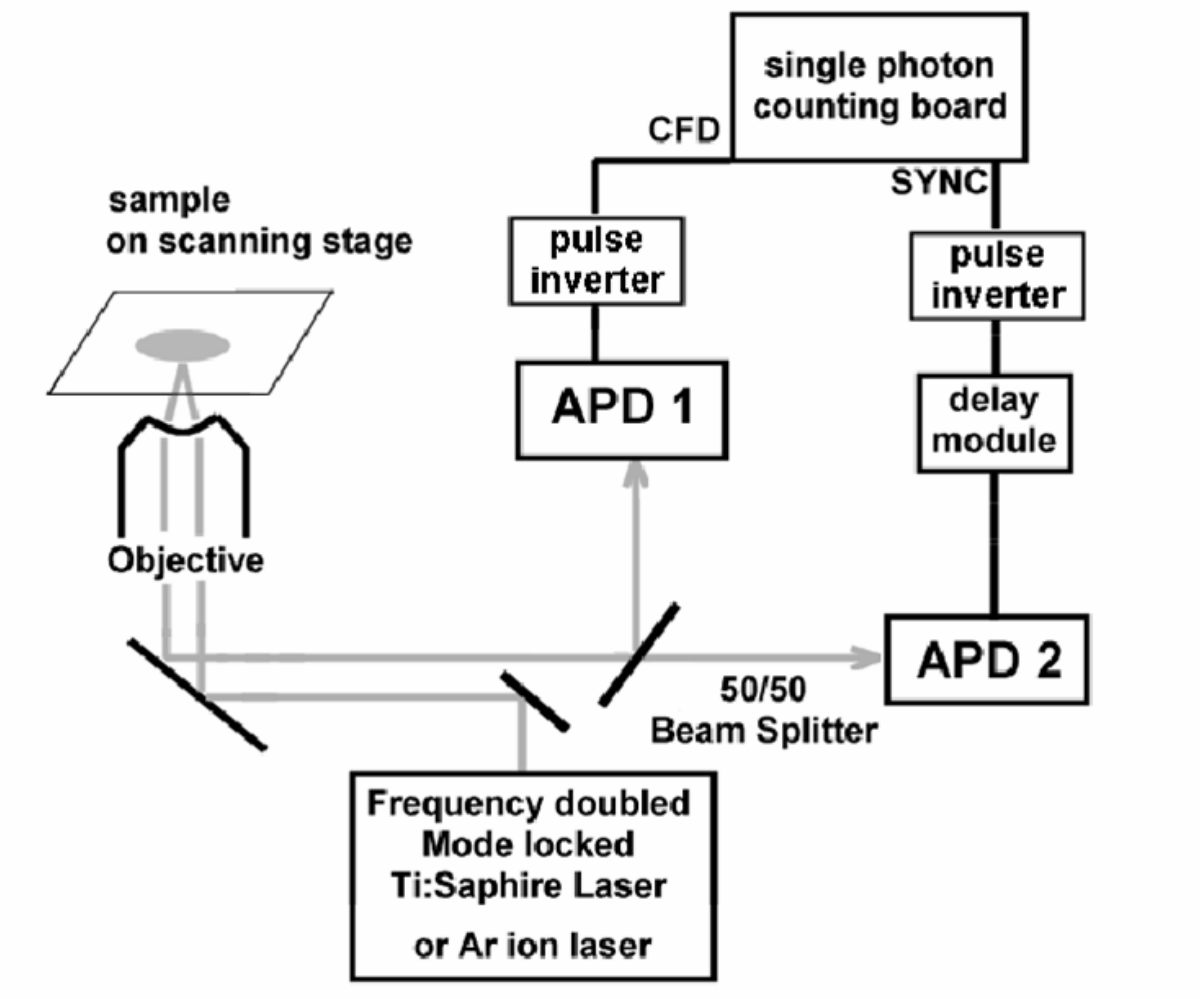

Figure 2.8.1. Hanbury- Brown and Twiss experimental setup for antibunching of silver nanocluster fluorescence. The photon stream from the sample was analyzed in coincidence pair format with two fiber-coupled APD's. The 50/50 beam splitter was mounted on a tri-nocular head of the eyepieces and served as the entrance for light coupling in to the two optical fibers.

also sufficient. The crucial part of the experiment is to make certain the APD's are looking at the same small spot, and also that any background fluorescence is minimized. Alternatively, electroluminescence can be generated at varying frequencies. The point at which the frequencies do not deviate (in period) is also an excellent estimate of zero delay. A very high signal to noise ratio is crucial for this experiment to work, as any discernable background level will foil the experiment. Photoactivation of the samples was often a problem so a dilute, dried sample should be used.

References

(1) Varkey, A.J. and A.F. Fort, *Some Optical-Properties of Silver Peroxide (AgO) and Silver- Oxide (Ag2)) Films Produced By Chemical-Bath Deposition.* Sol. Energy Mater. Sol. Cells 1993. **29**(3): p. 253.

(2) Kocareva, T., I. Grozdanov, and B. Pejova, *Ag and AgO thin film formation in Ag+-Triethanolamine solutions.* 2001. **47**: p. 319.

(3) Xiong, Y., et al., *Preparation and characterization of nanostructured silver thin films deposited by radio frequency magnetron sputtering.* 2000. **375**: p. 300.

(4) Buchel, D., et al., *Sputtered silver oxide layers for surface-enhanced Raman spectroscopy.* Appl. Phys. Lett. 2001. **79**(5): p. 620.

(5) Yip, W.T., et al., *Classifying the photophysical dynamics of single- and multiple- chromophoric molecules by single molecule spectroscopy.* J. Phys. Chem. A 1998. **102**(39): p. 7564.

(6) Vale, R.D., et al., *Direct observation of single kinesin molecules moving along microtubules.* Nature 1996. **380**: p. 451.

(7) Sanchez, E.J., et al., *Room-Temperature Fluorescence Imaging and Spectroscopy of Single Molecules by Two-Photon Excitation.* J. Phys. Chem. A 1997. **101**: p. 7019.

(8) Moerner, W.E., et al., *Optical Probing of Single Molecules of Terrylene in a Shpolskii Matrix - A Two-State Single-Molecule Switch.* J. Phys. Chem. 1994. **98**: p. 7382.

(9) Moerner, W.E. and L. Kador, *Optical detection and spectroscopy of single molecules in a solid.* Phys. Rev. Lett. 1989. **62**: p. 2535.

(10) Moerner, W.E., *A dozen years in single molecule spectroscopy in physics.* J. Phys. Chem B. 2002. **106**: p. 910.

(11) Haab, B.B. and R.A. Mathies, *Single DNA in Capillary Electrophoresis.* Anal. Chem. 1995. **67**: p. 3253.

(12) Ha, T., et al., *Single molecule dynamics studied by polarization modulation.* Phys. Rev. Lett. 1996. **77**: p. 3979.

(13) Ediger, M.D. and J.L. Skinner, *Single molecules rock and roll near the glass transition.* Science 2001. **292**(5515): p. 233.

(14) Bawendi, M., *Three-dimensional orientational measurements of symmetric single chromophores using polarization microscopy.* Nature 1999. **399**: p. 126.

(15) Bartko, A.P. and R.M. Dickson, *Imaging three-dimensional single molecule orientations.* J. Phys. Chem. B 1999. **103**(51): p. 11237.

(16) Bartko, A.P. and R.M. Dickson, *Three-Dimensional Orientations of Polymer-Bound Single Molecules.* J. Phys. Chem. B 1999. **103**: p. 3053.

(17) Zheng, J., et al., *Influence of pH on Dendrimer-pretected nanoparticles.* J. Phys. Chem. B 2002. **106**: p. 1252.

(18) Crooks, R.M., et al., *Dendrimer-encapsulated metal nanoparticles: synthesis, characterization, and applications to catalysis.* Acc. Chem. Res. 2001. **34**: p. 181.

(19) Ottaviani, M.F., *Internal structure of silver-poly(amidoamine) dendrimer complexes and nanocomposites.* Macromolecules 2002. **35**: p. 5105.

(20) Varnavski, O., et al., *Ultrashort time-resolved photoluminescence from novel metal-dendrimer nanocomposites.* J. Chem. Phys 2001. **115**(5): p. 1962.

(21) Zheng, J. and R.M. Dickson, *Individual Water-Soluble Dendrimer-Encapsulated Silver Nanodot Fluorescence.* JACS 2002. **124**(47): p. 13982.

(22) Slocik, J.M., J.T. Moore, and D.W. Wright, *Monoclonal antibody recognition of histidine-rich peptide encapsulated nanoclusters.* Nanolett 2002. **2**(3): p. 169.

(23) Brown, R.H. and R.Q. Twiss, *Correlation between photons in coherent light rays.* Nature 1956. **178**: p. 1447.

CHAPTER 3

INITIAL DISCOVERIES OF ROOM-TEMPERATURE PHOTOACTIVATED SILVER NANOCLUSTERS

Nanoparticle systems have generated great interest over the last few years due to their superb optical properties when properly surface passivated to display increased brightness, extreme photostability, and size tunability of fluorescence [1]. Synthetic enhancement of such semiconductor [2-5] and metallic nanoparticle [6-8] systems has elucidated a much fuller understanding of single nanoparticle photophysics and may find application in electroluminescent devices [9, 10], and biolabeling technology [4, 7, 11].

With respect to biological technology, II-VI and III-V compounds [12] have been the subject of increased research efforts to further explore nanoparticle system utility. Various complexes such metals as cadmium, mercury, and indium pair well with selenium, sulfur, phosphorous, or tellurium to produce a number of excellent photostable semiconductor quantum dots [13-18]. However, their utility is application limited do the inherent metallic toxicity both in health risks and in waste disposal. More environmentally friendly, metallic nanoparticle [6, 7] systems also find application in biolabelling as well as other materials. For example, nanosized gold efficiently scatters specific wavelengths but demonstrates greatly enhanced near-IR [6] and

visible [8] fluorescence relative to bulk metals. This chapter focus on the use of an even stronger visible optical material, silver, which has already demonstrated size-specific fluorescence [19-21].

Originally motivated by efforts to deduce the evolution of bulk structural and electronic properties from the molecular state [22], current nanocrystal research trends now eye the prospect of producing new, generally useful materials with unique physical properties [3]. One such property that remains of great use is the molecular nature of nanoparticles and how they interact with light based on their electronic transition dipoles. The strength of this nanoparticle absorption and emission enables facile observation of single particles [2, 3] with much higher and often more robust signals than those produced by organic dyes [23-25]. Such single-particle observations have furthered understandings of heterogeneity in molecular behavior. [26-28] Complementary to environment-influenced single molecule dynamics, [25, 27] nanoparticles are larger, more complex systems, and their fluorescence often reflects the nanoparticle/surface interactions that affect electron-hole recombination. [2, 3] For example, at room temperature, nanocrystals are often better photoemitters than are bulk systems due to selection rule relaxation more strongly coupling the electron and hole when quantum confined. However, inherent complexity in nanocrystalline ensembles arises due to the loss of spectral information from structural and environmental inhomogeneities [29]. Recently, it has been possible to reduce the inhomogeneous broadening spectral effects by the ability to image and take emission spectra of single nanocrystals [30-36]. This kind of “quantum-dot”

spectroscopy has seen tremendous success for its ability to extrapolate molecular level information from these ensemble systems without spectral broadening [30-36].

While less toxic materials than those mentioned above would be extremely advantageous, nanoparticle utility would also be greatly enhanced if their fluorescence were designed to be “caged” or photoactivated. Such caged fluorescent particles could be rapidly switched on and used, for example, as nanoscopic optical storage elements or as probes in living systems. Although photochromic molecules have been observed as single fluorescent entities [37-39], to date no photoactivated fluorescent nanoparticles have been produced, let alone ones that are observable on a single particle level. Such caged fluorescence should prove easier to observe from small clusters that are photochemically generated from, yet stabilized by a surrounding solid matrix. While many photochemical transformations are known, none yet produce strongly fluorescent photoproducts from initially non-fluorescent nanoparticles.

In photography, photoreactions produce small, surface-bound silver clusters from silver halide crystals, the fluorescence of which has been reported [40], but only at cryogenic temperatures. Although not yet harnessed for applications, strong visible fluorescence has been demonstrated from both neutral and charged small Ag clusters (2 to 8 atoms) in various environments [19-21, 41-43]. Even silver oxide (Ag_2O), which readily produces large surface-enhanced Raman signals resulting from photoinduced silver cluster formation, [44-47] had, to our knowledge, not previously been studied with fluorescence microscopy. Because Ag_2O has a band gap in the visible region (2.25 eV or ~550 nm)[48] and is readily photoreduced to yield metallic Ag

clusters, [44] Ag_2O provides a possible route to producing potentially fluorescent moieties upon visible illumination.

3.1 Characterization of thin silver films

In order to study nanoscale materials with photoactivated fluorescence, solid silver oxide (99.9%, Aldrich Chemical, or formed by combining $AgNO_3$ with KOH in aqueous solution) was ground, suspended in $CHCl_3$, and sonicated to break up larger aggregates. After settling, the supernatant was placed on a coverslip and the chloroform allowed to evaporate. Nanoscale (~80 nm diameter) particles were created in this manner, as determined by dynamic light scattering and atomic force microscopy (AFM) (Figure 3.1.1). Higher densities of much smaller Ag_2O particles (10 to 30 nm as determined from AFM and electron microscopy (Figure 3.1.2) were produced by the rapid oxidation of very thin silver films. The silver films were prepared in darkness by thermally evaporating silver onto glass at a deposition rate of 1 Å/s as described in section 2.1 with final thicknesses of 10.2, 11.5, 16.6, 18.2, 19.8, 30.4, 35.0, and 42.5 nm. On the thin films (<20 nm) used here, the presence of Ag_2O upon exposure to air was confirmed by x-ray photoelectron spectroscopy (XPS); only unoxidized metallic silver was observed on thicker films (Figure 3.1.3). On these films, no Ag_2S was observed for the lifetime of the samples. Although oxide growth on homogeneous silver films is self-passivating, silver films thinner than ~20 nm are not homogeneous, but form islands to minimize overall surface energy; [49] thicker films (>30 nm), however, produce much more homogeneous coverage. Thus, silver island formation is crucial to creating Ag_2O films because

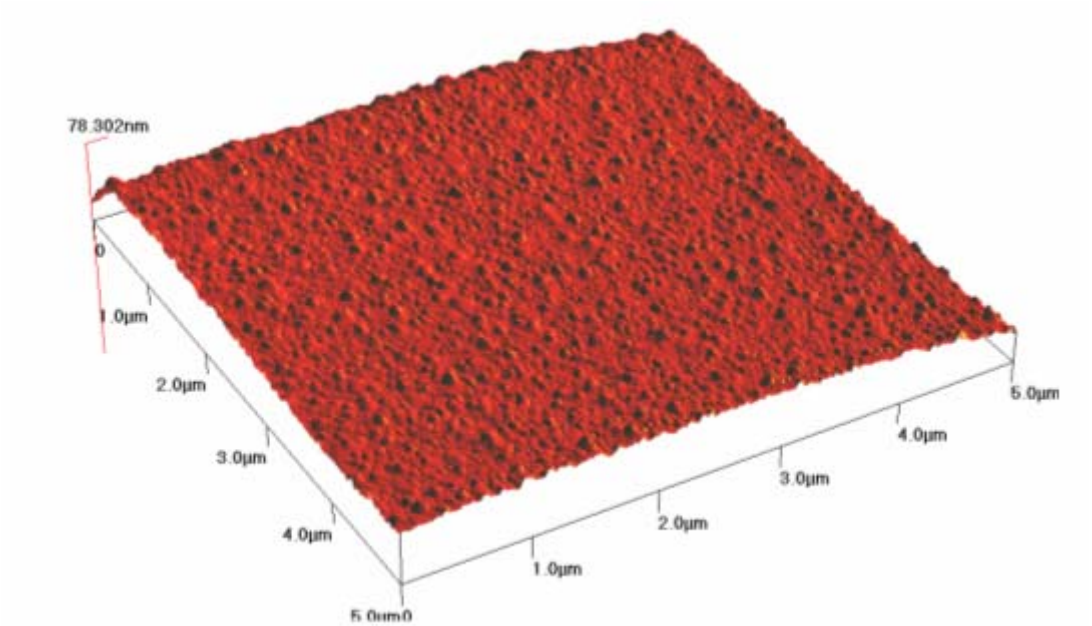

Figure 3.1.1. Atomic Force Microscope (AFM) image of a highly fluorescence 16.6nm silver film evaporated onto a glass coverslip. Features ranging in size from 10-50 nm form to minimize overall surface energy. These are the precursors to the small silver nanoclusters while form on exposure to light and exhibit strong fluorescence.

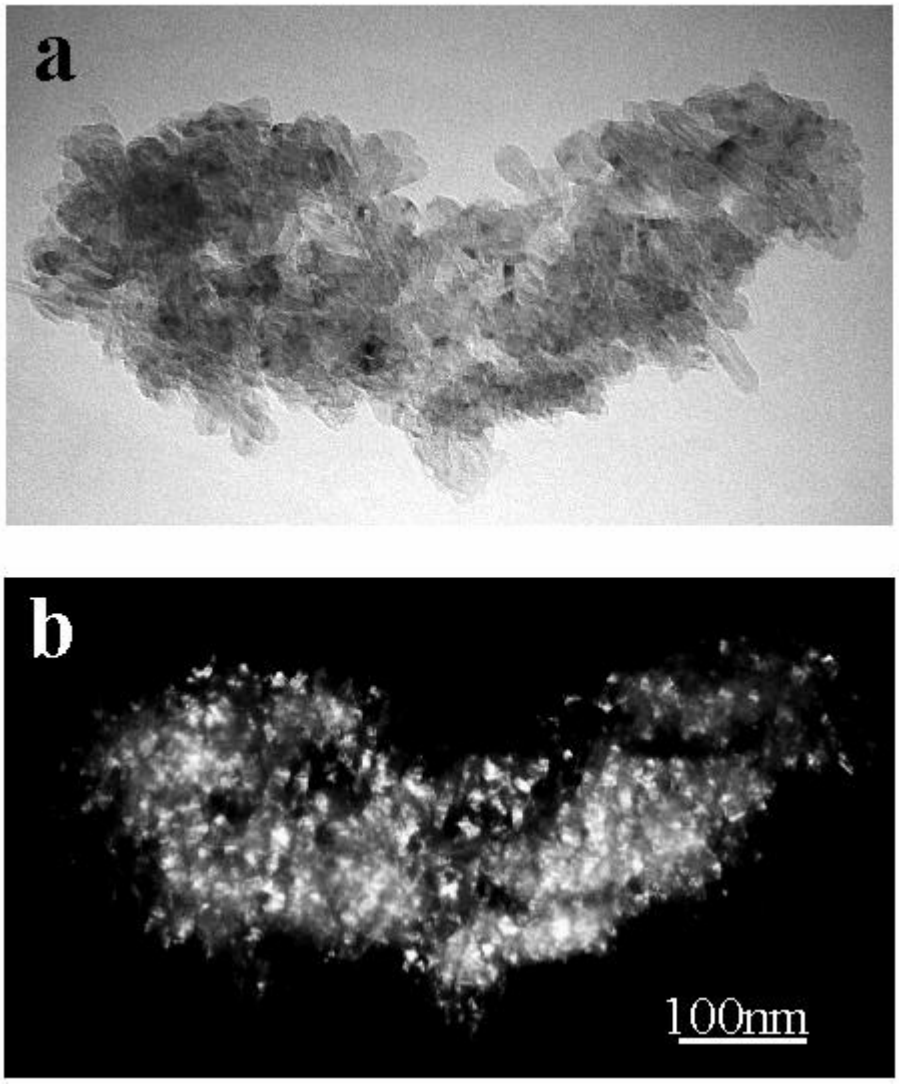

Figure 3.1.2. Electron microscopy images of the same evaporated silver film. The film coating was scraped off in order to place it in the EM grid. A) Bright field image showing slightly better contrast of the ~100nm features. B) Dark field EM image of the same features.

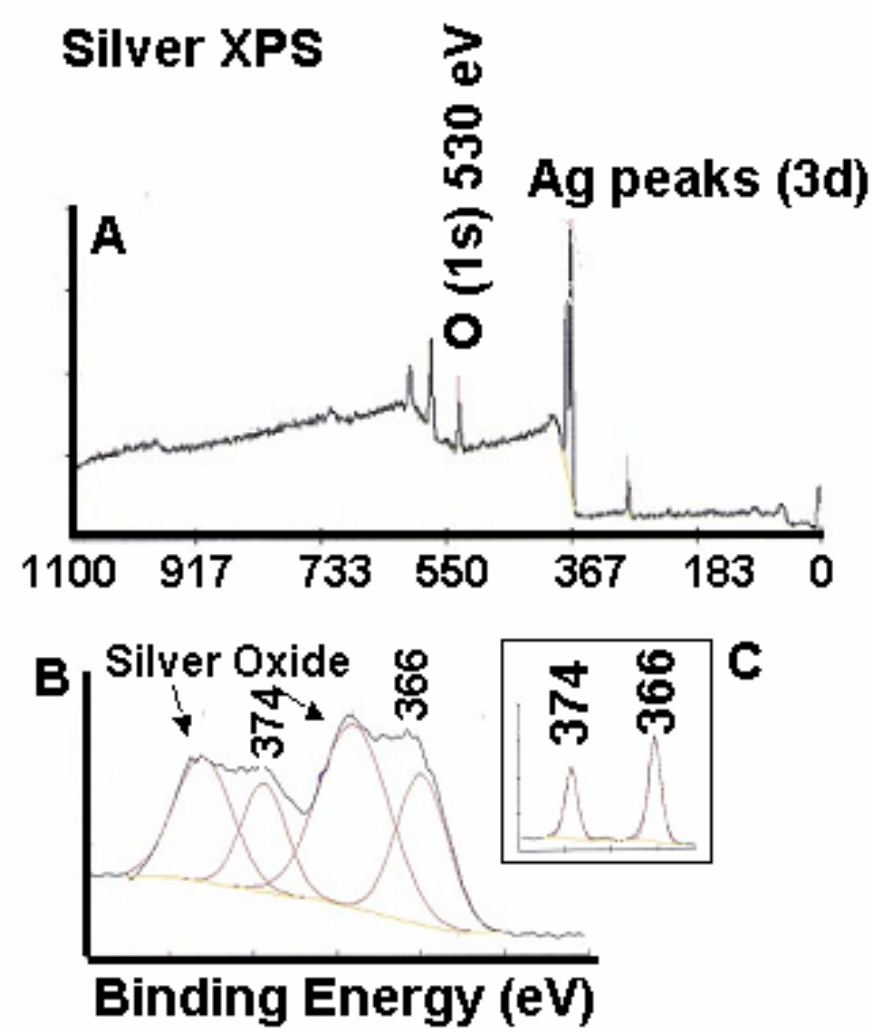

Figure 3.1.3. X-Ray photoelectron spectroscopy of a fluorescent oxidized silver film. A) The entire spectral range showing characteristic peaks of oxygen at 530 eV, silver at 374 eV, and 366 eV, and no sulfur (164 eV). The expanded view of the silver region of the fluorescence film in B clearly shows broadening due to silver oxide. Panel C shows the XPS peaks for a pure silver sample.

Ag_2O quickly overtakes Ag through the reactive, air-exposed, higher energy crystal faces. Both types of Ag_2O samples exhibited similar behavior, but the higher density films with smaller features are emphasized here. Samples were optically excited and observed from both sides of the silver film [28] to ensure that exciting or collecting emission through different thicknesses of silver did not affect the results.

Fluorescence from these dry, light-shielded Ag_2O samples was studied under both bandpass-filtered mercury lamp and argon-ion laser (514.5 nm and 488.0 nm) excitations [28]. In these samples, we observed that Ag_2O is initially non-fluorescent; however, upon illumination with wavelengths shorter than ~520 nm, multicolored fluorescence slowly grows in, one nanoparticle at a time (Figure 3.1.4). Once photoactivated, Ag_2O films exhibit bright, multicolored fluorescence under both blue (450-480 nm) and green (510-550 nm) excitation.

3.2 Single molecule studies

Emission pattern microscopy

With high numerical aperture objectives, direct imaging of single molecule fluorescence emission patterns is possible. For molecules oriented in the z (surface-normal) direction, only x-y polarized light can be collected due to the transverse wave nature of light. Since the dipole emission of oriented molecules is extremely anisotropic, an angle dependent projection is produced onto the x-y plane, and the emitting dipole at the interface

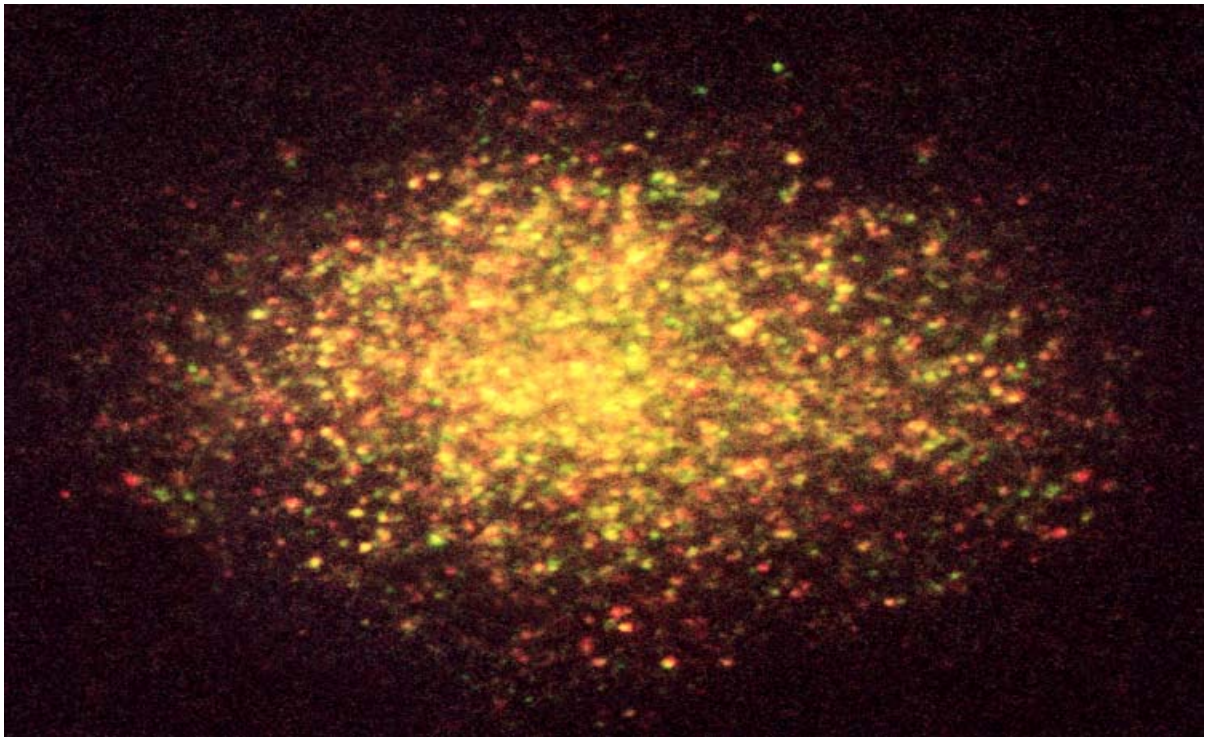

Figure 3.1.4. True-color 35mm film picture of the fluorescence from a 16.6nm Ag/Ag_2O film excited at 514.5nm. Individual nanoclusters grow in one at a time under continuous excitation. Excitation was performed on an Olympus IX-70 inverted microscope using a 1.4 N.A. Plan-Apochromat objective (color corrected, three wavelengths). The photograph was taken with ISO 400 film with a ~10sec exposure. The image is 29.5um wide.

emits over a wide range of angles. This makes each molecule's emission pattern uniquely dependent on its three dimensional orientation. Emission from a molecule aligned along the optic axis will give rise to an annular type emission pattern, while a slight defocus of the objective with respect to the interface (~300nm) to supplement the angle-dependent emission patterns is required to visualize the sine squared distribution of intensity about the dipole axis for molecules oriented within the x-y plane. Such x-y oriented molecules appear with wings perpendicular to the long axis of the central feature of the emission pattern. Visualization of such emission patterns and their changes on the CCD chip allow direct examination of a molecule's response to polarized light. For example, if a linear polarizer is placed in the emission path, and the molecule has linearly polarized emission, the visualized emission pattern will appear in one direction. While if the emission polarizer is rotated 90 degrees, the molecule's emission pattern will correspondingly rotate.

There is a tremendous amount of theory and an entire thesis projects in our lab devoted to the imaging and fitting of orientationally dependent emission patterns from anisotropic sources [50]. The above explanation though cursory, is intended only for the general understanding of an emission pattern, and its significance such that the reader is apt to properly place the information presented. For the purposes of this research, only the emission pattern projection onto a ccd camera is used to ascertain information about the polarization states of the emission, which gives still provides more information about reduced-dimension nanoclusters behaving as single entities. None of these molecules are fit, however, if in time the various sizes

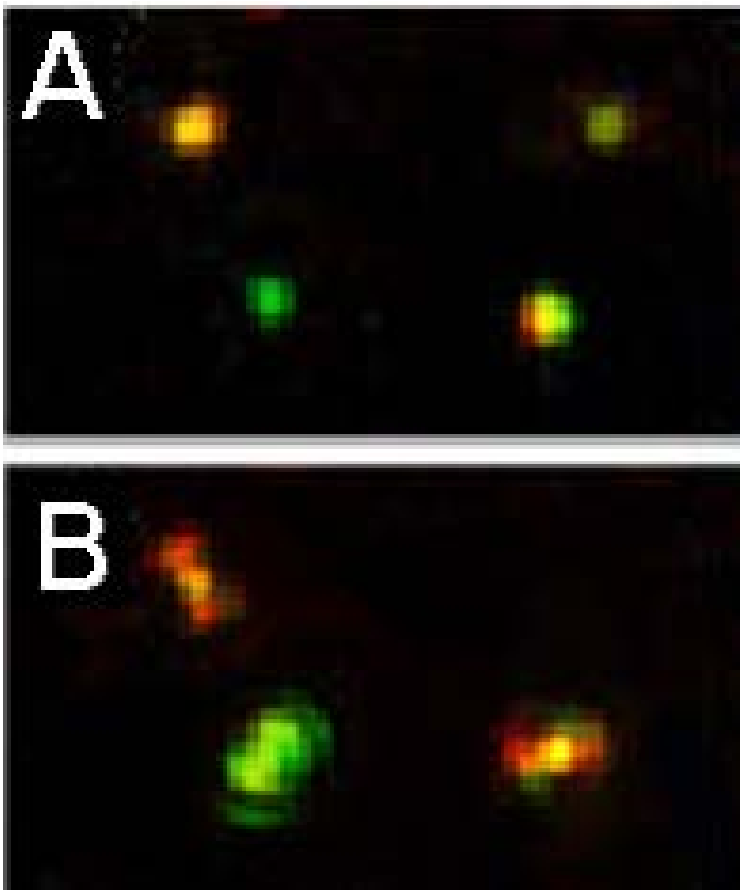

Figure 3.2.1. (A) Fluorescence of four individual features and (B) their emission patterns when excited with a 514.5nm laser. Each feature's unique emission pattern confirms single-nanocluster emission. The nanocluster in the upper right blinked off between photographs. The upper two molecules in (A) are separated by 4.0 microns and (B) is on the same scale. Multiple colors displayed in one emission pattern definitively indicates geometrical change.

were able to be separated, orientationally dependent dynamics as a function of nanocluster size and fluorescent properties would perhaps be very interesting. Although the average Ag_2O particle size is significantly greater than the nanometer scale, emission appears from a myriad of localized sites, each of which exhibited distinctive emission patterns characteristic of single Ag nanoclusters (Figure 3.2.1). [28] In this figure, distinct color changes even in the same emission pattern indicate the dynamic nature of the system. Under continuous excitation, the reflection of such drastic color changes in the emission pattern represents the changing geometry of the particle, even during collection of the data set.

Fluorescence intermittency (blinking)

Indicative of emission from a single quantum system, especially when combined with asymmetric emission patterns, fluorescence intermittency, commonly referred to as “blinking” occurs. Experimentally a nuisance, when properly analyzed, the dynamics of a blinking system can give useful information about the photophysical process occurring.

Once uncaged, very strong multicolored intermittent fluorescence, or "blinking," was clearly observed under continuous blue excitation. Under green excitation, however, even brighter, and significantly more stable (that is, less intermittent) red fluorescence was observed. Typical blinking traces and on-time histograms under blue and green excitation (Figure 3.2.2) not only further demonstrate single particle behavior, [3, 24, 26, 51] but also clearly demonstrate a spectral dependence of the blinking dynamics. Interestingly, an intensity dependence on the

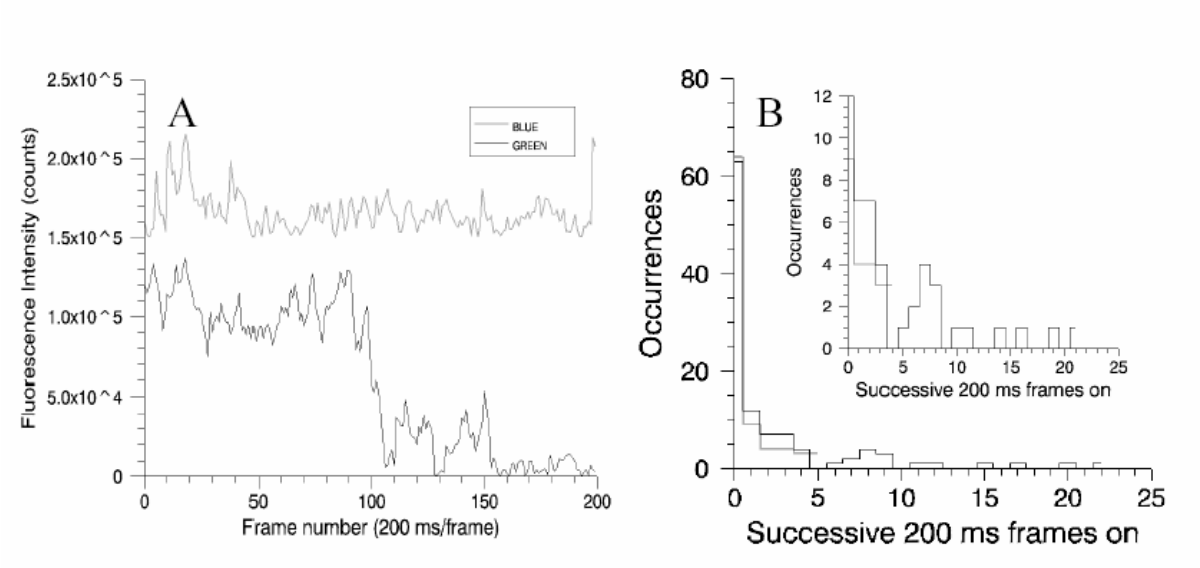

Figure 3.2.2. Wavelength- dependent fluorescence intermittency. (A) Typical single particle blinking traces for blue-excited (450-480nm, offset by 150,000 counts, gray trace) and green-excited (510-550nm) fluorescence acquired for 200 frames with 200ms time resolution (~30 W/cm2). Thresholding 93 such traces at 2.5 times the data set's average intensity for each trajectory yields the on-time histogram (B, on times less than two frames discarded). On times less than three frames were discarded in (B, inset) to emphasize the difference in long on-time behavior between blue and green excited emission. Green excited fluorescence was much more stable.

blinking dynamics also exists. Because all visible emission wavelengths are detected, this probes two different transitions – nanocluster creation and destruction.

Primarily, a silver nanocluster's transition from an "off" or non-emissive state to an emissive state is represented as the formation of a new cluster. However, the representation could also be perceived as the destruction of a created cluster that is too large to emit, and thus, it's parts emit after the photo-induced break up. Alternatively, a silver nanocluster's transition from an emissive state to a non-emissive state could signify that that particular cluster has been broken up, or perhaps that is has grown too large to emit. Though very qualitative in nature, the above explanation may initially be satisfied by an analysis of blinking dynamics of the system. Since we do not have the capability to physically test / monitor the nanocluster breakup on the atomic level in real time, nanocluster fluorescence (or lack thereof) is well served as an initial reporter of nanocluster dynamics since it is a direct probe of the nanocluster itself. Chapter 4 presents a more detailed study of the mechanism of nanocluster photoproduction.

Many such blinking traces were collected and their time trajectories analyzed to probe the creation and breakup of clusters under green excitation wavelengths. Performed with 514.5 nm excitation at intensities of 292 W/cm^2 (high) and 68 W/cm^2 (low), 150 individual molecule fluorescence intensity trajectory traces were collected for each excitation intensity. The resulting data sets were analyzed using a common threshold, defined as the square root of the maximum value plus twice the standard deviation of each single molecule trajectory to ensure that background and signal-to-noise levels are properly accounted for. Fluorescence intensities above this

threshold for each trace were deemed “on” events, while values below this level were identified as being “off”. The histograms of on and off times were each fit to a four parameter double exponential (Table 3.2.1) in which the “on” and “off” times for the fast initial decay, and long exponential tail behavior were compared between low and high intensities. In all cases examined, the exponential decays corresponding to initial decay and longer time behavior increased from low intensity to high. With respect to “on” times, this indicates that nanoclusters are being destroyed faster at higher intensities, analogously, the “off” times represent more efficient creation of nanoclusters at high intensity. The off time intensity dependence shows that while inefficient, high intensity green excitation is still able to photochemically write fluorescent Ag_n nanoclusters. The combination of efficient creation and breakup indicates that a dynamic equilibrium is being created as a function of the amount of energy put in to the system.

The clear asymmetries of single-particle emission patterns coupled with observed blinking dynamics non-destructively indicate single-particle behavior. This photoactivated emission represents a new type of nanoparticle behavior that is readily observable on a single particle level, even with weak mercury lamp excitation.

3.3 Optical properties

The necessity of Ag_2O formation for caged fluorescence is confirmed by the observation that thick (>30 nm) silver films showed no emission, even after strong illumination with blue light, whereas thin films were highly fluorescent after

Table 3.2.1. Fit parameters to the double exponential equation. Parameters *a* and *c* relate to the overall magnitude of the decay at short and long times. Parameters *b* and *d* increase from low intensity to high intensity for both on and off times indicating the efficiency of nanocluster creation / destruction.

$y=ae^{-bx}+ce^{-dx}$					
Intensity at 514.5 nm	State	a	b	c	d
68 W/cm^2	ON	3600.74	1.69	160.21	0.25
292 W/cm^2	ON	4573.11	1.96	193.65	0.32
68 W/cm^2	OFF	705.62	0.91	48.75	0.06
292 W/cm^2	OFF	621.44	1.07	52.65	0.09

photoactivation. Only films that are too thin to support a homogeneous Ag layer exhibit fluorescence, so island formation must occur such that oxide growth is not self-passivating. Thus, the emissive moiety is photochemically generated from the surrounding semiconductors, to produce a Ag - Ag_2O chromophore with an extremely high absorption cross-section, σ. Through these saturation intensity measurements (I_{sat} ~ 200 W/cm^2 at 514.5 nm) (Figure 3.3.1) and comparison to known single molecules (1,1´-dioctadecyl-3,3´,3-3'-tetramethylindocarbocyanine perchlorate ($DiIC_{18}(3)$): I_{sat} ~ 10,000 W/cm^2)[23], the absorption cross-section of our nanoparticles has been determined to be ~8 x 10^{-15} cm^2, a factor of ~50x stronger than the best organic dye molecules (e.g. $DiIC_{18}(3)$: σ ~ 1.6 x 10^{-16} cm^2).[23] In all cases, the highest density of emissive sites was observed on obviously oxidized samples. The additional observation of multicolored single-particle emission patterns [28] shows that individual particles can drastically change emission frequencies and that this change cannot result from several particles emitting from the same diffraction-limited volume.

Once a metallic impurity is formed, it becomes easier to continue the photoreduction process, creating Ag_2^+, Ag_2, Ag_3^+…, but this is balanced by the relative instability of AgO and the binding energy of each cluster relative to the excitation energy. [20, 41] This photochemical process enables small silver clusters to form from Ag_2O crystals (and subsequently from AgO) similar to those harnessed in silver halide-based photographic emulsions. Such small Ag clusters are known to produce strong visible fluorescence, [19-21, 41-43] and should exhibit emission wavelength

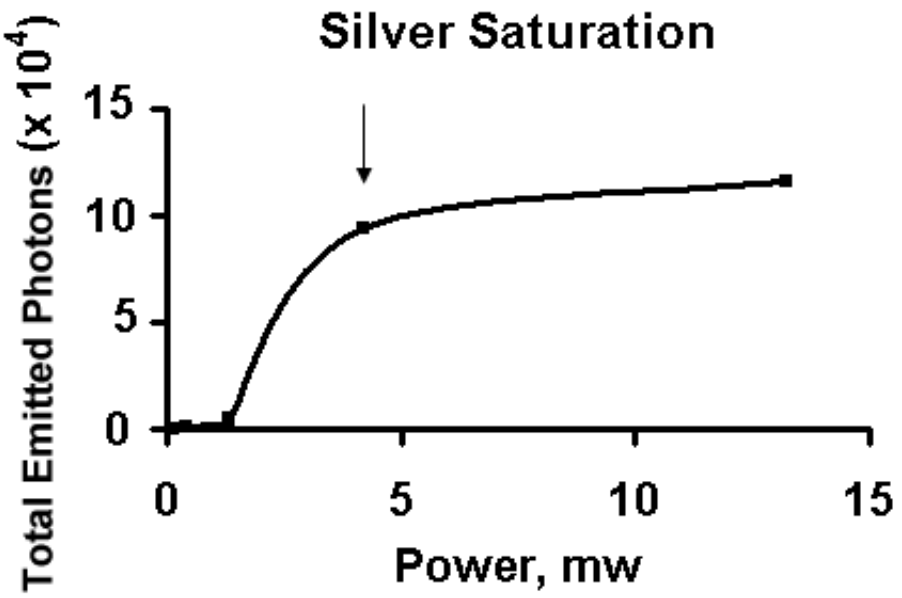

Figure 3.3.1. Measured saturation curve from an evaporated thin silver film. The arrow indicates the point used in calculation of the saturation point, or the point where the system is being excited much faster than it's radiative lifetime allows and with much more intensity. It is this point where a tremendous amount of photons are incident on the sample such that it's emission no longer increases linearly with intensity. Instead, the system "saturates" and emits a more or less constant amount. Exposure times were 100ms taken every 10 seconds at different excitation powers.

changes as they change geometry [52, 53] and size in the range from 2 to 4 atoms [19, 20, 40]. Because the Ag cluster size and charge are constantly being modified under constant illumination and chemical reaction, it is not surprising that the emission color of individual emissive sites changes.

Although Ag_2O must absorb the incident radiation, the photoactivation indicates photochemical change to produce Ag atoms and silver (II) oxide (AgO, best described as a combination of silver(I) and (III)), [44] the latter of which is unstable at room temperature relative to Ag_2O [54] and is readily photoreduced to form Ag^0 and 1/2 O_2. [55] Thus, we also prepared AgO samples similar to those for Ag_2O. Such samples of AgO (Aldrich Chemical) initially exhibited only very weak yellow fluorescence, but are also quickly photoactivated to yield the diverse colors observed from both Ag_2O and oxidized silver films. Because Ag_2O photochemically produces AgO, and both oxides not only yielded Ag clusters upon irradiation but also produced photoactivated multicolored fluorescence, the more stable Ag_2O must be the caged species yielding the observed fluorescence.

The wavelength-dependent photoactivation, blinking, and spectral diffusion of blue-excited Ag_n fluorescence, both on films and of supported nanocrystals, clearly indicate that the Ag_2O must absorb and form small neutral and cationic clusters of Ag metal and AgO, with subsequent fluorescence from the Ag clusters. Thus, while the Ag-clusters fluoresce under both blue and green illumination, the strong absorption cross-section indicates that the surrounding Ag_2O likely acts as a cage, similar to that of a rare-gas matrix [56] and in later work, to that of a dendrimer host [57]. However, because the blinking and spectral diffusion under green excitation are

greatly reduced, the Ag clusters must be directly excited by longer wavelengths. This wavelength dependence matches extremely well with the known band gap for Ag_2O [48] and the known green absorption and red emission lines of Ag clusters [19-21, 41-43]. The enhanced stability of the photoactivated red fluorescence excited by green light enables data to be written with blue light and nondestructively read with green, even on a single-particle level. Although the Ag_2O particles are 10 to 30 nm in size, the emissive site must consist of small Ag clusters either within or on the surface of the Ag_2O crystals. Thus, the Ag_2O serves as the photoactivatable material and Ag_2O simultaneously provides a protective overcoating that stabilizes the uncaged Ag-cluster fluorescence.

3.4 Read / write capabilities and current information storage methods

As the technological world continues to require better tools to communicate more data at higher rates, so does it require the ability to store larger amounts of information, preferably in the same amount of space. When compact discs (CD's) were first introduced in the 1980's, the concept of data storage was revolutionized. However, now following the trends of magnetic media, capacity requirements have again far exceeded what is available on CD. Even with the more recent introduction of digital versatile/video discs, we as a society continue to reach upper limits to the amount of storage we can obtain from these materials without changing the size of the system in which the media is compatible.

However, designing a new material which must compete with the high density storage capabilities of magnetic media, or the cost-effectiveness of serial methods is

challenging. Limited by both binary information, and the diffraction of electromagnetic waves, current single-layer read-only-memory (ROM) and write-once/read many (WORM) applications can only extend so far before an ultimate media size limitation is reached. Even WORM applications represent a significant advance in the technology by employing the use of phase-change materials which allow the storage of up to 5 gigabytes on one disc versus the traditional ~650MB on a compact disc[58, 59]. Techniques have been attempted to revolutionize the actual physical recording medium density by the introduction and modification of certain photopolymers, the introduction of a very high numerical aperture objective, the use of an NSOM tip, and even heat mode recording used in some optical materials where a thermal change in the material fosters readability [58, 60]. Fundamentally, material changes remain challenged by the (lack of) ability to reduce the bit data resolution distance for recording and reading to less than one-half of the laser beam wavelength. Current efforts to increase the storage density of optical devices are subsequently geared toward the design and development of very short wavelength, compact lasers that emit light in the blue or green region [61-63]. While frequency doubling of such light may offer temporary advances by effectively reducing the beam spot size by two (and increasing storage density by 4), to achieve even 100 times greater storage capacity over currently available technology, the output frequencies of these lasers would have to be ~10 times shorter than those on the market today.

In order to circumvent the above mentioned problematic issues to better push the envelope of optical storage, the use and combination of near-field recording

optics and methods [64-69] with photochromic materials [70-77] have been proposed as the next-generation of optical storage. The photoproduction of silver has also been used in a number of near-field storage applications [77, 78]. This particular optical storage scheme and many others of a similar nature utilize photoinduced nanoparticle formation and its' near field plasmon scattering to write data. Taking advantage of and harnessing the spectrally diverse emissive species that arise from nanocluster excitation, our nanocluster read/write system [76, 79] can create efficient storage in two dimensions at room temperature by using far-field stabilized fluorescence as the data-storing mechanism.

Because each of our silver individual particle is photoactivated, data are readily stored in and nondestructively read from these high-density nanoparticle films. Blue mercury lamp illumination enabled images of a field aperture to be written on the Ag_2O films. Two adjacent images were successively written on the same film, each with a 10-min exposure at an intensity of ~30 W/cm^2 (Figure 3.4.1). Although some emissive centers do seem to emit yellow light, images primarily grow in as individual red and green emissive sites. The final high-density images, however, exhibit only bits of red and green colors, which indicate that the yellow images result from color mixing of the dynamic red and green emission observed under blue excitation. Because blue light continues to write information, reading data with blue excitation will degrade data integrity. As these emissive features also absorb green light with concomitant stable red emission, these same features can be nondestructively read by green illumination, even up to many hours after being written without significant image degradation. Reading data with green excitation

very slowly bleaches the written image, without significantly increasing the background. Blue excitation, however, maintains nearly constant intensity in the written image due to the equilibrium resulting from photoactivation and bleaching, but the background intensity markedly increases.

As commercially pleasing as the technology may be, there are some technical risks that must be considered when considering the use of single molecules as optical storage entities. First, although single molecules are good candidates for reduced dimension storage because of their size, the problem of the diffraction limit (ability to focus light to a specific tightness) still exists. The problem can be circumvented by using a smaller laser spot as mentioned above, or designing the materials such that a larger amount of information can fit in the same space. Since the small nanoclusters manifest changes in color due to their changing geometry under continuous excitation, they possess the potential to store more information in each data point, a clear advantage over standard binary storage that is limited to one bit of information per data point.

This new class of nanoparticle behavior offers the potential to photochemically control fluorescent spectral features on both the single nanoparticle and bulk levels – a previously unattainable result. With the fundamental understanding obtained from the single molecule level experiments, bulk photoactivation properties can be linked such that emission may be better photochemically controlled.

On the other hand, while the bulk 2-D storage potential may be useful from a materials perspective, the chemical interactions on the molecular level possess

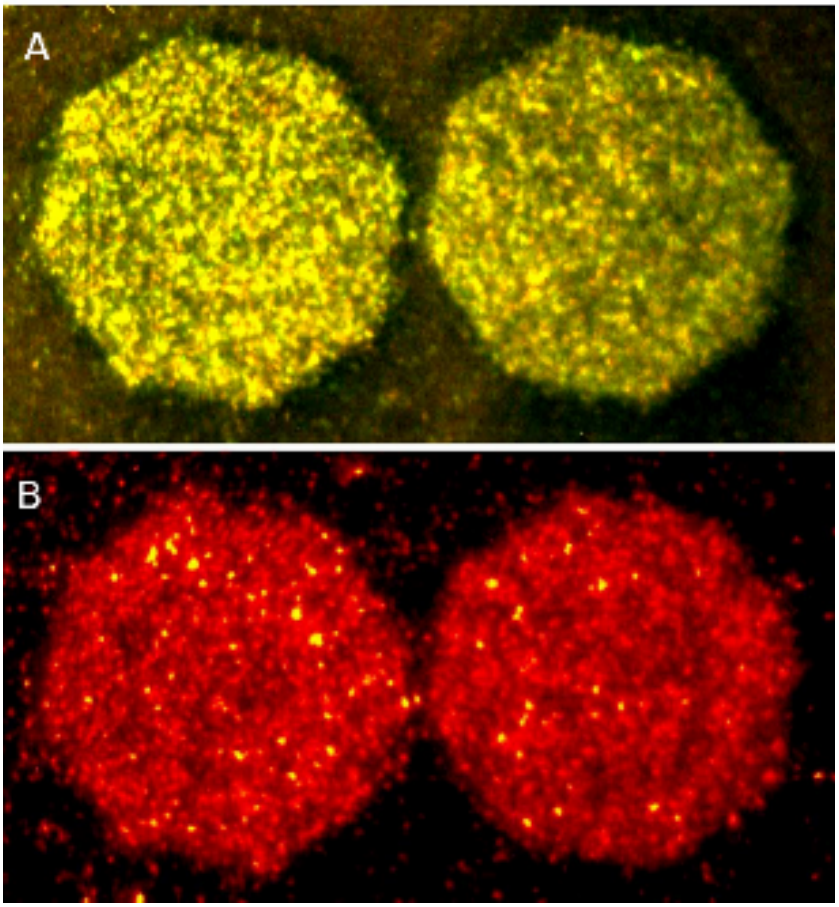

Figure 3.4.1. (A) Photograph (35mm, ISO 400 speed, ~10s exposure) of adjacent images of a field aperture successively written to a Ag film with blue Hg lamp excitation. (B) Red fluorescence from the same area in (A), instead illuminated with green excitation such that non-destructive probing of the images written in (A) is achieved. Opposite vertices of each aperture are 35 microns apart.

many more fundamentally challenging questions. Understanding a system at its lowest level opens up many more basic relationship questions such as cluster fluorescence spectroscopy and later, the potential relationship to SERS enhancement mechanisms. With the common ability to ascertain cluster fluorescence and geometric rearrangement dynamics on both single particle and bulk levels, the mysterious atom-bulk transition of these materials may be more easily probed.

3.5 Conclusions

Fluorescence microscopy of nanoscale Ag_2O revealed strong photoactivated emission for excitation wavelengths shorter than 520 nm. While blinking and characteristic emission patterns demonstrated single nanoparticle observation, large-scale dynamic color changes were also observed, even from the same nanoparticle. Identical behavior was observed in oxidized thin silver films that enabled Ag_2O particles to grow at high density from silver islands. Data were readily written to these films with blue excitation; stored data could be non-destructively read with the strong red fluorescence resulting from green $\lambda > 520$ nm) excitation indicating the potential for a novel silver-oxide data storage system with fluorescent readout. These properties arise solely from the individual luminescent species believed to be silver nanoclusters that are photochemically generated from the oxide.

References

(1) Gao, M.Y., et al., *Strongly photoluminescent CdTe nanocrystals by proper surface modification.* J. Phys. Chem. B 1998. **102**: p. 8360.

(2) Empedocles, S. and M. Bawendi, *Spectroscopy of Single CdSe Nanocrystallites.* Acc. Chem. Res. 1999. **32**: p. 389.

(3) Nirmal, M. and L. Brus, *Luminescence Photophysics in Semiconductor Nanocrystals.* Acc. Chem. Res. 1999. **32**: p. 407.

(4) Bruchez, M., et al., *Semiconductor nanocrystals as fluorescent biological labels.* Science 1998. **281**(5385): p. 2013.

(5) Xie, X.S. and H.P. Lu, *Single-molecule enzymology.* J. Biol. Chem. 1999. **274**(23): p. 15967.

(6) Bigioni, T.P., R.L. Whetten, and O. Dag, *Near-infrared luminescence from small gold nanocrystals.* J. Phys. Chem. B 2000. **104**(30): p. 6983.

(7) Schultz, S., et al., *Single-target molecule detection with nonbleaching multicolor optical immunolabels.* Proc. Natl. Acad. Sci. U. S. A. 2000. **97**(3): p. 996.

(8) Wilcoxon, J.P., et al., *Photoluminescence from nanosize gold clusters.* J. Chem. Phys. 1998. **108**: p. 9137.

(9) Rodriguez-Viejo, J., et al., *Evidence of photo- and electrodarkening of (CdSe)ZnS quantum dot composites.* J. Appl. Phys. 2000. **87**(12): p. 8526.

(10) Mattoussi, H., et al., *Electroluminescence from heterostructures of poly(phenylene vinylene) and inorganic CdSe nanocrystals.* J. Appl. Phys. 1998. **83**(12): p. 7965.

(11) Chan, W.C.W. and S.M. Nie, *Quantum dot bioconjugates for ultrasensitive nonisotopic detection.* Science 1998. **281**(5385): p. 2016.

(12) Peng, X.G., J. Wickham, and A.P. Alivisatos, *Kinetics of II-VI and III-V colloidal semiconductor nanocrystal growth: "Focusing" of size distributions.* J. Am. Chem. Soc. 1998. **120**(21): p. 5343.

(13) Alivisatos, A.P., et al., *From molecules to materials: Current trends and future directions.* Adv. Mater. 1998. **10**(16): p. 1297.

(14) Banin, U., et al., *Quantum confinement and ultrafast dephasing dynamics in InP nanocrystals.* Phys. Rev. B-Condens Matter 1997. **55**(11): p. 7059.

(15) Bawendi, M.G., et al., *Luminescence Properties of Cdse Quantum Crystallites - Resonance Between Interior and Surface Localized States.* J. Chem. Phys. 1992. **96**(2): p. 946.

(16) Chen, C.C., et al., *Size dependence of structural metastability in semiconductor nanocrystals.* Science 1997. **276**(5311): p. 398.

(17) Klein, D.L., et al., *A single-electron transistor made from a cadmium selenide nanocrystal.* Nature 1997. **389**(6652): p. 699.

(18) Schlamp, M.C., X.G. Peng, and A.P. Alivisatos, *Improved efficiencies in light emitting diodes made with CdSe(CdS) core/shell type nanocrystals and a semiconducting polymer.* J. Appl. Phys. 1997. **82**(11): p. 5837.

(19) Harbich, W., et al., *Deposition of mass selected silver clusters in rare gas matrices.* J. Chem. Phys. 1990. **93**: p. 8535.

(20) Rabin, I., W. Schulze, and G. Ertl, *Light emission during the agglomeration of silver clusters in noble gas matrices.* J. Chem. Phys. 1998. **108**(12): p. 5137.

(21) Tani, T. and M. Murofushi, *Silver Microclusters on Silver Halide Grains as Latent Image and Reduction Sensitization Centers.* J. Imag. Sci. Technol. 1994. **98**: p. 1.

(22) Rossetti, R., S. Nakahara, and L.E. Brus, *Quantum size effects in the redox potentials, resonance Raman spectra, and electronic spectra of CdS crystallites in aqueous solution.* J. Chem. Phys. 1982. **79**: p. 1086.

(23) Macklin, J.J., et al., *Imaging and time-resolved spectroscopy of single molecules at an interface.* Science 1996. **272**(5259): p. 255.

(24) VandenBout, D.A., et al., *Discrete intensity jumps and intramolecular electronic energy transfer in the spectroscopy of single conjugated polymer molecules.* Science 1997. **277**(5329): p. 1074.

(25) Moerner, W.E. and M. Orrit, *Illuminating single molecules in condensed matter.* Science 1999. **283**(5408): p. 1670.

(26) Dickson, R.M., et al., *Blinking and switching behavior of individual green fluorescent protein molecules.* Nature 1997. **388**: p. 355.

(27) Xie, X.S., *Single-Molecule Spectroscopy and Dynamics at Room Temperature.* Acc. Chem. Res. 1996. **29**(12): p. 598.

(28) Bartko, A.P. and R.M. Dickson, *Imaging three-dimensional single molecule orientations.* J. Phys. Chem. B 1999. **103**(51): p. 11237.

(29) Alivisatos, A.P.e.a., *Electronic states of semiconductor clusters: homogeneous and inhomogeneous broadening of the optical spectrum.* J. Chem. Phys. 1988. **89**(7): p. 4001.

(30) Empedocles, S.A. and M.G. Bawendi, *Influence of spectral diffusion on the line shapes of single CdSe nanocrystallite quantum dots.* J. Phys. Chem. B 1999. **103**(11): p. 1826.

(31) Empedocles, S.A. and M.G. Bawendi, *Quantum-confined stark effect in single CdSe nanocrystallite quantum dots.* Science 1997. **278**(5346): p. 2114.

(32) Empedocles, S.A., D.J. Norris, and M.G. Bawendi, *Photoluminescence spectroscopy of single CdSe nanocrystallite quantum dots.* Phys. Rev. Lett. 1996. **77**(18): p. 3873.

(33) Tittel, J., et al., *Fluorescence spectroscopy on single CdS nanocrystals.* J. Phys. Chem. B. 1997. **101**(16): p. 3013.

(34) Nirmal, M., et al., *Fluorescence intermittency in single cadmium selenide nanocrystals.* Nature 1996. **383**(6603): p. 802.

(35) Blanton, S.A., M.A. Hines, and P. Guyot-Sionnest, *Photoluminescence wandering in single CdSe nanocrystals.* Appl. Phys. Lett. 1996. **69**(25): p. 3905.

(36) Blanton, S.A.e.a., *Photoluminescence of single semiconductor nanocrystallites by two-photon excitation microscopy.* Chem. Phys. Lett. 1994. **229**: p. 317.

(37) Moerner, W.E., et al., *Optical Probing of Single Molecules of Terrylene in a Shpolskii Matrix - A Two-State Single-Molecule Switch.* J. Phys. Chem. 1994. **98**: p. 7382.

(38) Moerner, W.E., R.M. Dickson, and D.J. Norris, *Single-molecule spectroscopy and quantum optics in solids*, in *Advances in Atomic, Molecular, and Optical Physics*. 1998. p. 193.

(39) Dickson, R.M., et al., *On/off blinking and switching behaviour of single molecules of green fluorescent protein.* Nature 1997. **388**(6640): p. 355.

(40) Marchetti, A.P., et al., *Formation and spectroscopic manifestation of silver clusters on silver bromide surfaces.* J. Phys. Chem. B 1998. **102**(27): p. 5287.

(41) Konig, L., et al., *Chemiluminescence in the agglomeration of metal clusters.* Science 1996. **274**(5291): p. 1353.

(42) Fedrigo, S., W. Harbich, and J. Buttet, *Optical-Response of Ag2, Ag3, Au2, and Au3 in Argon Matrices.* J. Chem. Phys. 1993. **99**(8): p. 5712.

(43) Felix, C., et al., *Fluorescence and excitation spectra of Ag-4 in an argon matrix.* Chem. Phys. Lett. 1999. **313**(1-2): p. 105.

(44) Kotz, R. and E. Yeager, *Raman studies of the silver/silver oxide electrode.* J. Electroanal. Chem. 1980. **111**: p. 105.

(45) Brandt, E.S., *Selective Enhanced Raman Scattering from an Oxacarbocyanine Dye and 1-Phenyl-5-Mercaptotetrazole Adsorbed to Silver and Silver Halide Surfaces in Photographic Films.* Appl. Spectrosc. 1993. **47**: p. 85.

(46) Wang, X.Q., et al., *Enhancement mechanism of SERS from cyanine dyes adsorbed on Ag2O colloids.* Spectrochim. Acta A 1997. **53**: p. 2495.

(47) Watanabe, T., et al., *Evidence for surface Ag+ complexes as the SERS-active sites on Ag electrodes.* Chem. Phys. Lett. 1983. **102**: p. 565.

(48) Varkey, A.J. and A.F. Fort, *Some Optical-Properties of Silver Peroxide (AgO) and Silver- Oxide (Ag2)) Films Produced By Chemical-Bath Deposition.* Sol. Energy Mater. Sol. Cells 1993. **29**(3): p. 253.

(49) Yamaguchi, T., S. Yoshida, and A. Kinbara, *Effect of Retarded dipole-dipole interactions between island particles on the optical plasma-resonance absorption of a silver-island film.* J. Opt. Soc. Amer. 1974. **64**: p. 1563.

(50) Bartko, A.P., *Deciphering spatially heterogeneous polymer dynamics using single molecule microscopy.* Thesis 2002.

(51) Lu, H.P., L.Y. Xun, and X.S. Xie, *Single-molecule enzymatic dynamics.* Science 1998. **282**(5395): p. 1877.

(52) Bechthold, P.S., et al., *Guest-Host Interaction and Photochemical Transformation of Silver Particles Isolated in Rare Gas Matrices.* Z. Phys. D - Atoms, Molec. Clust. 1986. **3**: p. 263.

(53) Rabin, I., et al., *Absorption and fluorescence spectra of Ar-matrix-isolated Ag-3 clusters.* Chem. Phys. Lett. 2000. **320**(1-2): p. 59.

(54) Libardi, H. and H.P. Grieneisen, *Guided-mode resonance absorption in partly oxidized thin silver films.* Thin Solid Films 1998. **333**: p. 82.

(55) Ohtani, B., et al., *Photoactivation of silver loaded on titanium(IV) oxide for room-temperature decomposition of ozone.* J. Photochem. Photobiol. A 1993. **71**: p. 195.

(56) Rabin, I., W. Schulze, and G. Ertl, *Absorption spectra of small silver clusters Ag-n (n >= 3).* Chem. Phys. Lett. 1999. **312**(5-6): p. 394.

(57) Zheng, J. and R.M. Dickson, *Individual Water-Soluble Dendrimer-Encapsulated Silver Nanodot Fluorescence.* JACS 2002. **124**(47): p. 13982.

(58) Mansuripur, M. and G. Sincerbox, *Principles and techniques of optical data storage.* Proc. IEEE. 1997. **85**(11): p. 1780.

(59) Ashley, J., et al., *Holographic data storage.* IBM J. Res. Develop. 2000. **44**: p. 341.

(60) Kawata, S. and Y. Kawata, *Three-dimensional optical data storage using photochromic materials.* Chem. Rev. 2000. **100**: p. 1777.

(61) Haase, M.A., et al., *Blue-green laser diodes.* Appl. Phys. Lett. 1991. **59**: p. 1272.

(62) Nakamura, S., T. Mukai, and M. Senoh, *Candela-class high-brightness InGaN/AlGaN double-heterostructure blue-light-emitting diodes.* Appl. Phys. Lett. 1994. **64**: p. 1687.

(63) Nakamura, S., et al., *High-brightness InGaN blue, green and yellow light-emitting-diodes with quantum well structures.* Jap. J. Appl. Phys. 1995. **34**(7A): p. L797.

(64) Betzig, E., et al., *Near-field scanning optical microscopy (NSOM) - development and biophysical applications.* Biophys. J. 1986. **49**: p. 269.

(65) Betzig, E., et al., *Near-field magneto optics and high-density data storage.* Appl. Phys. Lett. 1992. **61**: p. 142.

(66) Martin, Y., S. Rishton, and H.K. Wickramashinghe, Appl. Phys. Lett. 1997. **71**: p. 1.

(67) Pohl, D.W., W. Denk, and M. Lanz, *Optical stethoscopy: image recording with resolution lambda/20.* Appl. Phys. Lett. 1984. **44**: p. 651.

(68) Tsujioka, T. and M. Irie, *Fluorescence readout of near-field photochromic memory.* Appl. Opt. 1998. **37**: p. 4419.

(69) Tominaga, J., et al., *The characteristics and the potential of super resolution near- field structure.* Jpn. J. Appl. Phys. Part 1 - Regul. Pap. Short Notes Rev. Pap. 2000. **39**(2B): p. 957.

(70) Toriumi, A., S. Kawata, and M. Gu, *Reflection confocal microscope readout system for three-dimensional photochromic optical data storage.* Opt. Lett. 1998. **23**: p. 1924.

(71) Ohko, Y., et al., *Multicolor photochromism of TiO2 Films loaded with Ag nanoparticles.* Nat. Mat. 2003`. **2**(1): p. 29.

(72) Newmann, D.M. and P. Panchmatia, *Nanoscale silver oxide: a rewritable optical recording medium.* Proc. IEEE. 2003. **150**(5): p. 214.

(73) Baba, K. and M. Miyagi, *Write-once optical data storage media for shorter wavelengths using aluminum-silver compound metal island films.* Elec. Lett. 2000. **36**(5): p. 453.

(74) Mihalcea, C., et al., *Intrinsic fluorescence and quenching effects in photoactivated reactively sputtered silver oxide layers.* J. Am. Chem. Soc. 2001. **123**(29): p. 7172.

(75) Nakano, T., et al., *Transmitted signal detection of optical disks with a superresolution near-field structure.* Appl. Phys. Lett. 1999. **75**(2): p. 151.

(76) Peyser, L.A., et al., *Photoactivated fluorescence from individual silver nanoclusters.* Science 2001. **291**: p. 103.

(77) Tominaga, J., et al., *New Recordable Compact-Disk With Inorganic Material, Agox.* Jpn. J. Appl. Phys. Part 1 - Regul. Pap. Short Notes Rev. Pap. 1992. **31**(9A): p. 2757.

(78) Fuji, H., et al., *A near-field recording and readout technology using a metallic probe in an optical disk.* Jpn. J. Appl. Phys. Part 1 - Regul. Pap. Short Notes Rev. Pap. 2000. **39**(2B): p. 980.

(79) Dickson, R.M., et al., *Photoactivated Nanoparticle Fluorescence for Optical Data Storage (#2362)*, in *Office of Technology Transfer, Georgia Tech*. 2002: USA.

CHAPTER 4

MECHANISM OF SILVER NANOCLUSTER PHOTOPRODUCTION

Size-dependent plasmon absorption of metal nanoparticles

One of the most characteristic physical phenomena representative of a bulk metal is conductivity which leads to the collective oscillation of valence electrons at optical frequencies, which is termed the plasmon resonance [1-3]. An interesting point of study is exactly the number of electrons within a particular metal that are needed to demonstrate this effect, especially as the number of atoms reaches the cluster level [3, 4]. Experimental studies on the subject for more than twenty years have aimed to trace the evolution of the metallic character of a cluster of atoms as a function of its size by directly examining electronic effects of cluster size [5-8]. Primarily performed on small particles with a 100 Å or less diameter, classical calculations [9] indicate that the observed strong absorption peak observed in small particles could also be attributed to the excitation of dipolar resonances.

Indeed, the optical and electronic properties of nanometer-sized metal particles do exhibit strong, size-dependent plasmon absorptions [10-15]. When in contact with intense electromagnetic fields such as a laser tuned to the proper frequency, the field around such nanoparticles becomes tremendously enhanced due to the creation of such an enormous dipole and subsequent polarizability [16, 17].

Discussed in detail in thesis sections 1.4 – 1.6, gold and silver have plasmon resonances accessible in the visible spectral range. The enhanced fields around such nanoparticles combined with single-molecule level concentrations of Raman-active molecules have been responsible for single molecule Raman scattering (SERS) [16] studies on Ag, Au, and Cu nanoparticles [18-20]. Control of such nanoscale optical properties on metal clusters has also led to applications ranging from nanosensors to waveguides [21, 22].

Silver nanocluster photoproduction in conjunction with near-field storage

The photoproduction of even smaller particles (2-8 atom nanoclusters) from silver halides finds important application in photography [23, 24] while Ag photoproduction from silver oxide has recently been utilized in near field optical storage materials [25-27]. Tominaga et. al. propose that the ability of silver oxide layers to enable sub-wavelength resolution to write data in the optical near field is directly connected to the local plasmons generated in silver nanoparticles which act as sub-wavelength sized, closely spaced masks. While these optical storage schemes utilize photoinduced nanoparticle formation and its near field plasmon scattering to write data, our significantly smaller Ag_n nanoclusters (n= 2-8 atoms) are also produced from AgO films with strong, size dependent fluorescence [28]. Since the small nanoclusters undergo changes in color due to their geometries changing under continuous excitation, they then possess the potential to store more information in each data point, surpassing the limits of standard binary storage. Contrary to magnetic storage methods, optical storage materials are more readily expandable to

3-D architectures, and can potentially store and retrieve data in parallel (see section 3.4).

Although the technology has the *potential* for making new materials, the reader should note that the surface bound nature of film-generated Ag_n is not the best synthetic route to take. Photolytically produced from the oxide, Ag nanoclusters are less than 1 nm in size, and thus not individually optically addressable. A further complication results from the surface bound clusters changing in size and geometry, making expansion to three dimensions effectively impossible. Since the introduction of Jie Zheng's water-based synthesis of the same Ag_n, opportunities for true three dimensional expansion may actually exist [29]. For either system, even contemplating the use of photoactivated nanoclusters for high-density optical storage involves significant characterization of the factors involved in writing different cluster size distributions, and therefore emission colors within each diffraction-limited spot have to be elucidated. Such studies can only be undertaken through detailed mechanistic understandings of Ag_n nanocluster creation dynamics. Though still limited by diffraction, the ability to write multiple properties with the same resolution can increase the storage capacity. By increasing bit depth within each data point, new optically active nanomaterials may thereby enable increased optical storage densities by encoding perceptibly different optical properties through readily controlled experimental parameters, preferably illumination intensity and time.

This chapter further characterizes the original findings of room temperature photoactivated fluorescence of such small nanoclusters presented in chapter three. The interesting part of the project at this point was the "reverse" characterization of

the thin –film optical properties. Clearly for use in any application, further study is needed to understand how such bright, stable nanoclusters are created at room temperature. Creation of nanocluster distributions has been demonstrated, however the bulk nature of the stored images effectively prevented characterization at the cluster level. We were able to perform a more detailed investigation of the factors effecting nanocluster creation as it occurs, and this chapter presents a mechanism within this context to address this question.

Silver nanocluster creation techniques at low temperature

The optical properties of embedded silver clusters have been thoroughly reviewed [5] and studied in matrix isolated conditions, [1, 14, 30-40] yet there is still a lack of agreement on the position of the plasmon, the size range for the existence of a plasmon, the effect that d-electrons have on the optical properties as a function of size. Spectroscopic data exists for the formation of these types of clusters at room temperature, for example, in photographic film, however at low temperature the matrix cage effect (section 1.2) is what allows stabilization of clusters up to 39 atoms for dynamic study [32]. Small metal clusters can also be created and their low-temperature dynamics studied in free beam experiments using techniques such as resonant two-photon ionization spectroscopy (R2PI) [41, 42], laser induced fluorescence (LIF)[43] and pump-probe techniques [44, 45], such as negative-neutral-positive (NeNePo) spectroscopy [46, 47], some of which are capable of time-resolved experiments [48]. The parameters directly investigated are usually cluster ionization potentials and electron affinities, both of which contribute to the understanding of how small clusters grow,

and break apart [2]. By definition, the ionization potential of a cluster measures the energy difference of the neutral and ionized cluster in the ground state while photoionization involves the removal of an electron by a photon. When taken together, both techniques generate information regarding the energies needed to add or take away an electron from a cluster. These values are used in experiment to generate and mass-select clusters of a known size [30, 36] while simultaneously minimizing fragmentation during deposition. Nanocluster fragmentation however, is also directly employed in some experiments to probe how clusters dissociate, and to determine binding energies corresponding to the break-up process [48-54]. For example, an Ag_8 cluster may dissociate into two Ag_4 clusters, or one Ag_7 cluster and an Ag atom. There is a characteristic energy threshold needed to ensure that atomic fragmentation does not occur such that such ionization potentials can be measured. Processes such as these have been heavily modeled and compared to experimental values [55, 56]. Both sets of calculations reproduce experimental observations of an even-odd alteration in electron affinities and predict the same alternation with respect to dissociation energies. Indeed, the prediction is valid. In general, for clusters with an even number of atoms, atom loss through collision is the predominant fragmentation channel. For odd numbered clusters, dimer loss is predominant, though the atom loss channel is still accessible [53]. In fact there is a pronounced competition between these two channels, the effect increasing with larger cluster size. Our room temperature studies do not have the capability at this time to mass-select and specifically study cluster formation and dissociation independently of one another. However, we can study the factors involved in Ag_n

cluster creation from the oxide with fluorescence microscopy techniques at room temperature. Since each cluster behaves as a molecule, room-temperature fluorescence can be studied in greater detail with respect to environmental and kinetic factors contributing to nanocluster creation and destruction. Combined with the gas-phase results, we can better understand room temperature nanocluster photoproduction. A proposed mechanism is presented.

Comparison of different film preparations

Thin AgO films ranging in thickness from 50 – 125 nm were produced by chemical bath deposition onto glass coverslips as described in thesis section 2.1 [57, 58]. Reported to produce pure AgO, the chemical bath procedure [57, 58] actually results in a mixture of oxides. Depending on the triethanolamine : $AgNO_3$ ratio, deposited film composition can range from nearly pure silver to a mixture of AgO and Ag_2O, which we subsequently further oxidize by ozone treatment [58]. Additionally, films of pure AgO (ranging in thickness from 50 – 125 nm) were prepared by reactive RF sputtering (thesis section 2.2) [59, 60]. The spectral dynamics of individual features were examined using green laser excitation (514.5 nm) and bandpass-filtered mercury lamp excitation. Optically interrogated in the same manner, all differently prepared AgO films exhibited similar writing ability and emission intensity, confirming AgO as the photoactive species.

Illumination of all nanocrystalline silver oxide samples with blue and UV mercury lamp excitation produces Ag_n nanoclusters that range in size from n=2~8 atoms with strong size and geometry dependent fluorescence [13, 28, 30, 40, 61]. With the

same writing wavelength, many different colored emissive species are simultaneously written to the same film. Investigating individual features on AgO films, however, becomes difficult due to the rapidly increasing fluorescence resulting from such efficient writing / photoactivation. On AgO films, each individual Ag nanocluster exhibits a unique emission pattern indicating alignment in the x-y plane [62, 63]. The absence of z-oriented (perpendicular to the film) molecules and the independence of written fluorescence intensity on film thickness both indicate that the emissive Ag_n nanoclusters are surface-bound. Probing the individual features of the nanoclusters becomes much easier when isolating them on an evaporated silver island film.[28] Since only very little AgO is present initially, the writing process does not occur rapidly, and we are able to clearly observe linearly polarized emission patterns from individual features as they slowly grow in. Interestingly, when unobscured by fast writing, a number of molecules oriented in the z-direction can be detected in aged, slightly oxidized Ag island films. Because oxidized silver-island films have highly curved surfaces, they are amenable to the detection of molecules oriented perpendicular to the substrate surface (Figure 4.0.0). In contrast, we have observed nothing but largely x-y oriented molecules on the much smoother and more homogeneous chemically deposited and RF sputtered AgO films.

4.1 Wavelength dependent dynamics

To separate the photoactivation and fluorescence excitation processes in these nanomaterials, we individually wrote images (4.1.1 A) with UV, blue, and green light. Each written spot was subsequently probed for fluorescence intensity

with each of UV, blue, and green excitation wavelengths. (4.1.1 B, C). The photoactivation efficiency clearly increases with decreasing wavelength, while fluorescence excitation peaks in the blue. While photoactivation of the AgO film to produce Ag_n nanoclusters is clearly much more efficient when excited with UV light, the fluorescence excitation spectrum of a written image exhibits very little UV-excited fluorescence. As these fluorescent patterns grow in through the photochemical transformation of silver oxides, this photochemical process enables small silver clusters to form on AgO surfaces similar to those harnessed in silver halide-based photographic emulsions [23, 24]. Contrary to nonfluorescent Ag nanoclusters on AgBr crystals, however, nanoclusters on AgO must be better stabilized by dispersive interactions to yield fluorescence when excited with energies exceeding the gas phase binding energy (1.68 eV for Ag_2) [64, 65].

4.2 Intensity dependence

While spectral diffusion has been observed in many single nanoparticle /molecule systems, [66-69] these surface bound individual emissive species produce dynamic single particle color changes among red, orange, yellow, and green. The fluorescence dynamics within a high-density diffraction-limited spot are illustrated by dispersing the fluorescence resulting from 514 nm laser excitation with an intensity of ~3 kW/cm^2 (Figure 4.2.1). At least five distinct spectral features (548 nm, 594 nm, 641 nm, 673 nm, 725 nm) are observed in each emission spectrum arising from distinctly differently sized and shaped Ag_n nanoclusters. These features clearly

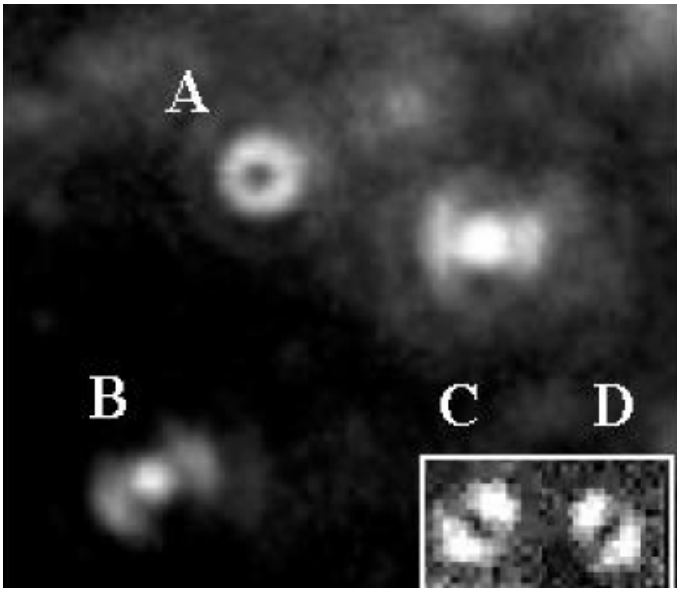

Figure 4.0.0. Typical fluorescence image from an oxidized Ag island film excited at 514.5 nm through a 100x 1.4NA objective. Individual features appear as either (A) doughnut or (B) bowtie patterns when slight defocus is introduced (see section 2.2). Because of the high surface curvature on Ag island films, z-oriented molecules can be observed. Although x-y oriented molecules exhibit nearly complete intensity modulation when passed through a rotating polarizer, the z-oriented molecules produce lobes parallel to the polarized transmission axis due to z-oriented molecules yielding equal collected intensities of x and y polarized light (C,D).

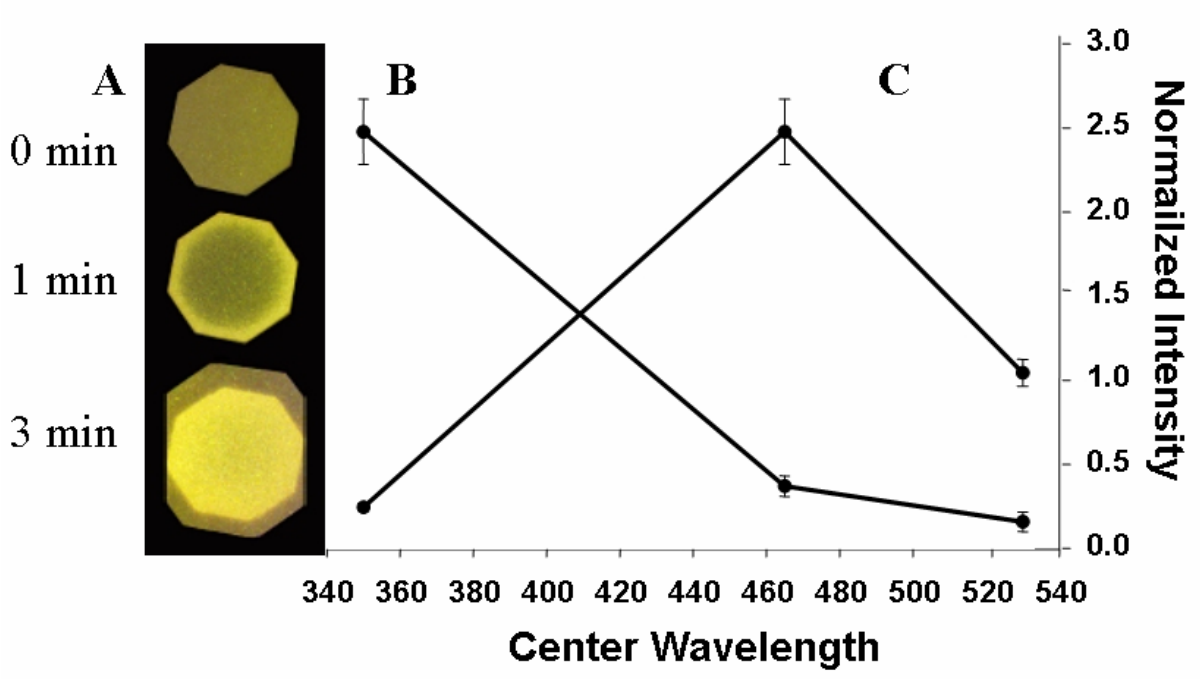

Figure 4.1.1 Fluorescence written to an AgO film with blue Hg lamp excitation. Species are written only in the region bound by the aperture for comparative purposes over time. Intensity is greatest at aperture edges due to diffraction. (B) Photoactivation spectrum of AgO film over varied spectral ranges (UV, blue, green). Features similar to (A) were written at each of these range center wavelengths and probed with blue excitation (long pass emission collected) to generate the spectrum. (C) Fluorescence excitation spectrum of previously written images with UV excitation. To generate the spectrum, fluorescence from the written images was measured with each UV, blue, and green excitation. Error bars represent 90% confidence limits.

change relative intensity with time, eventually reaching a light-dependent steady-state distribution of Ag_n nanocluster sizes that produces the final spectrum /composite emission color. The same emission wavelengths are maintained throughout the experiments; only the relative intensities change with time, indicating the equilibrium among various nanocluster sizes. Indicating that multiple colors are readily written through control of sample excitation, control of final cluster size distributions should allow specific colors to be written, thereby potentially enabling higher data storage densities to be achieved. The stabilizing and destabilizing interactions constantly increase and decrease the nanocluster size and modify molecular geometry under continuous illumination, thereby causing the dynamic emission color changes of individual emissive sites. Thus, the time-intensity product is an integral part in governing the written cluster size distributions resulting from the equilibrium between forming and breaking apart the fluorescent Ag_n nanoclusters.

Through writing varied distributions of Ag_n clusters, different composite colors can be created with UV and blue illumination. The photoactivation (writing) process clearly only produces nanoclusters within illuminated regions of the sample, with writing rate and final fluorescent intensity strongly dependent on excitation intensity.

4.3 Intensity-time product drives photoactivation

Because each individual particle is photoactivated, information is readily stored in these AgO films. Much faster writing is easily performed at higher incident intensities from a laser source, with the rate of fluorescent nanocluster formation being strongly dependent on the incident intensity at a given wavelength. While the

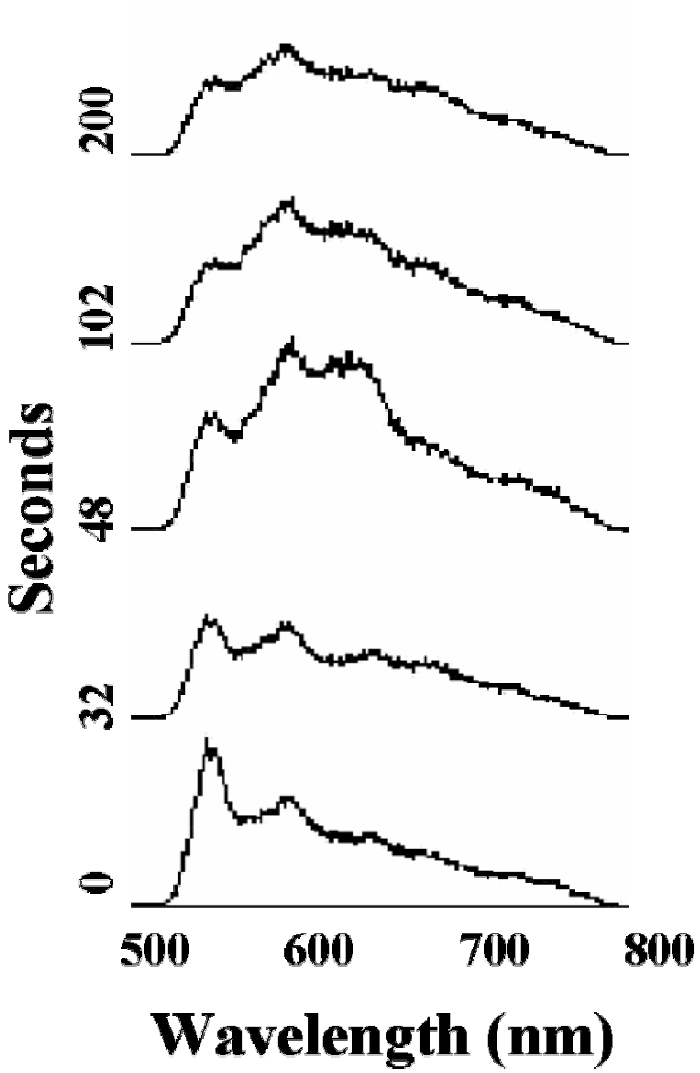

Figure 4.2.1. Spectral time series emission from a ~600 nm diameter region of a 514.5 nm excited AgO film. At least five distinct spectral features can be seen changing in time, and alternate in relative intensity as the Ag_n nanocluster size distribution continuously changes under constant excitation. Changes happen quickly in the early part of the spectrum but plateau off after about 1 minute at such high excitation intensity (~1 kW/cm^2) as indicated by only minor fluctuations in relative intensity.

final high-density image is yellow, it still exhibits bits of red and green colors, indicating that the yellow images result, at least in part, from color mixing of the dynamic multicolored emission observed under blue excitation. These written images on AgO films are quite stable in the dark for several days, even when otherwise exposed to ambient conditions. Also written with UV excitation, strong red and near IR fluorescent features are simultaneously observed within the illuminated region which can be more efficiently excited with green excitation.

Perhaps a clearer way of demonstrating the intensity dependence is by spectral visualization. With respect to Figure 4.2.1 above, we can consider one slice of the entire spectral series at random times, each of which shows a unique spectrum when taken by itself. However, when the entire data set as a whole is considered, one can watch changes occur within the spectral distribution rather dynamically until some final steady-state is reached of a certain size and geometry, as indicated by very little changes in the spectrum at later times. The prominence of specific peaks also changes with excitation intensity. The time-intensity product clearly has an effect on the observed spectrum, as the high-density spot written after a certain amount of time shows a specific cluster size distribution, while the same spot written for a different amount of time may show a very different spectrum. Additionally, if a change in wavelength or intensity were introduced into the system, the dynamics would no longer be in steady state, but again would change in time.

Investigations of the intensity dependent initial writing rate and final written fluorescence intensity demonstrate the light dependent equilibrium present in these systems (Figure 4.3.1). The three different curves each show an initial sharply rising

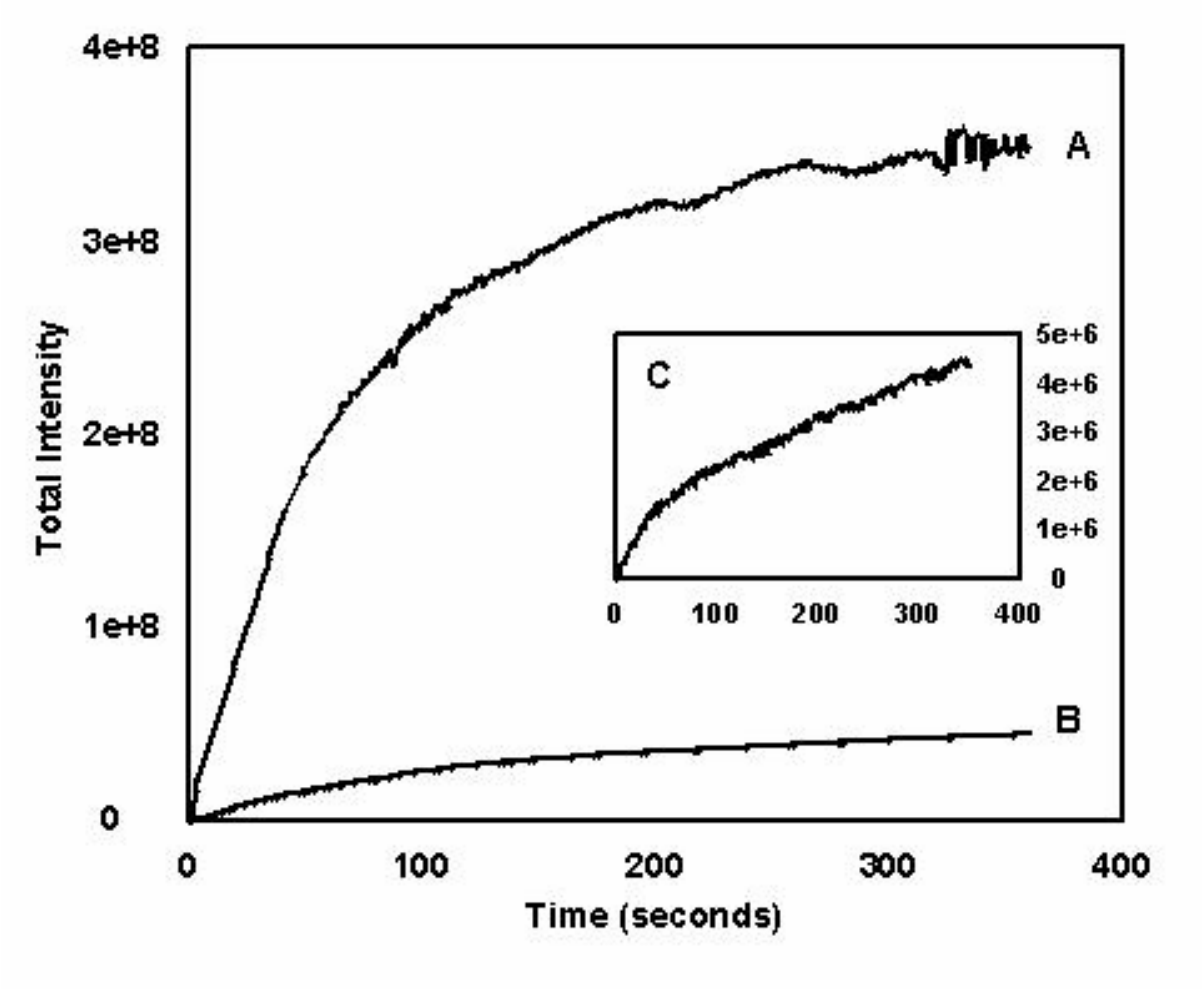

Figure 4.3.1. Total emission intensity vs. time for three different excitation intensities (A) 295 W/cm^2, (B) 77 W/cm^2, and (C) 18 W/cm^2. All three intensities demonstrate similar trends in that the initial area increases linearly and trails off to s steady state fluorescence intensity (nanocluster density). Of interest is the order of magnitude change in slope (rate of photoactivation) with only a factor of 3.5 change in excitation intensity. Ratios of the slopes yield a super-linear, but sub-quadratic intensity dependence scaling as $I_{Fluorescence} = I_{Exitation}^{1.65+/-0.010.}$

linear portion while eventually reaching an equilibrium written intensity. After the final nanocluster distribution and limiting written fluorescence intensity are reached, continued reading of fluorescence causes no further observed changes. While incident intensities were only varied by just over one order of magnitude, the final fluorescence intensities changed by two orders of magnitude. The initial slope (or writing rate) also exhibits a superlinear intensity dependence, indicating that multiple photons are involved in creating the fluorescent species, yielding an intensity dependence scaling as $I^{1.64 \pm 0.10}$. This excitation intensity dependence reflects the dynamic light-dependent equilibrium underlying the creation and destruction of multi-atom Ag_n nanoclusters.

Since the incident intensity is neither proportional to the emission in a linear nor a quadratic fashion, the creation dynamics do not result from simply single-photon or two-photon processes. Because dimers and larger nanoclusters must be created to produce fluorescence, at least two independent photochemical reactions of AgO must occur ($2AgO + 2h\nu \rightarrow 2Ag + 2O^{\cdot}$), suggesting a second-order process with respect to incident intensity. Since excitation energies exceeding gas phase nanocluster binding energies are used to excite fluorescence, a light-dependent equilibrium is established between the creation and destruction of the nanoclusters. The light dependent equilibrium between nanocluster creation and destruction is evidenced by the light-dependent blinking dynamics,[28, 70] (see discussion, section 3.2 and table 3.2.1) our observed relative intensity changes of emission peaks , and the light-dependent final fluorescence intensity for a given written feature. While both forward and reverse reaction rates are light-dependent, the forward reaction creating

Ag_n nanoclusters clearly dominates, favoring nanocluster creation at higher incident intensities and yielding a superlinear, but sub-quadratic, intensity dependence.

4.4 Environment-mediated dynamics

As oxygen atoms are produced in AgO photochemistry, environmental conditions will further affect Ag_n nanocluster dynamics and stability. Under moderate (10^{-5} torr) vacuum, the activation rate dropped 11.7-fold relative to that in air at atmospheric pressure, (Figure 4.4.1) while under nitrogen and argon atmospheres, the final written fluorescence intensity increased two-fold over ambient conditions. Writing fluorescent Ag_n nanoclusters in an O_2-enriched environment yields an activation rate slower than that in either Ar or N_2, but comparable to that in air. Because AgO is stable at room temperature, two processes must occur to generate stable Ag_n nanoclusters – removal of atomic oxygen and dissipation of energy. Including the optical excitation, AgO photodecomposition is exothermic, thereby requiring dissipation of the large amount of energy injected into the AgO system through light absorption. Evacuated environments seem to provide insufficient collisional rates to dissipate excess energy, thereby favoring reactants in this exothermic photochemical reaction. As a result, photoactivation is significantly less efficient in vacuum. Under even moderate vacuum conditions however, the reduced number of molecules present to undergo collisions hinders the system's ability to write data efficiently. As a result, while photoactivation still occurs in vacuum, it is considerably slower than in ambient conditions. While any gas will provide sufficient collisions to dissipate the excess energy and shift the equilibrium toward Ag_n

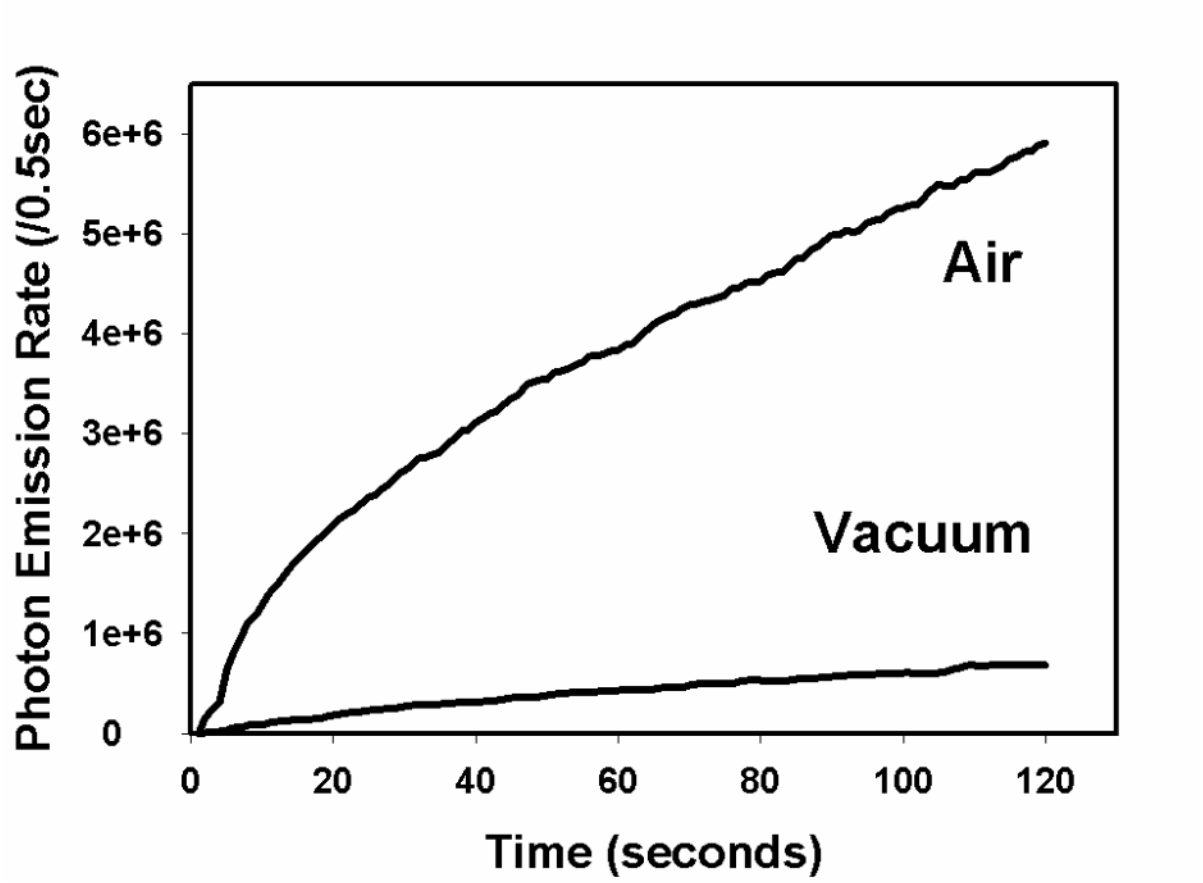

Figure 4.4.1. Moderate vacuum (10^{-5} Torr) shows a ~12 fold decrease in the rate of photoactivation. Photoactivation will still occur in vacuum, although considerably slower due to the lace of collision occurrences to dissipate excess surface energy.

nanoclusters, oxygen is a by-product of the AgO photodecomposition and could promote nanocluster re-oxidation to AgO. Due to these effects on the equilibrium between AgO and Ag, photoactivation is most efficient in non-evacuated, non-oxidizing environments. In fact, different nanocluster emission wavelengths are observed when excited in argon and nitrogen atmospheres, exhibiting significant emission even when excited with UV wavelengths. These presumably less stable nanoclusters are more easily oxidized back to non-fluorescent AgO, but are stabilized in inert environments.

4.5 Conclusions

Through varied sample preparation and control of external conditions, the important chemical species involved in photoactivation of silver oxides have been studied. AgO films are readily photoactivated with UV excitation, preferably in inert atmospheres to produce highly fluorescent, surface-bound Ag_n nanoclusters. Because only nanoclusters containing 2~8 atoms are known to exhibit significant oscillator strengths at visible wavelengths [13, 30, 39] and superlinear, but sub-quadratic intensity dependences of writing have been observed, we have obtained further evidence that the emissive species, as on cryogenic AgBr crystals, are small Ag_n nanoclusters.

The most directly related application at this point remains the potential of a novel silver-silver oxide system for optical data storage with fluorescent readout. These information bearing properties arise from photolytic production of highly fluorescent single Ag_n molecules (n = 2-8 atoms) from silver oxide. Single molecule

and bulk fluorescence experiments have begun to elucidate the dynamics of AgO photoactivation and subsequent Ag_n nanocluster emission which when taken together may have the potential to unlock new storage techniques. Additionally, excitation, wavelength and intensity dependent dynamics are investigated to this extent and clearly show dependence on Ag_n nanocluster creation and destruction. By characterizing the size, intensity, wavelength, and chemical factors governing photoactivation and characterizing the fluorescence dynamics, we have begun to elucidate the interactions yielding the dynamic multicolored emission giving rise to the stored images. The potential of these nanoparticles remains very large: in just 10 data points, binary storage enables 2^{10} = 1024 pieces of information while the ability to distinguish just 4 colors yields a storage capacity of 4^{10} = 1,048,567. Because of the Ag-cluster size dependent emission colors, high optical storage densities should be achievable through optical and chemical control of silver /silver oxide photoactivation and the resulting Ag_n nanocluster fluorescence.

Not only have factors for potential later applications been suggested, but the fundamental properties of small silver nanocluster creation at room temperature have been determined, which is the relevant species of interest. With the spectral, kinetic, and photoactiavation information gathered from this study, we can move toward the fuller study of the non-two dimensionally limited dendrimer and peptide encapsulated Ag_n system for more direct study of this nanocluster involvement in surface-enhanced Raman spectroscopy.

References

(1) Fedrigo, S., W. Harbich, and J. Buttet, *Collective Dipole Oscillations in Small Silver Clusters Embedded in Rare-Gas Matrices.* Phys. Rev. B-Condens Matter 1993. **47**(16): p. 10706.

(2) de Heer, W.A., *The physics of small metal clusters.* Rev. Mod. Phys. 1993. **65**(3): p. 611.

(3) Henglein, A., *Physicochemical Properties of Small Metal Particles in Solution - Microelectrode Reactions, Chemisorption, Composite Metal Particles, and the Atom-to-Metal Transition.* J. Phys. Chem. 1993. **97**(21): p. 5457.

(4) Brack, M., *The physics of simple metal clusters: self consistent jellium model and semiclassical approaches.* Rev. Mod. Phys. 1993. **65**(3): p. 677.

(5) Kreibig, U. and L. Genzel, *Optical absorption of small metal particles.* Surf. Sci. 1985. **156**: p. 678.

(6) Kreibig, U. and C. von Fragstein, *Limitation of electron mean free path in small silver particles.* Z. Phys. 1969. **224**(4): p. 307.

(7) Welker, T. and T.P. Martin, *Optical absorption of matrix-isolated lithium, sodium, and silver clusters and microcrystals.* J. Chem. Phys. 1979. **70**(12): p. 5683.

(8) Abe, H., et al., *Surface plasmon absorption of various colloidal metal particles.* Chem. Phys. 1982. **68**(1-2): p. 137.

(9) Mie, G., *Contributions to the Optics of Turbid Media, Especially Colloidal Metal Solutions.* Ann. Phys. 1908. **25**: p. 377.

(10) Mostafavi, M., et al., *Ultraslow aggregation process for silver clusters of a few atoms in solution.* Chem. Phys. Lett. 1990. **167**(3): p. 193.

(11) Linnert, T., et al., *Long lived nonmetallic silver clusters in aqueous solution: preparation and photolysis.* J. Am. Chem. Soc. 1990. **112**: p. 4657.

(12) Bigioni, T.P., R.L. Whetten, and O. Dag, *Near-infrared luminescence from small gold nanocrystals.* J. Phys. Chem. B 2000. **104**(30): p. 6983.

(13) Bonacic-Koutecky, V., V. Veyret, and R. Mitric, *Ab initio study of the absorption spectra of Agn (n=5-8) clusters.* J. Chem. Phys. 2001. **115**(22): p. 10450.

(14) Rabin, I., W. Schulze, and G. Ertl, *Absorption spectra of small silver clusters Ag-n (n >= 3).* Chem. Phys. Lett. 1999. **312**(5-6): p. 394.

(15) Wilcoxon, J.P., et al., *Photoluminescence from nanosize gold clusters.* J. Chem. Phys. 1998. **108**: p. 9137.

(16) Moskovits, M., *Surface-enhanced spectroscopy.* Rev. Mod. Phys. 1985. **47**: p. 783.

(17) Creigton, J.A., C.G. Blatchford, and M.G. Albrecht, *Plasma resonance enhancement of Raman scattering by pyridine adsorbed on silver or gold sol particles of size comparable to the excitation wavelength.* 1978: p. 790.

(18) Kneipp, K., et al., *Single molecule detection using surface-enhanced Raman scattering (SERS).* Phys. Rev. Lett. 1997. **78**: p. 1667.

(19) Nie, S.M. and S.R. Emory, *Probing single molecules and single nanoparticles by surface-enhanced Raman scattering.* Science 1997. **275**: p. 1102.

(20) Michaels, A.M., M. Nirmal, and L.E. Brus, *Surface enhanced Raman spectroscopy of individual rhodamine 6G molecules on large Ag nanocrystals.* J. Am. Chem. Soc. 1999. **121**(43): p. 9932.

(21) *Nanostructured Materials and Nanotechnology*, ed. H.S. Nalwa. 2000, New York: Academic Press.

(22) Timp, G., *Nanotechnology*. 1999, New York: Springer-Verlag.

(23) Ehrlich, S.H., *Spectroscopic Studies of AgBr With Quantum-Sized Clusters of Iodide, Silver, and Silver Sulfides.* J. Imaging Sci. Technol. 1993. **37**(1): p. 73.

(24) Eachus, R.S., A.P. Marchetti, and A.A. Muenter, *The Photophysics of Silver Halide Imaging Materials.* Ann. Rev. Phys. Chem. 1999. **50**: p. 117.

(25) Tominaga, J., et al., *New Recordable Compact-Disk With Inorganic Material, Agox.* Jpn. J. Appl. Phys. Part 1 - Regul. Pap. Short Notes Rev. Pap. 1992. **31**(9A): p. 2757.

(26) Fuji, H., et al., *A near-field recording and readout technology using a metallic probe in an optical disk.* Jpn. J. Appl. Phys. Part 1 - Regul. Pap. Short Notes Rev. Pap. 2000. **39**(2B): p. 980.

(27) Tominaga, J., et al., *Super-resolution near-field structure and signal enhancement by surface plasmons.* Jpn. J. App. Phys. 2001. **40**(3B): p. 1831.

(28) Peyser, L.A., et al., *Photoactivated fluorescence from individual silver nanoclusters.* Science 2001. **291**: p. 103.

(29) Zheng, J. and R.M. Dickson, *Individual Water-Soluble Dendrimer-Encapsulated Silver Nanodot Fluorescence.* JACS 2002. **124**(47): p. 13982.

(30) Harbich, W., et al., *Deposition of mass selected silver clusters in rare gas matrices.* J. Chem. Phys. 1990. **93**: p. 8535.

(31) Harbich, W., S. Fedrigo, and J. Buttet, *The Optical-Absorption Spectra of Small Silver Clusters (N = 5- 11) Embedded in Argon Matrices.* Chem. Phys. Lett. 1992. **195**(5-6): p. 613.

(32) Harbich, W., S. Fedrigo, and J. Buttet, *The Optical-Absorption Spectra of Small Silver Clusters (N=8- 39) Embedded in Rare-Gas Matrices.* Z. Phys. D-Atoms Mol. Clusters 1993. **26**(1-4): p. 138.

(33) Harbich, W., et al., *Optical spectroscopy of size-selected silver clusters embedded in solid neon: A cluster-support interaction study.* Surf. Rev. Lett. 1996. **3**(1): p. 1147.

(34) Fedrigo, S., et al., *Evidence For Electronic Shell Structure of Small Silver Clusters in the Optical-Absorption Spectra.* Chem. Phys. Lett. 1993. **211**(2-3): p. 166.

(35) Fedrigo, S., W. Harbich, and J. Buttet, *Optical-Response of Ag2, Ag3, Au2, and Au3 in Argon Matrices.* J. Chem. Phys. 1993. **99**(8): p. 5712.

(36) Felix, C., et al., *Fluorescence and excitation spectra of Ag-4 in an argon matrix.* Chem. Phys. Lett. 1999. **313**(1-2): p. 105.

(37) Konig, L., et al., *Chemiluminescence in the agglomeration of metal clusters.* Science 1996. **274**(5291): p. 1353.

(38) Rabin, I., et al., *Absorption and fluorescence spectra of Ar-matrix-isolated Ag-3 clusters.* Chem. Phys. Lett. 2000. **320**(1-2): p. 59.

(39) Rabin, I., W. Schulze, and G. Ertl, *Light emission during the agglomeration of silver clusters in noble gas matrices.* J. Chem. Phys. 1998. **108**(12): p. 5137.

(40) Rabin, I., W. Schulze, and G. Ertl, *Light emission in matrix assisted cluster-cluster reactions.* Cryst. Res. Technol. 1998. **33**(7-8): p. 1075.

(41) Duncan, M.A., in *Advances in metal and semiconductor clusters*, M.A. Duncan, Editor. 1993, JAI Press: New York. p. 123.

(42) Morse, M., *Clusters of transition-metal atoms.* Chem. Rev. 1986. **86**: p. 1049.

(43) Kramer, H.-G., et al., *Sub-Doppler laser spectroscopy of silver dimers Ag2 in a supersonic beam.* Chem. Phys. Lett. 1992. **193**(5): p. 331.

(44) Woste, L., *Laser spectroscopy of metal clusters.* Z. Phys. Chem. 1996. **196**: p. S121.

(45) Wolf, S., et al., *Spectroscopy of size-selected neutral clusters: femtosecond evolution of neutral silver trimer.* Phys. Rev. Lett. 1995. **74**: p. 4177.

(46) Ho, J., K. Ervin, and W.C. Lineberger, *Photoelectron spectroscopy of metal cluster anionsL Cun-, Agn- and Aun-.* J. Chem. Phys 1990. **93**(10): p. 6987.

(47) Hess, H., et al., *Vibrational wave paclet dynamics in the silver tetramer probed by NeNePo femtosecond pump-probe spectroscopy.* Eur. Phys. J. 2001. **16**: p. 145.

(48) Hild, U., et al., *Time-resolved photofragmentation of stored silver clusters Agn+ (n=8-21).* Phys. Rev. A 1998. **57**(4): p. 2786.

(49) Francisco, P.R., et al., *Ultrafast fragmentation and vibrational dynamics of triatomic hetero-and homonuclear alkali metal clusters.* J. Chin. Chem. Soc. 2000. **47**: p. 705.

(50) Haupt, S., et al., *Photofragmentation of Ag-4(N-2)(x)(+), x=0-3: N-2 binding energies.* Z. Phys. D-Atoms Mol. Clusters 1997. **40**(1-4): p. 331.

(51) Kruckeberg, S., et al., *The dissociation channels of silver clusters Agn+ 3<n<20.* Int. J. Mass. Spec. 1996. **155**: p. 141.

(52) Shi, Y., V. Spasov, and K. Ervin, *Competitive fragmentation and electron loss kinetics of photoactivated silver cluster anions: dissociation energies of Agn- (n = 7-11).* J. Chem. Phys. 1999. **111**(3): p. 938.

(53) Spasov, V., et al., *Measurement of the dissociation energies of anionic silver clusters (Agn-, n= 2-11) by collision-induced dissociation.* J. Chem. Phys. 1999. **110**(11): p. 5208.

(54) Vogel, M., A. Herlert, and L. Schweikhard, *Photodissociation of small group-11 metal cluster ions: fragmentation pathways a nd photoabsorption cross sections.* J. Am. Soc. Mass. Spectrom. 2003. **14**: p. 614.

(55) Bonacic-Koutecky, V., et al., *Effective core potential-configuration interaction study of electronic structures and geometries of small neutral and cationic silver (Agn) clusters: predictions and interpretation of measured properties.* J. Chem. Phys. 1993. **98**(10): p. 7991.

(56) Bonacic-Koutecky, V., et al., *Effective core potential-configuration interaction study of electronic structure and geometry of small anionic Agn clusters: predictions and interpretation of photodetachment spectra.* 1994. **100**(1): p. 490.

(57) Varkey, A.J. and A.F. Fort, *Some Optical-Properties of Silver Peroxide (AgO) and Silver- Oxide (Ag2)) Films Produced By Chemical-Bath Deposition.* Sol. Energy Mater. Sol. Cells 1993. **29**(3): p. 253.

(58) Kocareva, T., I. Grozdanov, and B. Pejova, *Ag and AgO thin film formation in Ag+-Triethanolamine solutions.* 2001. **47**: p. 319.

(59) Xiong, Y., et al., *Preparation and characterization of nanostructured silver thin films deposited by radio frequency magnetron sputtering.* 2000. **375**: p. 300.

(60) Buchel, D., et al., *Sputtered silver oxide layers for surface-enhanced Raman spectroscopy.* Appl. Phys. Lett. 2001. **79**(5): p. 620.

(61) Weis, P., et al., *Structures of small silver cluster cations (Ag_n^+, n<12): ion mobility measurements versus density functional and MP2 calculations.* 2002. **355**: p. 355.

(62) Bartko, A.P. and R.M. Dickson, *Imaging three-dimensional single molecule orientations.* J. Phys. Chem. B 1999. **103**(51): p. 11237.

(63) Bartko, A.P. and R.M. Dickson, *Three-Dimensional Orientations of Polymer-Bound Single Molecules.* J. Phys. Chem. B 1999. **103**: p. 3053.

(64) Ferrari, A.M., et al., *Pd and Ag dimers and tetramers adsorbed at the MgO(001) surface: a density functional study.* 1999. **1**: p. 4655.

(65) Oku, Y. and M. Kawasaki, *Diffuse Transmittance Spectroscopy of Diatomic Ag Nuclei on AgBr Microcrystals.* J. Phys. Chem. B 1998. **102**: p. 9061.

(66) Geva, E. and J.L. Skinner, *Single molecule spectral trajectories in low-temperature glasses.* Chem. Phys. Lett. 1998. **287**(1-2): p. 125.

(67) Lu, H.P. and X.S. Xie, *Single-Molecule Spectral Fluctuations at Room Temperature.* Nature 1997. **385**: p. 143.

(68) Empedocles, S.A. and M.G. Bawendi, *Influence of spectral diffusion on the line shapes of single CdSe nanocrystallite quantum dots.* J. Phys. Chem. B 1999. **103**(11): p. 1826.

(69) Skinner, J.L. and W.E. Moerner, *Structure and dynamics in solids as probed by optical spectroscopy.* J. Phys. Chem. 1996. **100**(31): p. 13251.

(70) Peyser, L.A., T.-H. Lee, and R.M. Dickson, *Mechanisn of Ag_n nanocluster photoproduction from silver oxide films.* J. Phys. Chem B. 2002. **106**: p. 7725.

CHAPTER 5

THE ROLE OF THE SILVER NANOCLUSTER IN SINGLE-MOLECULE RAMAN SPECTROSCOPY

Ordinarily exceedingly weak, Raman spectroscopy cross sections can be sufficiently enhanced when near 40-100-nm Ag and Au nanoparticle surfaces to even enable facile single molecule observation. [1-3] While single molecule Raman spectroscopy (SM-Raman) is currently the only tool capable of combining chemical information with single molecule sensitivity, the enhancement mechanism remains enigmatic as presented in section 1.5, thereby limiting application. SM-Raman cross sections are only thought to become comparable to those of fluorescence through a combination of chemical/charge transfer interactions combined with large metal nanoparticle-assisted plasmon enhancement of the incident electromagnetic field. [1-6] The chemical or charge transfer process mixes energy levels to produce new electronic states in resonance with the laser excitation [7-10], but until the results presented in this chapter [11], the chemical interaction was thought to only yield a small contribution (~10^3) to the overall enhancement.

The "hot spot" concept

Early results of both Kneipp et. al. and Nie and Emory were crucial to investigating SERS enhancements giving rise to the observed 15 orders of magnitude gained from near infrared excitation of crystal violet or Rhodamine 6G[2] in colloidal metal solutions[1]. By exploiting the properties of SERS and resonance effects, these incredible enhancements were attributed to rare surface interactions present on a very small subset of nanoparticles on the surface. Since only a few nanoparticles demonstrated the unusually high enhancement, they were deemed "hot particles" or "hot spots". The primary effect today is still widely thought to arise from extreme plasmon-assisted field enhancements at these ill-defined "hot spots" [3, 12, 13] [1, 2]. Some groups define/characterize hot spots by combined spectroscopic and topographical imaging [3, 14], while others assume a constant nanoparticle concentration and account for "hot spots" by tracking the number of enhanced molecules as the nanoparticles diffuse through the laser focus [15], usually less than 1% [3].

The Brus Ag nanocrystal junction model

While still under debate, the largest such enhancements should occur at nanoparticle junctions – a prediction that largely correlates with experimental evidence. [14, 16] Brus et. al. have propsed that the nanoparticles yielding SM-SERS on their Rhodamine 6G-colloidal Ag system are actually compact aggregates of a minimum of two ~50nm Ag particles. Their model stems from interpretation of Otto and Persson's results which consider a metal with a strong

chemisorbed molecule, and its interaction with ballistic electrons [7, 9]. They increased the Rhodamine concentration by a factor of one hundred, and the increase in the number of SERS active particles only increased five-fold. As this postulates the number of SERS active particles is not limited by the number of SERS active molecules, they suggest a rare chemisorption site may be the "critical and limiting factor" for SM-SERS. Brus proposed from adding NaCl to test the "anion effect", that nanoparticle junctions may be the rare site. It has been proposed that anions serve as activating agents [4, 17], and when NaCl was added, still only a small number of molecules exhibited SERS and the scattering spectra of such particles were characterized by multiple resonances, suggesting that NaCl induced aggregation. Classical calculations demonstrated that the junction (assuming Angstrom scale separation) experiences a higher magnetic field than for any other site on the surface of a single particle [18, 19]. Very briefly, capacitive coupling of one particle to the other supports Otto and Persson's theory that current density of ballistic carriers on the surface creates the field in the junction.

The underlying continuum – electronic Raman or "spurious SERS"?

Even with the consideration that the SM-SERS is enhanced by the field produced by the junction of two nanoparticles, the Raman vibrational lines are still accompanied by omnipresent scattering, an observation that has been noted since the early work on SERS. This continuum is proposed to arise from either luminescence [20] or electronic Raman scattering from the metal [21, 22], and is only

an aspect of SERS, and not manifested in traditional free-space Raman scattering. Electronic Raman is characterized by an inelastic photon scattering process exciting an electron from below to above the Fermi surface of the metal (creating an electron-hole pair in the metal). In metals such as silver, electronic Raman is generally extremely weak since the momentum transferred to the e-h pair is only large enough to create an e-h pair a few wavenumbers in energy above the Fermi surface [14]. When rough, curved or other wise dirty systems are considered, momentum selection rules become relaxed, (for a full description of momentum, see section 1.5) and electronic Raman allowed to occur over wide energy ranges, and has been reported [21, 23-28]. As Brus proposes, the "simplest" assumption indicates that the continuum could be a result of Ag electronic Raman scattering caused by one surface defect – defined by an adsorbed R6G molecule exchanging electrons with the metal. Scattering from the plasmon-driven surface electrons can create both R6G "first layer" SERS and Ag electronic Raman [14]. The "first layer" effect is described in detail in section 1.5 as it relates to the chemical enhancement mechanism. More recent results indicate that the continuum is simply "spurrious", only displaying the super-imposed Raman scaterring when resonant with the "Raman active" spectral region [29].

Recent results and the connection to photoactivated Ag_n

Even in the most advantageous case, the total calculated enhancements ($\sim 10^{11}$) [30, 31] typically fall far short of those observed ($\sim 10^{15}$) in nanoparticle-based SM-surface enhanced Raman (SM-SERS) experiments. Such enhancements

make SM-SERS 10-100 times more sensitive than SM-fluorescence [1-3]. Additionally, the nanoparticle Rayleigh spectrum (corresponding to plasmon enhancement) was shown to be independent of the spectral dependence yielding Raman enhancement,[3] questioning the role of the plasmon in SM-Raman. Very recently, the strong, broad, non-resonant background and blinking signals were even shown to be present without (purposely) added analyte and seem to arise solely from the large metal nanoparticle itself. [29, 32]

Well known at low temperature [33], strong luminescence has been reported for small (<10 atom) silver clusters. Chapter three discusses the strong, photoactivated fluorescence from individual 2-8 atom silver nanoclusters discovered both on thin silver films and encapuslated in a dendrimer host matrix at room temperature [34-36]. The absorption cross sections of these few-atom materials were both ~10^{-14} cm^2, or ~100 times stronger than those of the best organic fluorophores, and therefore easily observable on the single molecule level. The similar excitation and emission spectra and comparable emissive lifetimes suggest that these few-atom solution phase and thin film-bound nanoclusters are the same species and are likely a contributing factor to the omnipresent, strong non-resonant background characteristic of SERS experiments. With very high polarizibilities, these strongly absorbing few-atom metal nanoclusters should strongly interact with analytes in a charge-transfer mechanism to enhance Raman signals. In this chapter, we demonstrate that large metal nanoparticles are actually unnecessary to produce SM-Raman signals, with the enhancement arising solely from coupling with the strong optical

transitions of few-atom Ag nanoclusters. In fact, our results challenge the current framework by which SM-SERS is justified in the literature. As we have shown that there is not necessarily a need for a nanoparticle, SM-Raman may arise from Ag_n enhancement alone, or possibly from Ag_n on top of larger nanoparticles. With scaffold-specific Raman scattering, biocompatibility, and even SM-antistokes Raman being observed, these sub-nm Ag nanoclusters open exciting opportunities in single molecule biolabeling and a window into how SM-Raman signals occur.

5.1 Early indicators that small silver nanoclusters may have an important role in enhancing Raman spectra

In the beginning stages of this work, all spectroscopy was performed on thin metal films. With some degree of uncertainty about the single-molecule nature of the experiments, some interesting results were obtained. Since the photoactivation properties of such films was so fast, addressing individual features became quite challenging and experiments were relegated to bulk studies partly due to this and in part due to the resolution of the monochromator at that time (Spex, fixed 150 l/mm grating). Originally, these experiments were intended to investigate the origin of the omnipresent and poorly understood non-resonant background present in high-sensitivity SERS experiments. As the tremendous ~10^{15} SERS enhancement is postulated to arise from combinations of chemical and electromagnetic factors. Although direct experimental evidence is scant, the major effect is thought to arise within strongly enhancing

electromagnetic environments at the junction of two nanoparticles. Estimates of the enhancements possible at such sites qualitatively reproduce observed enhancements, but are unable to explain the corresponding non-resonant background and generally ignore the charge-transfer interactions. [4, 37]

The spectral characteristics of the strong non-resonant background are very similar to those observed in the strong photoactivated fluorescence from our individual Ag_n nanoclusters. [34, 35] It is these few-atom, possibly cationic nanoclusters that are also thought to interact with analytes in a charge-transfer mechanism further enhancing SERS signals. In fact, when synthesized in a radiolytic process specifically without cationic nanoclusters on the Ag nanoparticle surfaces, neither SM-SERS nor the non-resonant background signals can be observed [38]. The strong similarity in spectral, intensity, and photoactivated dynamics common to both SERS and Ag_n nanocluster fluorescence on silver and AgO substrates suggests that highly fluorescent, highly polarizable neutral and cationic Ag_n nanoclusters can strongly interact with analyte molecules to yield the chemical enhancements necessary to observe single molecule SERS (SM-SERS). While electromagnetic interactions can be an important component yielding SM-SERS enhancements, the charge-transfer interaction is thought to yield comparable enhancements in light of our recent results, which can also push detection limits to the single molecule level. If either process turns off, the Raman enhancement may be temporarily reduced to a level unobservable on the single molecule level.

On the same type of thin Ag/silver oxide films used in chapter three, we identified and characterized nanocluster fluorescence and subsequently added 100uL of aqueous sub-nanomolar concentration R6G solution to the surface to mimic amounts of dye per active site consistent with the calculations of Nie and Emory [2], and subsequent reports by Michaels and Brus [3]. This enabled us to directly observe sharp Raman transitions superimposed on a fluorescent background with lines consistent with SM-R6G Raman. No Raman signal was ever observed without the continuous non-resonant background (Figure 5.1.1), but the fluorescent background was occasionally observed without any Raman peaks, consistent with others' observations. [2, 3, 16] The background fluorescence signal constituted approximately 85% of the observed signal. When the underlying fluorescence of these Raman spectra is subtracted out, the resulting pure Raman spectrum remained at both low and high signal to noise. (Figure 5.11A, B)

Experiments investigating the nanocluster's contribution to the non-resonant background were performed with the assistance of a confocal/scanning/imaging system. The setup allowed direct examination of individual particles for precise determination of SERS activity. It was designed such that the focal point of the monochromator/ camera leg mirrors that of the APD focal plane by the use of a small slit in the emission path, and a 50 micron multi mode fiber coupled to the APD (Figure 5.1.2A). Thus we are able to obtain a spectrum from the same single entities revealed by the confocal scan, while retaining spatial and temporal information about the particle (Figure 5.1.2 B).

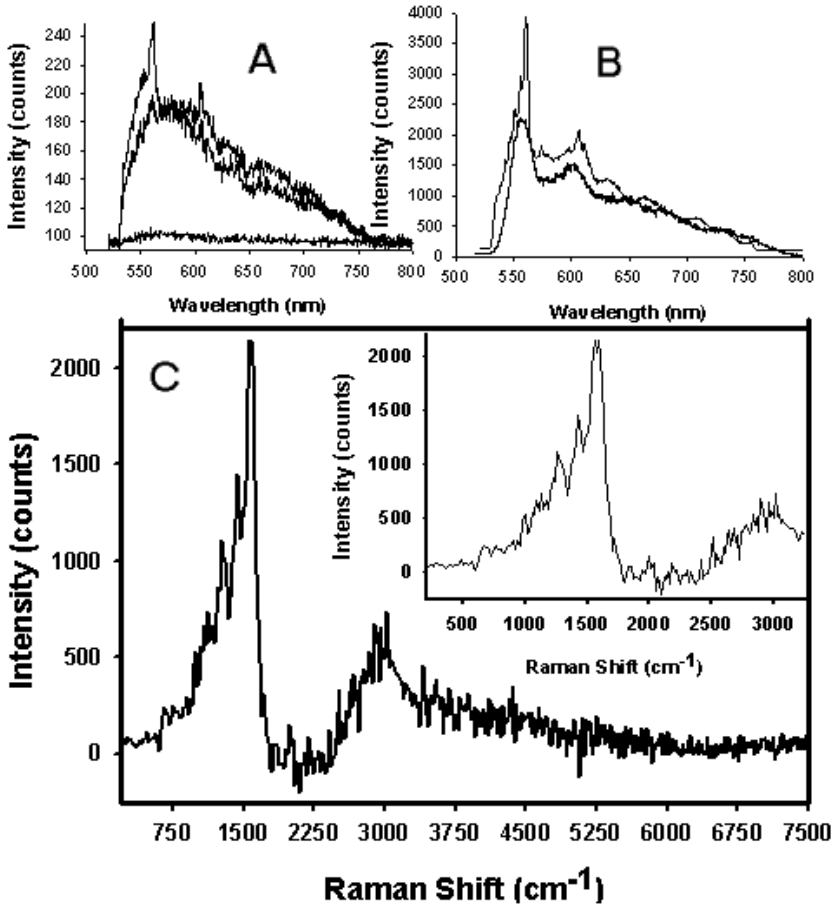

Figure 5.1.1. Raman spectra from thin silver films with underlying background fluorescence at both (A) low (300W/cm^2) and (B) high (50,000W/cm^2) excitation intensities. Blinking of both fluorescence and Raman together is shown in (A). Due to the low resolution monochromator used, many Raman peaks are poorly resolved but this enables collection of the entire spectrum. (C) A background-subtracted spectrum with the "fingerprint" region for Rhodamine as the inset. All exposure times were 2 sec.

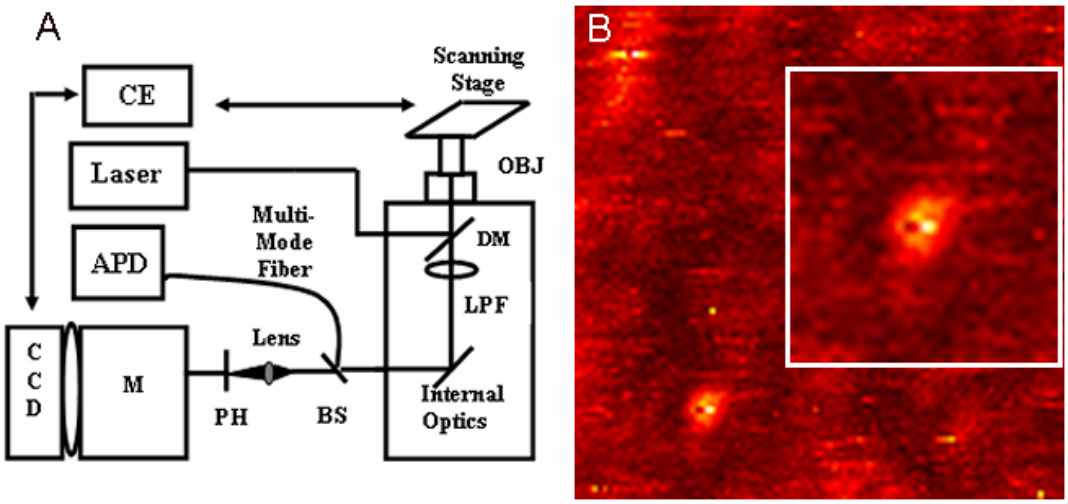

Figure 5.1.2. 5 micron square confocal scan of an evaporated silver island film (~16 nm thick). Two particles can be seen, though the top left molecule appears to have blinked off or bleach during the scan time. The bottom molecule is expanded in the inset to show the intermittency in fluorescence in time. The dark spot in the center indicates that the molecule blinks during the scan. The scan rate is 500ms / pixel.

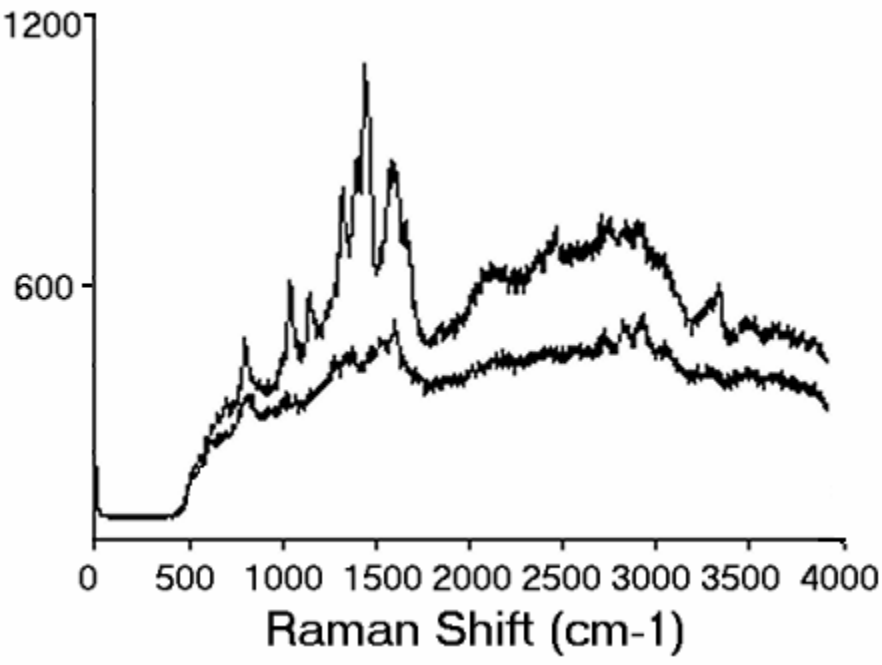

Figure 5.1.3. Example of a Raman spectrum obtained from a bulk silver film in the absence of any rhodamine or otherwise added analyte molecule. The lower trace shows that the Raman still appears on top of a fluorescent background, but similar to the previous figure, the Raman has not been seen to appear without the background. These suggestive experiments prompted further exploration on a better controlled system.

Results demonstrated that even with no analyte present, strong Raman spectra were still observed with the same underlying fluorescence (Figure 5.1.3). Experiments proceeded to further characterize this interesting result on the single particle level, but film based experiments proved too “dirty” to accurately characterize the system.

Coupled with reports over the last few years detailing the interplay of Ag_n fluorescence [34] with SERS of analytes bound to partially cationic Ag_n nanoclusters,[39, 40] these experiments established a solid foundation with which to continue investigating the role of the silver nanoclsuter in SERS. The film based experiments are the precursors to the current work presented in the rest of this thesis. Since spectral features such as these are often more easily seen on the bulk level, it is possible that none of the current spectroscopy on the encapsulated dendrimer/peptide system would have been done if not for early insights on silver films.

5.2 Dark-Field Microscopy as a means to confirm the small size of the Raman emitting features

As a cleaner system to study Raman, Jie Zheng has recently devised solution based routes to producing small, 2-8 atom nanoclusters within both PAMAM G4-OH and G2-OH dendrimers (fourth- and second-generation OH-terminated poly(amidoamine)) [36] and short amine-rich peptides known to interact with metal ions (AHHAHHAAD). [41] Exceedingly strong, multicolored single molecule fluorescence is observed from the distribution of small silver

nanoclusters with excitation spectra for all nanoclusters peaking at ~475 nm, [35] essentially independent of emission wavelength. Any large nanoparticles that may have been produced are removed through centrifugation at 13,000 RPM for one half hour before study. No plasmon absorption (~400-nm) is seen from these small particles indicating they are smaller than a nanometer in size. Further, none of the fluorescent species from the sample scatter light when observed with dark-field microscopy, indicating the complete absence of large nanoparticles in the sample. Although the strongly emissive species are 2-8 atom nanoclusters as confirmed by mass spectrometry, [36] to provide an additional upper limit on nanocluster sizes, Jie synthesized nearly monodisperse (as determined by transmission electron microscopy) 4-nm diameter Ag nanoparticles in PAMAM [42] and also thiol-encapsulated 1.8-nm Au nanoparticles, both of which are clearly observed with dark-field microscopy and removed from solution by centrifugation. Consequently, any feature observed that does not correlate with dark-field scattering must be smaller than 1.8 nm and should correspond to our 2-8 atom nanoclusters if the emission is similar to that previously reported. [34-36]

Simultaneous dark-field microscopy, wide-field fluorescence and fluorescence/Raman spectra of features within the same field of view were collected on a high-sensitivity CCD through a 300-mm imaging monochromator on the side port of an inverted microscope with either a mirror (for imaging) or a 600 l/mm grating rotated into the emission light path. Raman spectra were collected upon excitation from various lines of an Argon-Ion laser with an inverted fluorescence microscope in an epi-fluorescent configuration (Olympus). A small

drop of the aqueous nanocluster solution was imaged on a cleaned glass coverslip – dried and solvated samples produced indistinguishable results. The lack correlation between dark-field and single molecule fluorescence microscopy images of the same field of view directly demonstrate that the strong peptide- (Figure 5.2.1 A,B) and dendrimer- (Figure 5.2.1 C,D) encapsulated Ag_n nanocluster emission does not arise from nanoparticles, but instead only from these sub-nm Ag nanoclusters.

5.3 Resonant Raman scattering from small silver nanoclusters

Surprisingly, when excited with narrow-band laser illumination, Raman scattering is observed from both samples at the single molecule level with unique scaffold-specific spectra (Figure 5.3.1). Of note is that the spectra are neither from highly polarizable dyes, nor do they result from interactions with large plasmon-supporting metal nanoparticles, but are signatures of protein backbones and amino acid residues *without* attached fluorophores. The measured single-molecule level excitation shows the maxima of both systems appears at ~475nm. Since this corresponds to resonance, we investigated whether such intense, matrix specific single molecule Raman could also be seen when excited with this wavelength. The result is presented with the measured single particle excitation spectrum presented in Figure 5.3.2. 476nm-excited Raman is easily seen from both peptide and dendrimer encapsulated Ag_n, seemingly with very little difference to the 514.5nm excited spectra.

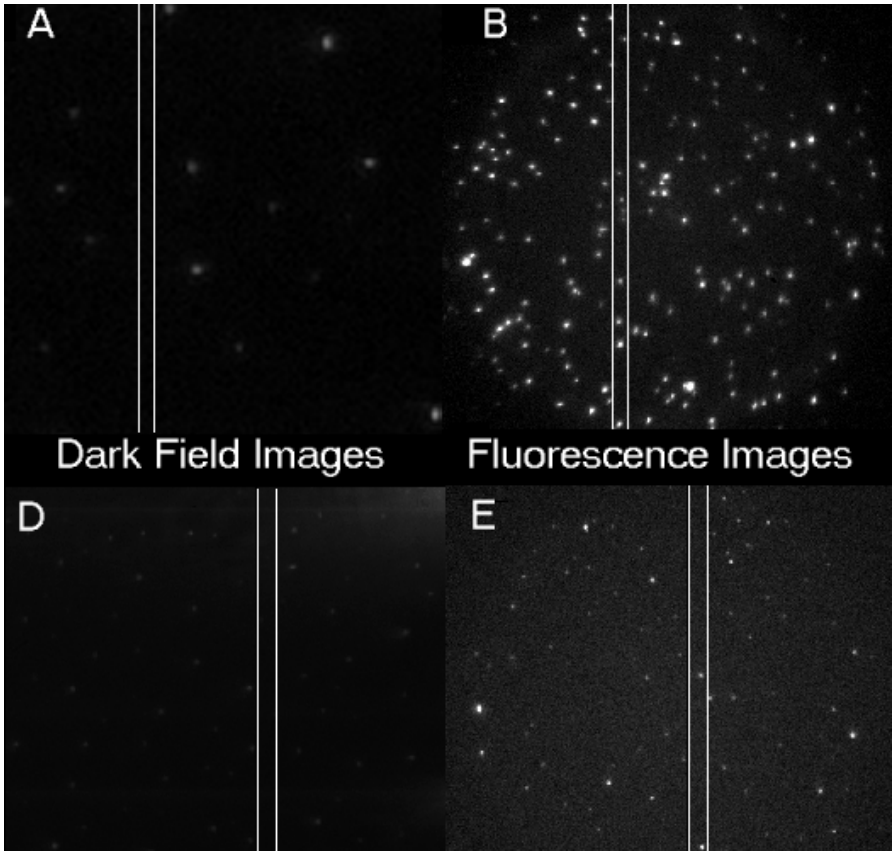

Figure 5.2.1. Dark-Field and stokes shifted emission from encapsulated small silver nanoclusters. Both peptide (A, B) and dendrimer (C,D) exhibit un-correlated Dark field and (A,D) and Stokes shifted emission (B,E) images of the same field of view. The white lines represent the entrance slits of the monochromator for spectral measurements. Images here correlate with spectra in Figure 5.3.1.

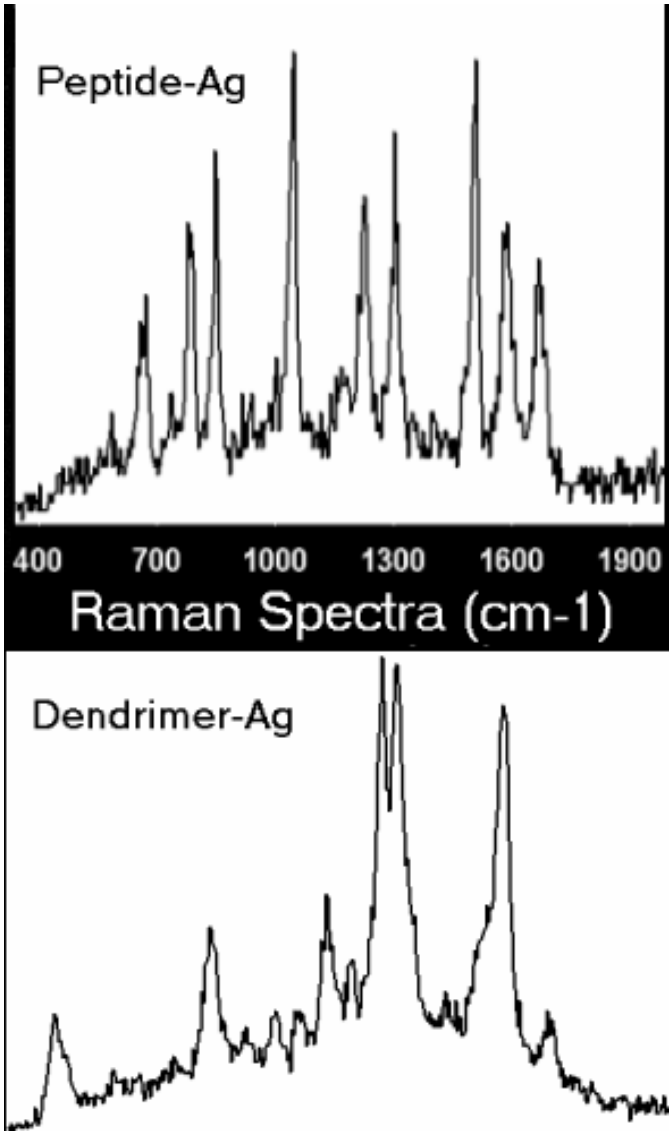

Figure 5.3.1. Scaffold specific single molecule Raman in complete absence of any analyte molecule of plasmon supporting nanoparticle. The spectra arise from clusters not detectable with dark-field spectroscopy, indicating the extremely small size.

Often considered evidence of single molecule behavior, emission intermittency in both the fluorescence and Raman is readily observed. Such stochastic intermittency will disappear into noise at the level of even several emitters within a given probe volume. The Raman spectra in Figure 5.3.1 suggest that the scaffold Raman spectrum is measured on top of the strong Ag_n nanocluster fluorescence. Because individual molecule Raman spectra are known to shift with dynamic relative intensities, the sum of 100 single dendrimer Raman spectra was compared to the summed spectra of 100 peptide encapsulated Ag nanoclusters, thus accounting for any spectral shifts arising from environmental differences. All fitting was carried out with the use of the built-in "multi-peak-fit" algorithm in IgorPro software. This allowed accurate determination of peak positions, as well as independent fitting of the fluorescent background which clearly is similar in both the peptide and dendrimer samples (Figure 5.3.3 A). However, the sharp peaks are unique to each scaffold (Figure 5.3.3 B,C). As broad nanocluster fluorescence is unchanged and only the scaffold differs, the background arises from Ag_n fluorescence while the SM-Raman is characteristic of the scaffold. In fact, our single dendrimer Raman spectra (Figure 5.3.4) are consistent with the recently reported ordinary bulk PAMAM Raman spectrum. [43]

5.4 Spectrally selected fluorescence lifetime measurements

Using frequency doubled Ti:sapphire laser (890 nm center frequency, 84 MHz, ~200 fs) excitation at 445 nm (10-nm bandwidth), we probed the

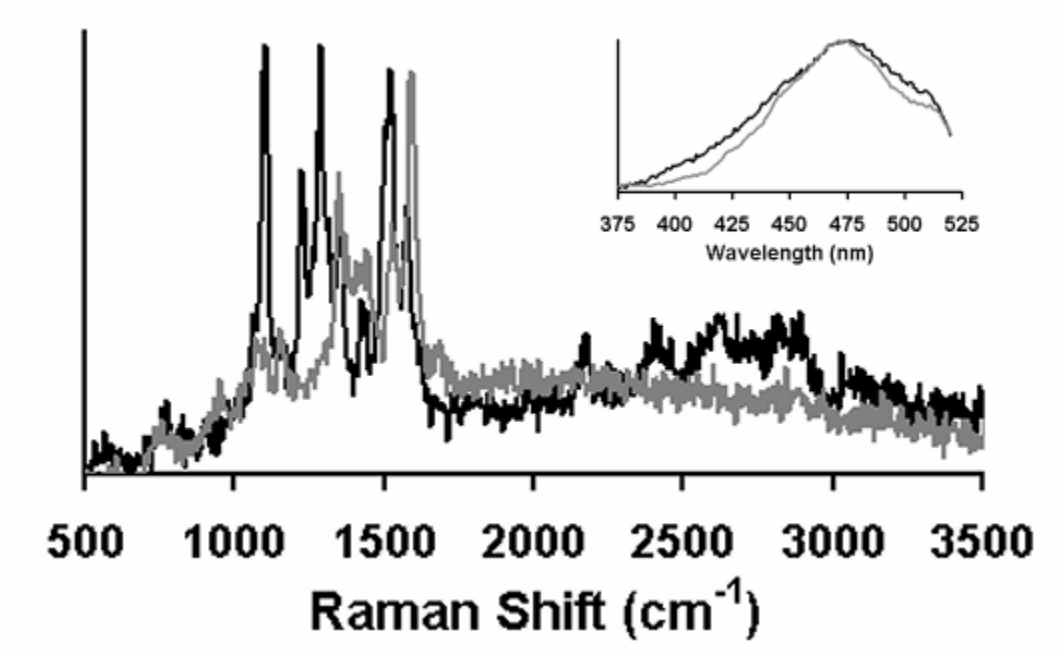

Figure 5.3.2. On- resonance (476nm excited) Raman spectra for both peptide (gray trace) and dendrimer (black trace) Ag_n. Inset: Room-temperature ensemble excitation spectra were collected through an excitation wavelength scanning monochromator - equipped scanning inverted optical microscope (Zeiss Axiovert 200) in an epi-fluorescent configuration. Samples were short-pass excited (<520nm) and long pass emission was collected (>535 nm) with an exposure time of 500ms/nm.

wavelength dependent lifetimes of the peptide- and PAMAM-encapsulated nanocluster emission (see setup, thesis section 2.5). Instead of imaging with a CCD, light was diverted to a multichannel plate photomultiplier tube (MCP-PMT) at the side port of the monochromator, which with time correlated single photon counting electronics (Becker-Hickl SPC-630), exhibits an instrument response of 35ps. After deconvolution, we obtain reliable fluorescence lifetimes down to 7 ps.

Lifetime measurements within 10-nm bandwidths selected through the monochromator yield instrument response-limited lifetimes for all emission shorter than 500 nm. Wavelengths longer than 500 nm give time responses longer than the instrument response which fit to single component decays of ~ 30 ps (Figure 5.4.1). The results are summarized in Table 5.4.1. A longer second component is also measured, but is directly attributed to measured background from plain cover glass at each wavelength range. An instrument response was taken every time a lifetime experiment was carried out. Accounting for the pulse width, all Raman lines in the fingerprint region would be expected below 500 nm (~2200cm^{-1} shift), consistent with the instrument response-limited, effectively instantaneous time response of the emission. Once sufficiently shifted away from the excitation line to avoid Raman processes, the lifetime becomes a very fast, but measurable ~30 ps corresponding to the broad fluorescent Ag nanocluster background on which the sharp Raman lines appear. As an indicator of the connection between the connection of ground and excited states from which the lifetime is measured, these lifetimes not only indicate very fast dynamics, but also

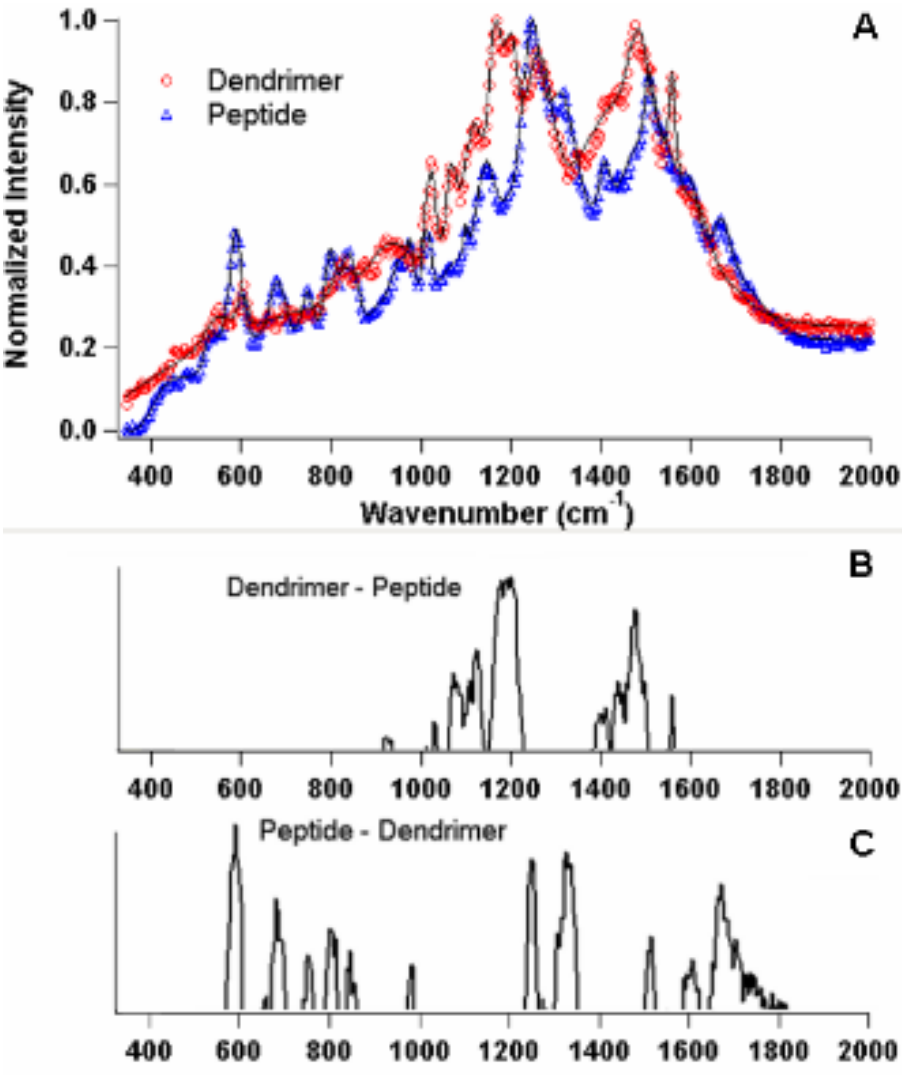

Figure 5.3.3. Scaffold-specific single molecule Raman spectra. (A) Summed Raman spectra from 100 PAMAM- (o) and 100 peptide- (Δ) encapsulated nanoclusters. Spectral subtractions remove the similar Ag nanocluster fluorescent background, and yield characteristic dendrimer (B) and peptide (C) Raman lines when only positive peaks are retained for each subtraction order.

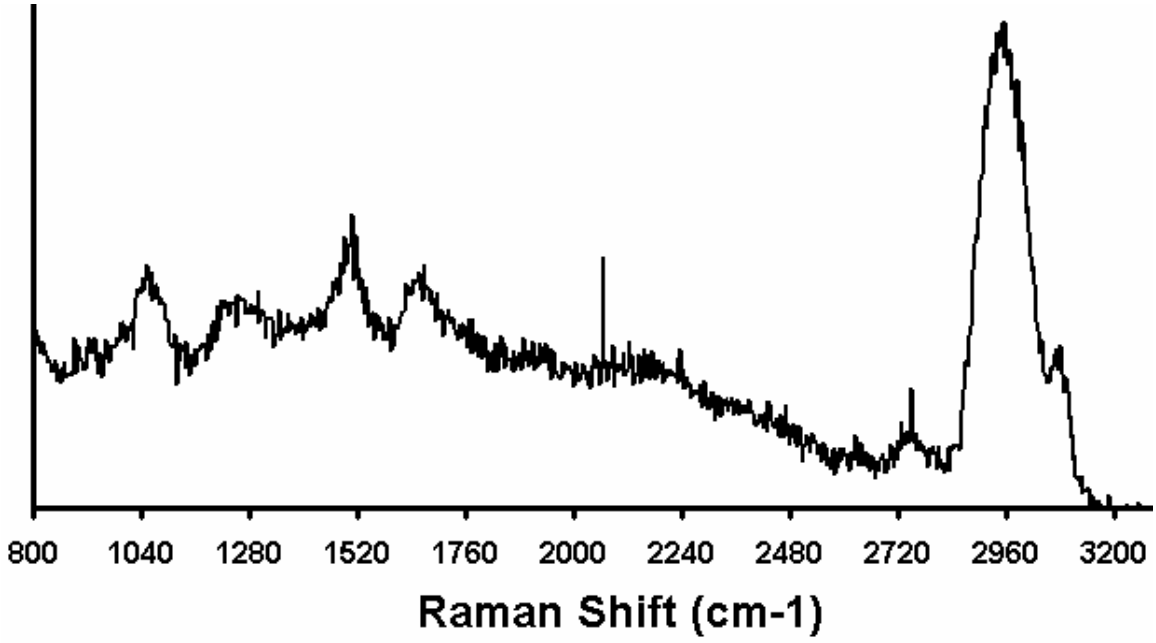

Figure 5.3.4. Raman scattering spectrum from the dendrimer solution in the absence of any silver nanocluster being present. Extremely weak, this was collected under 514.5nm excitation with a 60 second integration with a 150l/mm grating at an intensity of ~30 W/cm^2.

suggest an extremely close connection between the two states, pointing toward a large transition moment and high polarizability in these small nanoclusters again in the absence of a supporting nanoparticle. Further, both the spectrally selected and bulk lifetimes for the peptide- and dendrimer- encapsulated samples differ statistically from one another (Figure 5.4.2) further confirming the that the host matrices are dynamically different from one another with respect to their encapsulation of and interaction with the same Ag_n species. Although it has been reported that nanocluster binding inside dendrimers may involve the amine, [43] this remains to be investigated with this specific peptide sequence. This could also be a function of the nanocluster size in various matrices since the dendrimer encapsulated systems shows no fluorescence when excited with light in the UV (~350nm) range while the peptide sample does. This would indicate smaller cluster sizes being more prevalent in such a system (Figure 5.4.3), as indicated by the low-temperature trend that red-shifted absorption wavelengths correspond generally to larger cluster sizes [44].

5.5 Antibunching of silver nanocluster fluorescence

Figure 5.5.1 A shows pulsed-excitation antibunching data for a well-known single quantum system, Cadmium selenide rods (CdSe, provided by Dr. Mostafa El-Sayed). The antibunching feature shown here (and for other systems) is described well by the minimum $g_2(t)$ at t=0 as described in section 1.8 and performed with the setup in section 2.7. Error is due in part to jitter of the APD's

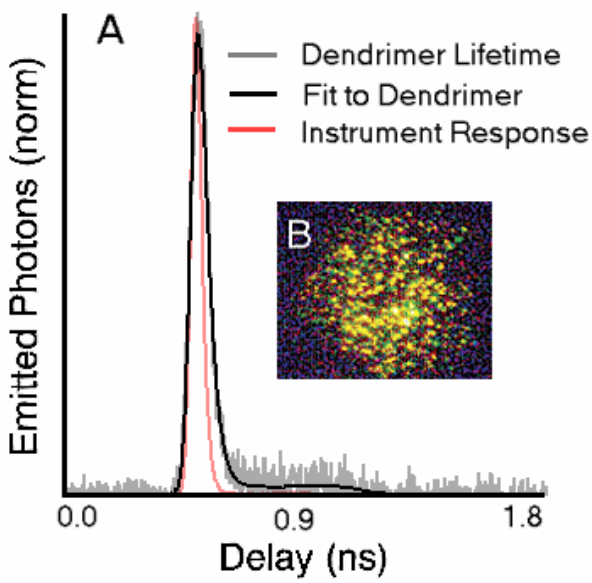

Figure 5.4.1. Typical single exponential fit to a silver nanocluster fluorescent lifetime. In red, the ~35ps instrument response function (IRF) is clearly shorter than the measured lifetime decay of the sample (gray trace). The fit yields a ~30 ps lifetime (black line).

Table 5.4.1. Summary of spectrally selected fluorescence lifetime data for both the peptide and dendrimer encapsulated samples. All fitting to single exponentials as in Figure 5.4.1, the data taken within ~50nm of the excitation wavelength (here, ~420nm) is limited to the instrument response due to Raman scattering occurring in those areas. Percentages represent relative amounts of that spectral component in the sample. Once shifted past about ~650nm, very little signal is collected, due to PMT insensitivity, but a measurable lifetime is still discernable. The "all" column represents data taken with a mirror rotated into the path in order to properly gather all components through the visible where any radiative lifetime can be measured.

	Peptide		Dendrimer	
	Intensity	T1(ns)	Intensity	T1(ns)
480 nm	99%	0.009	97%	0.011
495 nm	99%	0.008	96%	0.011
510 nm	97%	0.008	99%	0.025
525 nm	89%	0.011	93%	0.029
540 nm	87%	0.013	89%	0.031
555 nm	88%	0.017	90%	0.035
570 nm	59%	0.016	95%	0.035
585 nm	18%	0.023	86%	0.040
600 nm	10%	0.019	70%	0.029
615 nm	7%	0.024	43%	0.038
630 nm	4%	0.062	21%	0.037
645 nm	2%	0.108	36%	0.078
ALL	55%	0.018	76 %	0.033

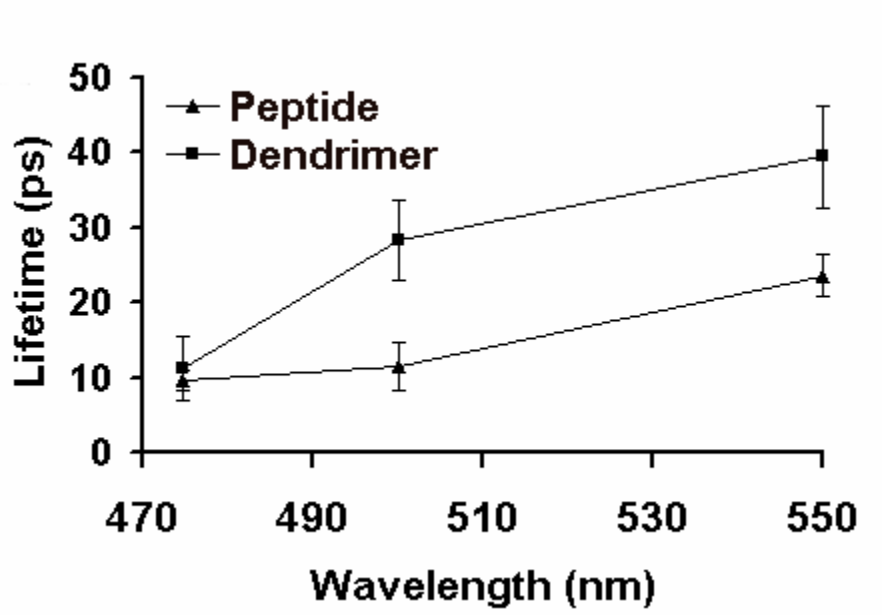

Figure 5.4.2. Statistical differences showing that the peptide and dendrimer systems have different overall fluorescence lifetimes. Averaged over 5 trials, the error bars represent confidence limits of 95%. Averages for the peptide fall at ~18ps while those of the dendrimer at a measurable higher ~33ps.

(~1.1ns total error - 1ns for one, and 0.4ns for the other). Though the jitter severely limits the depth of the zero delay feature, the system lifetime (~4 ns) is not significantly longer than the detector error (1.1ns) which also contributes. A simulation of the depth of the zero delay peak accounting for the 1.1ns jitter indicated that the dip should be about 0.6. The ideal case for pulsed excitation is in thesis section 1.8. The baseline in this experiment (Figure 5.5.1, A) is not flat because the lifetime is comparable to the repetition rate of the laser (~12ns) and therefore shows some cut-off.

The finite lifetime of the measured surface-bound silver nanoclusters however, suggests that if indeed Raman enhancement and the fluorescent background arise from excitation of an individual Ag nanocluster, fluorescence antibunching should be observed, once shifted sufficiently far to avoid all Raman processes. Using a 590-nm long pass filter with 445 nm excitation, all possible Raman transitions and any background fluorescence from optics are avoided and antibunching from the small amount of Ag nanocluster emission that remains is clearly observed (Figure 5.5.1 B). Unfortunately, due to Ti:sapphire excitation exciting significant background fluorescence from the internal microscope optics, more than 90% of the total emission is discarded in order to perform these antibunching experiments, thereby severely limiting the contrast. With short pulse excitation, only one photon can be emitted per excitation pulse if each pulse is extremely short relative to the nanocluster lifetime. Measured as arrival time histograms between photons arriving on two high sensitivity avalanche

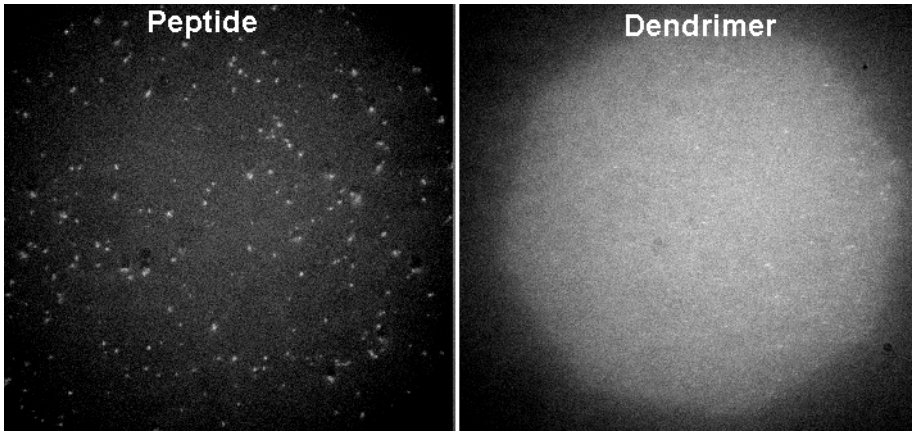

Figure 5.4.3. Hg lamp UV-excited fluorescence collected with a ~420lp filter shows much resolvable more fluorescence in the peptide sample collected at a three second exposure time than does the dendrimer which is basically auto-scaled background to better show the contrast).

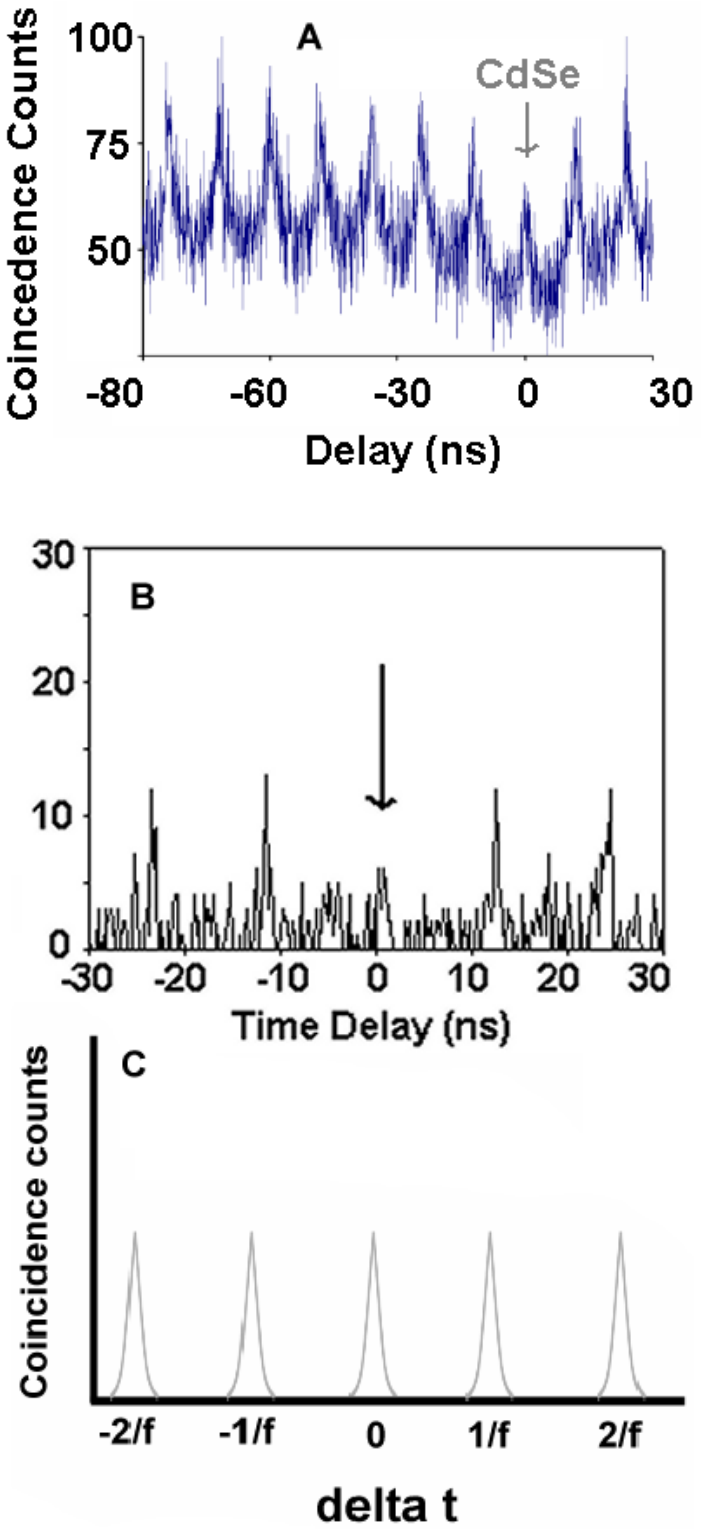
A
CdSe
Coincedence Counts
100
75
50
-80
-60
-30
0
30
Delay (ns)
B
30
20
10
0
-30
-20
-10
0
10
20
30
Time Delay (ns)
C
Coincidence counts
-2/f
-1/f
0
1/f
2/f
delta t

Figure 5.5.1. (A) Antibunched emission from a sample CdSe nanorod system excited with ~400nm (1.4kW/cm^2) from a Ti:Sapphire laser. Due to the single quantum nature of this system and its long lifetime relative to the pulses of the laser (~200fs), this sample shows a representative, albeit still weak antibunching signature and provides an estimate of where the zero delay peaks should show up on the small silver samples. Photochemically much less stable than our silver samples, the CdSe data had to be collected using a scanning stage (Nanonics) and adding together the signals from hundreds of molecules. Under pulsed excitation, the probability of detecting two photons at the same time should be zero if the pulse width is significantly shorter that the excited state lifetime (see ideal case section 1.7). However here, Raman signals are broadened beyond discernable levels with pulsed, broad bandwidth (~10-nm) excitation so short pulse (~200 fs) Ti:Sapphire laser excitation was necessary to collect the antibunching signal due to the very short-lived (30 ps) emission, while retaining overlap with the excitation profile. Shifting far away to avoid Raman while highly filtering the sample to avoid any background issues, the attenuated data in trace (B) was collected. Figure 5.5.1 C shows an ideal case for a classical system where all peaks have equal intensity building up at the periodic repetition rate of the excitation laser.

photodiode detectors in a Hanbury-Brown and Twiss interferometry arrangement, [45] such histograms are an excellent approximation of the true intensity autocorrelation function at short times. [46, 47] The long wavelength portion of the nanocluster emission exhibits a reduced intensity at zero inter-photon arrival delay due to two photons having zero probability of being simultaneously emitted by a single quantum system, thereby proving that emission is from a single nanocluster. This reduced feature only appears at zero delay and cannot be observed at wavelengths where Raman is present because of its instantaneous nature. In contrast, a classical system (i.e. large number of independent emitters) would display peaks that build up in equal intensity everywhere (Figure 5.5.1 b). This confirms for the first time that Raman can be definitively observed from a single molecule system and concurrently, that individual Ag nanoclusters enhance Raman scattering well above observable single molecule levels. These nanoclusters are also likely a source of the commonly observed, but overlooked, non-resonant background in SM-Raman experiments employing Ag nanoparticles and roughened silver films.

5.6 Observation of antistokes shifted Raman

Observed when a system is already in an excited state, the interaction of laser radiation with the populated system can also cause a downward transition from higher to lower energy resulting in an emitted photon at *higher* energy than that of the incident radiation (anti-stokes shifted). With respect to Stokes shifted transitions, A-S transitions are rarely studied because of their inherent weakness,

unless very small shifts in wavenumber are considered as the thermal population of the excited state decreases exponentially with energy as given by the Boltzmann distribution. Though the direct study of A-S shifted peaks study may be limited by low population, the intensity ratio of stokes to antistokes peaks provides important temperature information about a system in accordance with a Boltzmann distribution of excited state populations [48] (Equation 5.6.1).

$$\frac{I_{stokes}}{I_{antistokes}} = \frac{(\upsilon_0 - \upsilon_m)^4}{(\upsilon_0 + \upsilon_m)^4} e^{hc\upsilon_m / kT} \qquad (5.6.1)$$

In (5.6.1), υ_0 is the frequency of the laser, υ_m, is the vibrational energy of a Raman band of the system, *h* is Planck's constant, and *c* is the velocity of light.

Antistokes spectra in our system are excited at the same 30W/cm^2 intensities at 514.5 nm and are collected at 10 second exposures through a short pass dichroic mirror and emission filter to image the higher energy emission. Stokes and antistokes emission from the exact same encapsulated nanoclusters are measured by switching filters within the microscope filter turret during the same data set. The Raman transitions are so surprisingly strong that the antistokes lines are readily observed on the single molecule level for both the

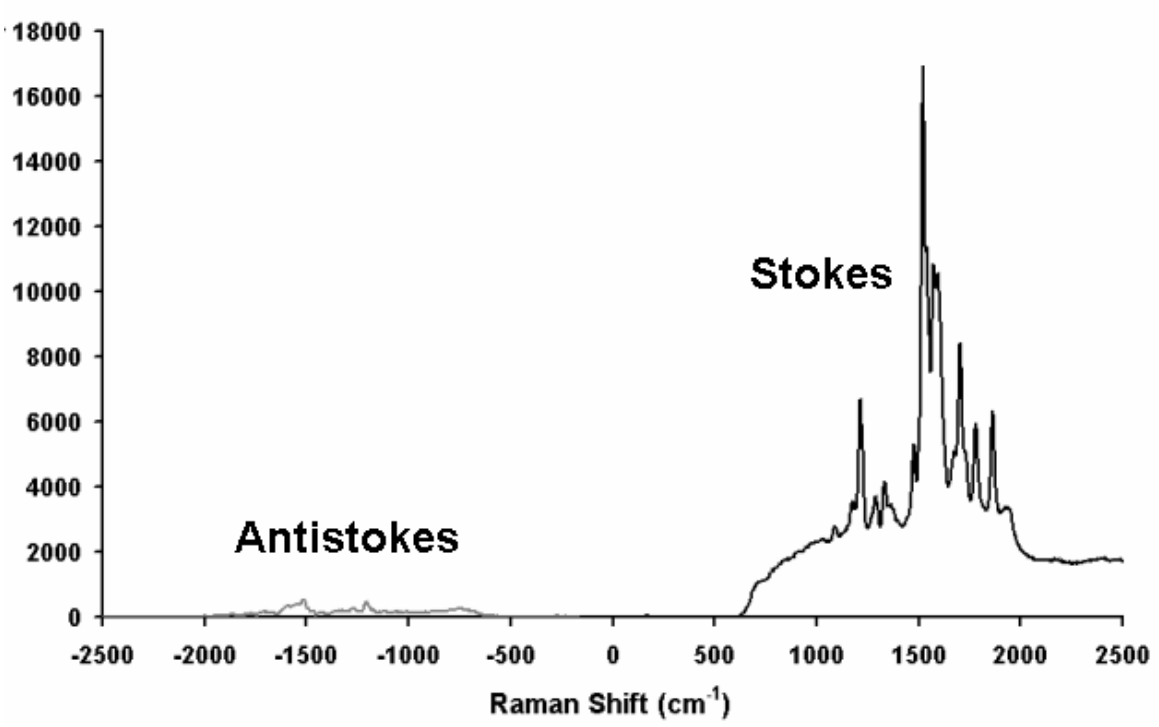

Figure 5.6.1. Typical scaling differences between measured stokes and anti-stokes emission from the same nanocluster. The measured antistokes emission intensities are about 1/30th than that of the stokes -shifted emission. The above example is from a dendrimer encapsulated sample excited at ~30W/cm^2 and collected for 10 seconds.

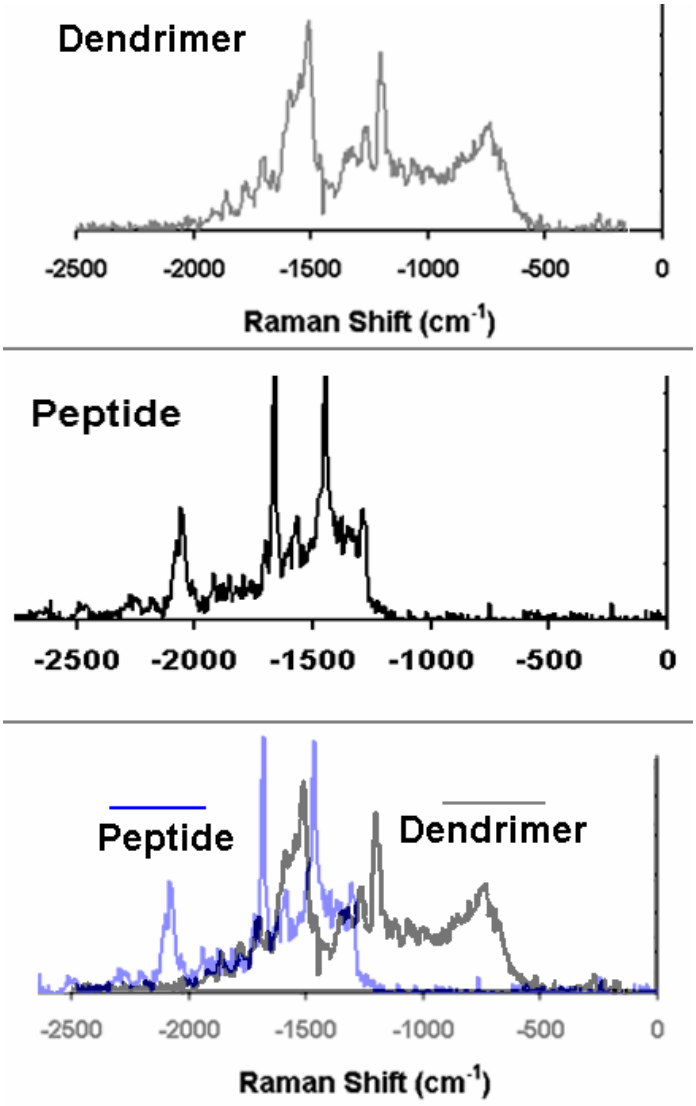

Figure 5.6.2. Scaffold dependent antistokes emission. Much weaker compared to stokes when excited at the same intensity, both systems still yield measurable antistokes spectra that are comparable in intensity. The lower panel overlaps the two and again displays scaffold dependent behavior.

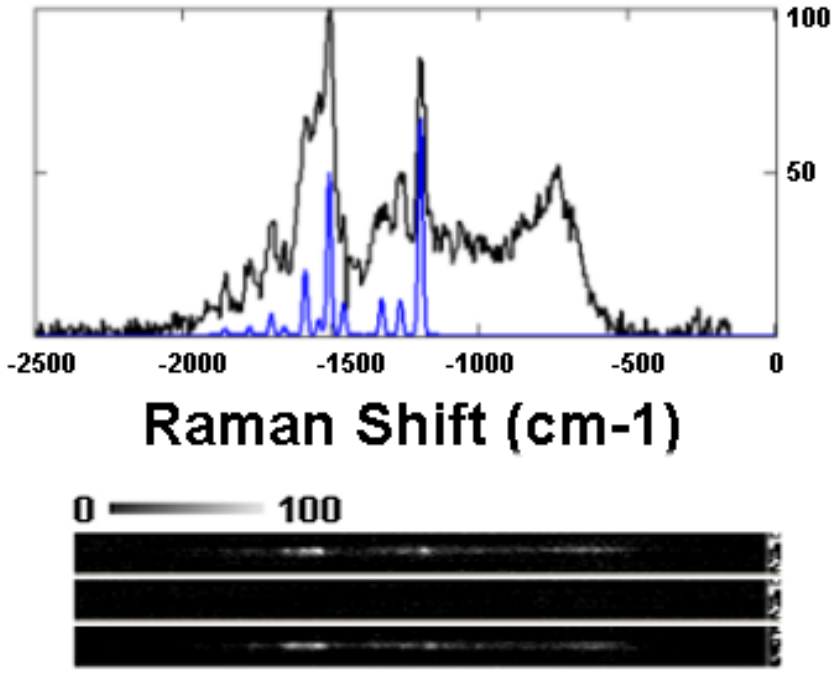

Figure 5.6.3. Simulated Boltzmann weighting of the antistokes spectrum in Figure 5.6.1 suggests thermal population of higher vibrational levels with correct relative intensities. (C) Shown for three successive 10-sec frames, intermittency of the antistokes emission is also readily observed further indicating single molecule behavior especially when taken together with the measured antibunched emission from its stokes-shifted counterpart.

peptide and dendrimer systems, with drastic differences in scaling as compared to the Stokes shifted lines (about 1/30th stokes intensity) (Figure 5.6.1).

Exhibiting identical shifts to the stokes-shifted transitions, they are also scaffold-dependent (Figure 5.6.2). Since, consistent with a Boltzmann distribution of thermally populated vibrational levels, a simulation was necessary to determine if the observed AS-spectrum was due to thermal energy, or an alternative mechanism. At 1/30th of the strength of the Stokes shifted lines, these higher energy transitions nicely mirror a thermal distribution of excited vibrational state populations in the scaffold with correct relative intensities (Figure 5.6.3), as the intensities of the stokes transitions were used in simulation. They also provide a single molecule temperature measurement as explained above. The thermal population of each AS-Raman state also exhibits intensities that are comparable to single molecule fluorescence from the best organic dyes available. They blink, and occur on top of a very weak background of currently unknown origin, which again confirms the single molecule nature of the scaffold-specific Raman information.

This is the first observation of single molecule antistokes Raman and should provide opportunities for true background free windows for biological imaging by measuring emission at *higher* energy than the excitation. [49] With the antistokes signal being ~1/30th of the stokes lines, antistokes Raman transitions reflecting the thermal populations of each state exhibit intensities comparable to standard single molecule fluorescence from the best organic dyes. Again, as

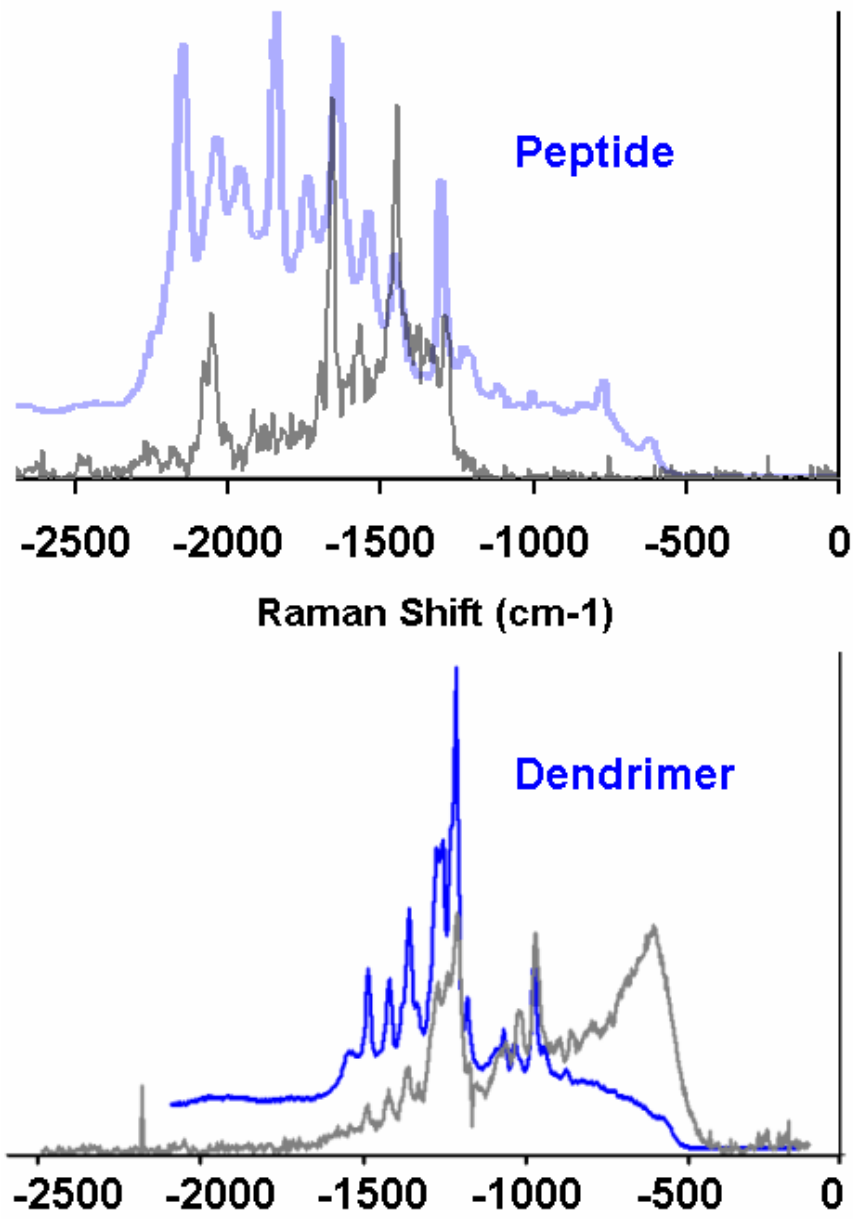

Figure 5.6.4. Both systems exhibit direct overlap of their measured stokes and antistokes spectra. Here they are presented overlapped on the higher energy axis for clarity since the AS-spectra are so comparably weak.

observed with the stokes-shifted lines, the SM-antistokes of the peptide and of the PAMAM are distinctly different and the frequencies of each matches up perfectly with their respective stokes-shifted counterpart (Figure 5.6.4). All Raman lines and fluorescent backgrounds are also observed when excited closer to resonance at 476 nm (e.g. Figure 5.3.2).

5.7 Potential mechanisms

The observed total Raman absorption cross sections are comparable to those observed for Ag nanoclusters on roughened thin Ag and AgO films as well as those encapsulated in PAMAM dendrimers in solution ($\sigma = 10^{-14}$ cm^2) [34, 36]. Accordingly, both the SM-Raman and Ag_n fluorescence likely stem from initial Ag nanocluster electronic excitation. Since the laser excitation is well overlapped with the electronic absorption of the silver nanoclusters, [50] a type of resonance or pre-resonance enhancement likely occurs, but without plasmon enhancement as our few-atom Ag nanoclusters are too small to support such a collective electron oscillation. As metal nanoclusters are highly polarizable [51-54] and exhibit giant resonances in their gas phase photofragmentation spectra, [55] it is possible that a predissociative process is accessed in the excited state leading to significant transfer of charge to the scaffold similar to the models presented in section 1.5. While the scaffold stabilizes the Ag nanocluster and prevents photodissociation characteristic of gas phase Ag_n, [51-55] a large excited state charge separation most likely produces the large oscillator strength, fast radiative lifetime, and Raman-enhancing ability of these few-atom nanoclusters. Consequently, while not well-

understood at this time, the Raman transitions seem to “piggy-back” off the strong Ag nanocluster optical transition to yield the strong SM-Raman signals. A potential mechanism based on current literature is discussed in the context of the presented results next.

In general, Raman-exciting lasers are selected below the first electronically accessible state of the molecule. However, since the excitation energy of the laser at 514.5nm in our experiments is well-overlapped with the electronic structure of the silver nanoclusters [50], a type of resonance or pre-resonance enhancement may occur. As mentioned, this is not a surface effect, nor are these large enough metal nanoparticles to support a plasmon of their own capable of generating the polarizibility necessary for such large Raman enhancements. It is known in the literature that small silver nanoclusters of 2 to 8 atoms have well characterized oscillator strengths, and demonstrated by our group that the magnitude of the cross section is extremely large ($\sigma = 10^{-14}\,cm^2$). This combination would allow sufficient oscillator strength to assist a resonance Raman transition yielding an enhancement of ~10^{14}, [56] but still lacks the needed change in polarizibility and cannot account solely for the intensities reported.

Continuous laser excitation of Ag_n nanoclusters above the gas phase dissociation energy (~2.2 eV for Ag_2) results in a continuously changing geometry in clusters from 2-8 atoms [34]. Reports of large resonances associated with the coupling of the electronic motions of nearly-free s and localized d-electrons of small silver clusters [55] makes it feasible to assume that there is a large polarizability present with differently sized clusters as they move toward

dissociation. In fact, specifically with the gas phase complex Ag_2 (and other small metal clusters in the gas phase) [51-55] a large separation of charge is observed when the cluster is in a pre-dissociative state, allowing for a large polarizability. Since classically, Raman selection rules mandate a change in polarizability of the material during a transition, this pre-dissociative state may be the key connecting the large oscillator strength of small silver clusters with the largely enhanced Raman spectra of the host matrix.

During scattering, the Ag nuclei experience forces associated with excited state potential energy surfaces and move from their equilibrium positions, leaving the molecule in a vibrationally excited state. The more the bond is stretched, the greater the shift in frequency of the scattered photon will be. Since overtones and state-mixing can be particularly prominent when the motion on the excited PES corresponds to a particular vibrational mode of the ground state for Ag_n (the beginning of bond-breaking motion, leading to photo-dissociation) complex and different Raman spectra can be observed [57, 58]. As resonance Raman benefits from strong Franck-Condon overlap, theoretical studies have shown and independently compared to experiment that geometry changes from small clusters (Ag_n n= 2 – 4) contribute to large F-C overlap, specifically from linear to bent structures [52, 59].

Bonding in coinage metal (Au,Ag,Cu), dimers for example, primarily involves the valence *s* electrons. However, the (n-1)*d* shell is also fully occupied thus contributing very little to the bonding characteristics of the metal. It should not be overlooked however, that *np* orbitals *are* available, and have energies

close to the valence *ns* orbitals. Thus the indication that dissociation (and pre-dissociation) energies increase simply with size is not valid, suggesting why the intensity profiles of the observed Raman peaks are not consistent with either absorption profiles or wave packet dynamics of excited state transient clusters of similar size[52]. Due to their varied geometries, different sized encapsulated silver nanoclusters will interact differently with the excited state PES of the peptide and the dendrimer matrices due to this electronic structure alone (ground state atoms with closed d-shell and single s-valence electron), possibly giving rise to such dynamic resonant Raman scattering [53]. Additionally, the encapsulated nanoclusters display extremely short fluorescence lifetimes (~30 ps) which increases slightly over their entire spectral range (Figure 3). The short lifetime together with the strong oscillator strength of the silver clusters, and the lack of a plasmon indicates a very strong coupling between the ground and excited states. This strong transition moment connecting the two then creates a direct pathway for the demonstrated resonance Raman to occur between tightly connected electronic states.

The existence of polarizibility in a predissociative (versus completely dissociative) state is also supported by the observation of fluorescence in these systems. Stokes-shifted Raman spectra are almost always observed superimposed on a fluorescent background as in figure 5.3.3. If the excited state nanocluster wave packet were to continue along the excited state PES of the peptide or dendrimer and cross over to a completely dissociative state, it would break apart and no fluorescence would be seen. However, we believe it is the

existence of the surrounding matrix that may stabilize the nanoclusters after experiencing a pre-dissociative state by changing the PES crossing toward preferential fluorescence recombination. The induced charge separation is sufficient to induce a Raman transition between the intermediate and final electronic states, depositing vibrational energy into the molecule, but subsequently being pulled back down the excited state PES via stabilization of the surrounding matrix. Fluorescence may then still be generated by the intact nanocluster, that may be comparable with luminescence previously reported [35, 36, 60].

5.8 Conclusions

In the absence of a large, plasmon-supporting nanoparticle or conjugated analyte system, dendrimer and peptide-encapsulated sub-nm silver nanoclusters produce strong, single molecule resonance - enhanced Raman scattering. Matrix dependent strong stokes, and weaker but observable antistokes scattering signatures are also observed from even the same individual nanocluster, the first such observation of emission from higher energy excitation on the single molecule level. Background fluorescence and fluorescence intermittency (blinking) characteristic of single molecules are simultaneously observed, while weak antibunching of the emission in the fluorescent background directly confirms the single molecule nature of the emissive species. As the nanoparticle is unnecessary for single molecule Raman, these Ag nanoclusters may enable

unprecedented sensitivities in biolabeling with high-brightness, narrow-band, unbleachable signals.

The observation of SM Stokes- and antistokes-shifted Raman without a nanoparticle offers new insights into the nature of SM-Raman. The combination of few-atom Ag nanocluster- enhanced Raman signals of the encapsulating peptide suggests unparalleled opportunities in biolabeling by imaging either the stokes or the antistokes emission of designed Ag-binding peptide sequences. The observation of antibunching from the underlying Ag nanocluster emission definitively proves that emission arises from individual molecules and begins to help us understand possible Raman-enhancement mechanisms enabled by these molecular Ag nanoclusters. The extremely high oscillator strength of these sub-nm nanoclusters presents many possibilities for use as Raman labels and potentially as sensors for various scaffolds with bio-friendly single molecule sensitivity correlated with true chemical information.

5.9 Future Directions

With the new discovery in this thesis that small photoactivated silver nanoclusters are able to assist in the generation of such intense Raman spectra of an absorbed scaffold *without* a large silver nanoparticle, many future directions for continued study on scaffold dependent Raman from these systems exist. From a detailed mechanistic understanding of the strong enhancements to potential use as biologically relevant in-vivo labels, the experimental paths in continuation of this project are many. The results presented in this thesis open

doors for such studies on the non resonant background present in many SERS experiments in which the small silver nanocluster might play a role. The results also give yet another means for studying the (electromagnetic vs. charge-transfer) enhancement mechanism for generally applicable SERS experiments. The rest of this chapter details preliminary results from which further study could elucidate many more interesting and useful dynamics of this system. Also presented with these results are other experimental avenues for which the system may be suited for study, along with thesis conclusions.

Intensity dependence of stokes and antistokes and the correlation of fluorescence to Raman

The applied laser field to the system is the first step in the generation of such intense Raman spectra, however, when changed, the system's response also changes. Many reports in the literature make reference to an intensity dependence relating to their results on surface enhanced studies. Perhaps the most logical example of bulk studies report the intensity dependence of observed SERS signals from various substrates as dependant on the number or concentration of particles and the particle spacing on various surfaces [61, 62]. Other reports detail both in theory and by experiment the dependence of certain pyridine SERS peak enhancements on intensity based on specific similarities noted between the SERS charge transfer mechanism and the resonance Raman (RR) process [63, 64]. Since the results in this thesis are based on consideration of a RR process, there may be some connection with the results in these papers

citing surface electronic states of the substrate metal as the responsible party for their results. Our preliminary results on this issue indicate a linear dependence with intensity as measured on the Stokes-shifted side of the spectrum. Figure 5.9.1 shows measured Raman spectra at five different intensities that display a more or less linear trend in total emitted intensity (that is, fluorescence plus the super-imposed Raman spectra) as a function of excitation intensity for the same spot. Concurrently as the total emitted intensity increases linearly, fitting of the resulting spectra allows separation of fluorescence and Raman peaks. When comparing the (integrated intensity) ratio of fluorescence to Raman peaks as the excitation intensity increases, the ratio remains constant at about 6%. Because this initial result was only measured at a factor of three difference, it may change with a greater difference in intensity points, however, bulk SERS reports by Kneipp et. al and Malinauskas and Niaura indicate a linear dependence of Stokes-shifted Raman with excitation intensity on various systems including effects from chloride ions on copper electrodes [65, 66]. The Kneipp paper also indicates a quadratic dependence on the antistokes spectrum attributed to population pumping of accessible vibrational states which we have not yet measured since the signal is so weak. Typically a very high laser power and a longer integration time are needed to observe the signal. Even though the initial results on the intensity dependence at this particular wavelength (514.5 nm) appear to be linear, there may be a dependence at other wavelengths as suggested by some [67] who have done experiments looking at the wavelength dependence on surface-enhanced hyper- Raman scattering to SERS.

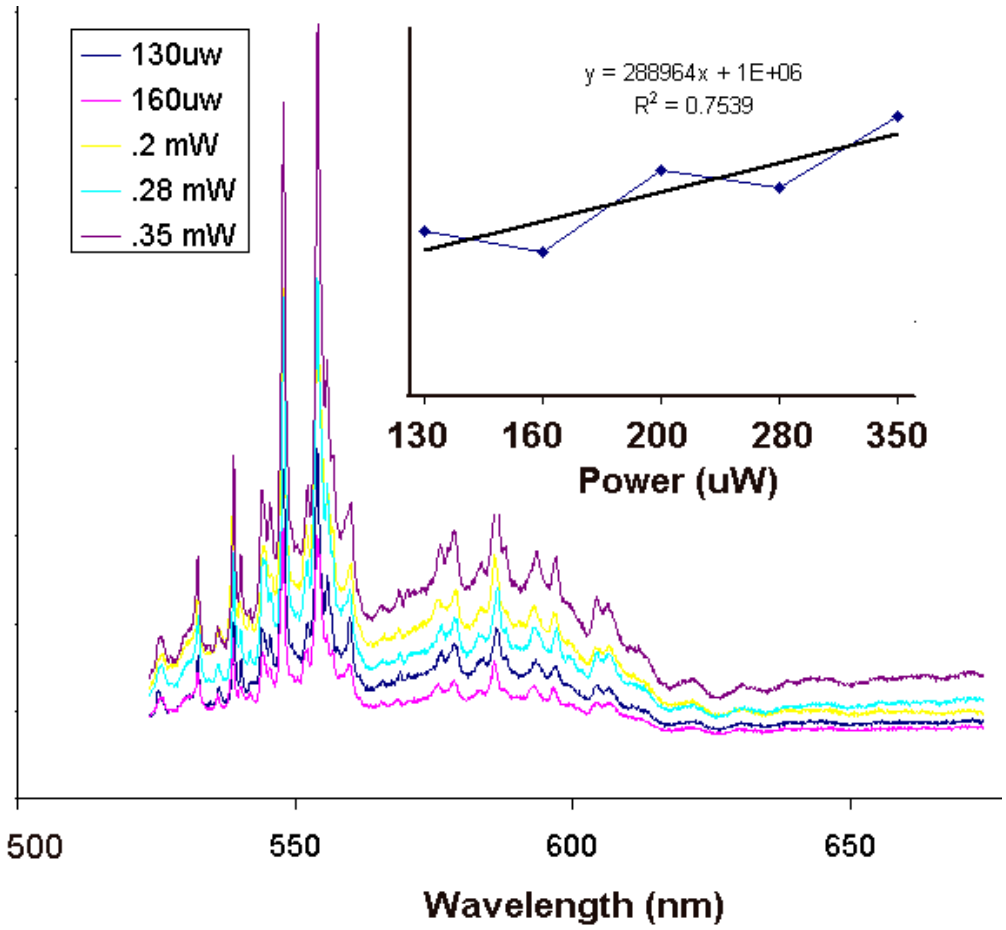

Figure 5.9.1. Measured spectra over five difference intensity values shows a linear trend in total emitted light. Fitting in Igor allows elucidation of the fluorescent background to be statistically distinguished from measured Raman peaks. Once this is completed for one intensity value, the same peaks can be watched over other intensities and the results tabulated.

Threshold activity

Concurrently with experiments investigating any intensity dependence, a threshold must be considered. Many experiments especially those involving biologically relevant samples can suffer from the high powers needed to generate sufficient signals. In these systems, optical damage thresholds have not been shown to be problematic since the cross section is so large, however there is an indication that a threshold may exist for the a Raman transition to occur between the Ag_n and the organic scaffold (Figure 5.9.2). Again, these experiments are very preliminary, only investigating a few particles and can use a more thorough investigation, but it appears that below a certain intensity level, only fluorescence can be observed from a single particle. Very little literature exists with respect to a threshold for other than that of optical damage [68] or with respect to stimulated Raman experiments [69]. However, a group from China summarizes that Raman scattering is proportional to the excitation power below the threshold power. Above the threshold, the intensity of the Stokes light strongly increases [70]. Though they do not refer to single-molecule experiments, and in fact their experiments are decidedly non-spontaneous Raman (versus stimulated), the results are still helpful and provide a starting point for many-particle trends to look for. Hundreds of molecules will have to be examined in order to decisively conclude anything about a true SM-Raman threshold from this unassisted system. A tremendous amount of information cannot be garnered from any one-molecule in this system, especially since the molecules turn on so quickly and blink intermittently. The best approach is to observe many, and look more

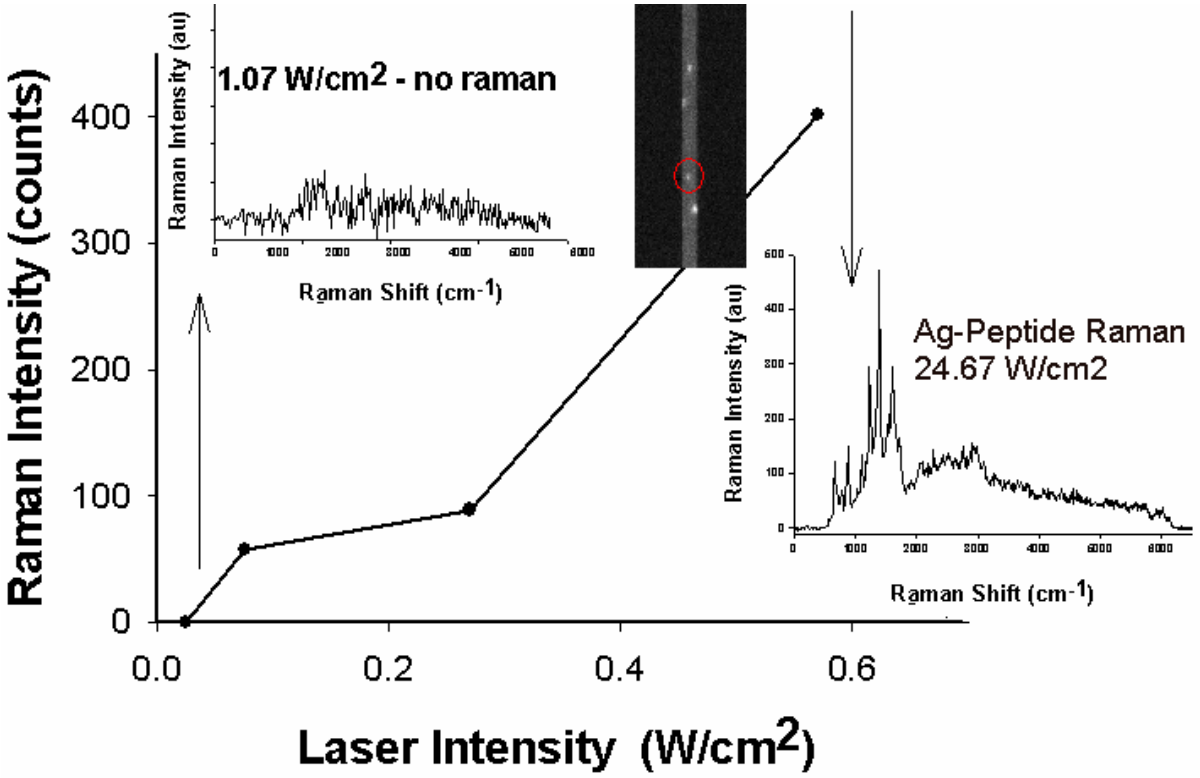

Figure 5.9.2. Initial experiments investigating the threshold behavior for a single Ag-peptide molecule. Below ~25 W/cm^2 no Raman is seen from this particular particle, only fluorescence, but above, a typical Raman spectrum is observed.

carefully for trends and closer distinctions between the amounts of Raman and fluorescence being emitted from certain molecules at certain intensities. Of recent observation is also the appearance of single nanoclusters whose emission gets tremendously brighter and more stable when brought directly into the laser focus. Nanoclusters of this type have been observed in all colors and there is some question as to whether these may be aggregates from older samples or something comparable to observed “hot spots” in the literature mentioned in the thesis introduction. AFM may help clarify this issue when used in conjunction with optical microscopy.

Polarization effects of Raman transitions

As discussed in the thesis introduction, Raman spectroscopy can be thought of classically or quantum mechanically. The classical relation involves more directly a consideration of the induced dipole as it relates to the electric field applied to the system through a polarizability tensor. If the induced dipole is broken up into each of its matrix elements in the x, y, and z directions (see equation below), the molecular response can be conceptually thought of as changing with respect to the polarization of the incident light. Since the behavior of individual silver nanoclusters already models that of single molecules in that fluorescence emission dependence on polarization has been demonstrated [35] (see thesis section 3.2) it follows that excitation polarization only in one direction should preferentially allow a Raman transition in that direction only. Unless an anisotropic source is present, Raman should also be seen in the directions x and

$$\begin{pmatrix} \mu_x \\ \mu_y \\ \mu_z \end{pmatrix} = \begin{pmatrix} \alpha_{xx} & \alpha_{xy} & \alpha_{xz} \\ \alpha_{yx} & \alpha_{yy} & \alpha_{yz} \\ \alpha_{zx} & \alpha_{zy} & \alpha_{zz} \end{pmatrix} \begin{pmatrix} E_x \\ E_y \\ E_z \end{pmatrix} \quad (5.9.1)$$

y, but should be different based on the input polarization. Various reports have confirmed this in conventional SERS experiments [71-74], however most of them tie together the dependence on polarization with the existence of such "hot spots" or describe the system as an ensemble of polarizable dipoles.

Initial experiments to investigate this theory demonstrated strange, but interesting results. Changes in polarization on the dendrimer system were made in all combinations on both the emission side and the excitation side (vertical, horizontal and even circular) with seemingly no change in preferential emission of the particles. It should be mentioned however that these changes were not monitored spectrally. This experiment was only performed in an imaging configuration to observe any visual changes in particle that either emitted or did not emit any light with respect to changes in polarization before moving to a spectral investigation. For use as a more specific label application, this manifestation of polarization of the Raman signal could be extremely useful.

5.10 Thesis conclusions

Photoactivated fluorescence from individual silver nanoclusters

The research presented in this thesis drew its roots from the plethora of available literature on small silver clusters and their relation to the photographic process, specifically, the behavior of small silver clusters when exposed to light. Originally intended as an extension of the laser dye Di-IC_{18}(3) single molecule orientational studies, the properties of this amazing silver system gave it a place of its own in the single-molecule community. The demonstration that a molecule's state could be controlled by light, or the local environment at room temperature was a major driving force for this research and extended nicely from Dickson et.al.'s room temperature optical switch behavior of Green Fluorescent Protien (GFP)[75]. Previously unavailable, new avenues of research were opened up at room temperature where photochemistry can be used to control molecular properties.

By simply shining visible light on thin (~10nm) Ag/AgO films, small silver clusters of Ag_2-Ag_8 can be formed. Extremely responsive to continuous excitation, many of these small sized clusters are stabilized on the surface, even creating written (stored) fluorescent patterns of many different colors whose fluorescence can be non-destructively read even after many days. The demonstration that small silver clusters act as single molecules in their behavior such as blinking, orientationally unique emission patterns, and even antibunching of fluorescence helps probe the molecular to bulk transition of the system while understanding the factors important to both such as excitation polarization and image fidelity. Additionally, photochemical control and measurement of spectral

features both on the single particle and bulk levels was gained. Revealed by this research, the important chemical species involved in photoactivated fluorescence of 2-8 atom silver nanoclusters on thin films was discovered. As these small clusters are the only ones with characterized oscillator strengths at visible wavelengths [50, 76, 77], and correspondingly the same emissive species as in low temperature silver halide studies, the emissive species possessing such superior optical properties are small silver clusters.

The silver nanocluster connection to Raman spectroscopy

The spectral, intensity, and photoactivation dynamics that are similar to both silver nanocluster fluorescence and SERS experiments have been found to be tightly connected. Common to most SERS experiments, the existence of a large metallic nanoparticle is required to generate reported 10^{15} and greater enhancements over ordinarily extremely weak Raman scattering. Combined with reports outlining the interplay of exactly this nanocluster fluorescence potentially with Raman scattering [40, 78], this research resulted in a very interesting addition to the current mysteries surrounding what factors prevail in surface-enhanced studies. As the nanoparticle is not needed to generate such signals, the argument that the majority of the enhancement mechanism arises from the electromagnetic field generated by a plasmon supporting nanoparticle cannot explicitly hold for all situations. Future studies armed with this knowledge will be forced to consider the effect of the generally ignored charge transfer interactions

resulting from binding interactions with the analyte molecule and metal nanoparticle support.

Not only is another piece to this some thirty year old problem introduced, but also, Raman scattering resulting from various silver encapsulated systems is dependent on the scaffold (peptide or dendrimer). Having such a short measured lifetime at visible wavelengths (~30ps), and such a high absorption cross section (10^{-14} cm^2), an extremely close connection between the ground and excited states of these nanoclusters is established allowing a strong transition moment to occur. Coupling this with state mixing with electronic states of the scaffold while also catering to enhanced Raman signals by using an excitation laser on or near resonance, such large enhancements can be obtained even generating antistokes transitions on a detectable level which model a thermal distribution of excited vibrational states. The first true demonstration of single molecule Raman was confirmed by the results in this thesis, specifically the observed antistokes shifted Raman and antibunching of silver nanocluster fluorescence.

Combining the fluorescent and photoactivatable properties of small silver nanoclusters with their ability to assist large Raman transitions on the single molecule level, many otherwise unattainable experimental possibilities exist. Potentially for later study in the Dickson group, this technology is useful specifically in biological labeling applications which currently suffers from chemical photobleaching, toxicity, and generally limited utility in in-vivo systems. These systems need only weak excitation for narrow-band single molecule

fluorescence to be generated and are much smaller than the current standard (CdSe) for biological labeling which is comparable in size to a protein which it could potentially label.

References

(1) Kneipp, K., et al., *Single molecule detection using surface-enhanced Raman scattering (SERS).* Phys. Rev. Lett. 1997. **78**: p. 1667.

(2) Nie, S.M. and S.R. Emory, *Probing single molecules and single nanoparticles by surface-enhanced Raman scattering.* Science 1997. **275**: p. 1102.

(3) Michaels, A.M., M. Nirmal, and L.E. Brus, *Surface enhanced Raman spectroscopy of individual rhodamine 6G molecules on large Ag nanocrystals.* J. Am. Chem. Soc. 1999. **121**(43): p. 9932.

(4) Hildebrandt, P. and M. Stockburger, *Surface enhanced Raman Spectroscopy of Rhodamine 6G adsorbed on colloidal silver.* J. Phys. Chem. 1984. **88**: p. 5935.

(5) Moskovits, M., *Surface roughness and enhanced intensity of Raman scattering by molecules adsorbed on metals.* J. Chem. Phys. 1978. **69**: p. 4159.

(6) Jeanmaire, D.L. and R.P. Van Duyne, *Surface-enhance spectroelectrochemistry part 1: Heterycyclic, aromatic, and aliphatic aminesadsorbed on the anodized silver electrode.* J. Electroanal. Chem. 1977. **84**: p. 1.

(7) Otto, A., *Surface enhanced Raman scattering: "Classical" and "Chemical" origins*, in *Light Scattering in Solids IV*, M. Cardona and G. Gundtherodt, Editors. 1984, Springer-Verlag: Berlin. p. 289.

(8) Lombardi, J.R., et al., *Charge-transfer theory of surface enhanced Raman spectroscopy: Herzeberg-Teller contributions.* J. Chem. Phys. 1986. **84**: p. 4174.

(9) Persson, B.N.J., *On the theory of surface enhanced Raman scattering.* Chem. Phys. Lett. 1981. **82**(3): p. 561.

(10) Kambhampati, P., et al., *On the chemical mechanism of surface enhanced Raman scattering: experiment and theroy.* J. Chem. Phys. 1998. **108**(12): p. 5013.

(11) Capadona, L.P., J. Zheng, and R.M. Dickson, *Nanoparticle-Free Single Molecule Antistokes Raman Spectroscopy.* 2004. **submitted**.

(12) Kneipp, K., L.T. Perelman, and H. Kneipp, *Coupling and scattering power exchange between phonon modes observed in surface-enhanced Raman spectra of single-wall carbon nanotubes on silver colloidal clusters.* Phys. Rev. B. 2001. **63**(19): p. 193411.

(13) Doering, W.E. and S. Nie, *Single-molecule and single nanoparticle SERS: Examining the role of surface active sites and chemical enhancement.* J. Phys. Chem. B 2002. **106**: p. 311.

(14) Jiang, J., et al., *Single molecule raman spectroscopy at the junctions of large Ag nanocrystals.* J. Phys. Chem. B. 2003. **107**: p. 9964.

(15) Osbourne, M.A., et al., *Optically Biased Diffusion of Single Molecules Studied by Confocal Fluorescence Microscopy.* J. Phys. Chem. B. 1998. **102**(17): p. 3160.

(16) Michaels, A.M., J. Jiang, and L.E. Brus, *Ag Nanocrystal Junctions as the Site for Surface-Enhanced Raman Scattering of Single Rhodamine 6G Molecules.* J. Phys. Chem. B 2000. **104**: p. 11965.

(17) Schneider, S., et al., *Stabilization of silver colloids by various types of anions and their effect on the surface-enhanced Raman spectra of organic dyes.* J. Ram. Spec. 1996. **27**(1): p. 57.

(18) Garcia-Vidal, F.J. and J.B. Pendry, *Collective theory for surface enhanced Raman scattering.* Phys. Rev. Lett. 1996. **77**(6): p. 1163.

(19) Inoue, M. and K.J. Ohtaka, *Enhanced Raman scattering by two-dimensional array of polarizable spheres.* J. Phys. Soc. Jpn. 1983. **52**(4): p. 1457.

(20) Birke, R.L., J.R. Lombardi, and J. Gersten, *Observation of a continuum in enhanced Raman scattering from a metal-solution interface.* Phys. Rev. Lett. 1979. **43**(1): p. 71.

(21) Otto, A., *Raman spectra of cyanide ion adsorbed at a silver surface.* Surf. Sci. 1978. **75**(2): p. L392.

(22) Burstein, E., et al., *"Giant" Raman scattering by adsorbed molecules on metal surfaces.* Sol. St. Commum. 1979. **29**(8): p. 567.

(23) Cardona, M., *Raman scattering in high-Tc superconductors: Phonons, electrons, and magnons*, in *Raman scattering in materials science*, W.H. Weber and R. Merlin, Editors. 2000, Springer: New York.

(24) Zawadowski, A. and M. Cardona, *Theory of Raman scattering on normal metals with impurities.* Phys. Rev. B. 1990. **42**(16): p. 10732.

(25) Itai, K., *Theory of Raman scattering in coupled electron-phonon systems.* Phys. Rev. B. 1992. **45**(2): p. 707.

(26) Gass, A.N., et al., *The nature of the inelastic background in surface enhanced Raman scattering spectra of coldly-deposited silver films. The role of active sites.* Sol. St. Commun. 1989. **71**(9): p. 749.

(27) Otto, A., *Enhanced infrared absorption of SERS-active lines of ethylene on Cu.* Phys. Status. Soldi A: Appl. Rev. 2001. **188**(4): p. 1471.

(28) Portales, H., et al., *Raman scattering by electron-hole excitations in silver nanocrystals.* Phys,. Rev. B. 2001. **63**(23): p. 233402.

(29) Andersen, P.C., M.L. Jacobson, and K.L. Rowlen, *Flashy Sliver Nanoparticles.* J. Phys. Chem. B. 2004. **108**(7): p. 2148.

(30) Kelly, K.L., et al., *The optical properties of metal nanoparticles: the influence of size, shape, and dielectric environment.* J. Phys. Chem. B. 2003. **107**(3): p. 668.

(31) Haynes, C.L. and R.P. Van Duyne, *Plasmon-sampled surface-enhanced Raman excitation spectroscopy.* J. Phys. Chem. B. 2003. **107**(30): p. 7426.

(32) Monti, O.L.A., J.T. Fourkas, and D.J. Nesbitt, *Diffraction-limited photogeneration and characterization of silver nanoparticles.* J. Phys. Chem. B. 2004. **108**(5): p. 1604.

(33) Fedrigo, S., W. Harbich, and J. Buttet, *Optical-Response of Ag2, Ag3, Au2, and Au3 in Argon Matrices.* J. Chem. Phys. 1993. **99**(8): p. 5712.

(34) Peyser, L.A., et al., *Photoactivated fluorescence from individual silver nanoclusters.* Science 2001. **291**: p. 103.

(35) Peyser, L.A., T.-H. Lee, and R.M. Dickson, *Mechanisn of Ag_n nanocluster photoproduction from silver oxide films.* J. Phys. Chem B. 2002. **106**: p. 7725.

(36) Zheng, J. and R.M. Dickson, *Individual Water-Soluble Dendrimer-Encapsulated Silver Nanodot Fluorescence.* JACS 2002. **124**(47): p. 13982.

(37) Moskovits, M., *Surface-enhanced spectroscopy.* Rev. Mod. Phys. 1985. **47**: p. 783.

(38) Kneipp, K., *Ion-induced SERS of dye molecules on very small colloids in aqueous solution.* Spec. Acta. A. 1994. **50A**(6): p. 1023.

(39) Mihalcea, C., et al., *Intrinsic Fluorescence and Quenching Effects in Photoactivated Reactively Sputtered Silver Oxide Layers.* J. Am. Chem. Soc. 2001. **123**(29): p. 7172.

(40) Buchel, D., et al., *Sputtered silver oxide layers for surface-enhanced Raman spectroscopy.* Appl. Phys. Lett. 2001. **79**(5): p. 620.

(41) Slocik, J.M., J.T. Moore, and D.W. Wright, *Monoclonal antibody recognition of histidine-rich peptide encapsulated nanoclusters.* Nanolett 2002. **2**(3): p. 169.

(42) Zheng, J., et al., *Influence of pH on Dendrimer-pretected nanoparticles.* J. Phys. Chem. B 2002. **106**: p. 1252.

(43) Davis, A.P., G. Ma, and H.C. Allen, *Surface vibrational sum frequency and Raman stidues of PAMAM G0, G1 and acylated PAMAM G0 dendrimers.* Anal. Chim. Acta. 2002. **496**: p. 117.

(44) Marchetti, A.P., et al., *Formation and spectroscopic manifestation of silver clusters on silver bromide surfaces.* J. Phys. Chem. B 1998. **102**(27): p. 5287.

(45) Hanbury- Brown, R.H. and R.Q. Twiss, *Correlation between photons in coherent light rays.* Nature 1956. **178**: p. 1447.

(46) Kumar, P., et al., *Photon antibunching from oriented semiconducting ploymer nanostructures.* J. Am. Chem. Soc. 2004. **126**(11): p. 3376.

(47) Loudon, R., *The Quantum Theory of Light*. 2nd ed. 2000, New York: Oxford University Press.

(48) Ferraro, J.R., *Introductory Raman Spectroscopy*. 1994, Boston: Academic Press.

(49) Cheng, J.-X., et al., *Laser-scanning coherent anti-stokes Raman scattering microscopy and applications to cell biology.* Biophys. J. 2002. **83**: p. 502.

(50) Bonacic-Koutecky, V., V. Veyret, and R. Mitric, *Ab initio study of the absorption spectra of Agn (n=5-8) clusters.* J. Chem. Phys. 2001. **115**(22): p. 10450.

(51) Kruckeberg, S., et al., *The dissociation channels of silver clusters Agn+ 3<n<20.* Int. J. Mass. Spec. 1996. **155**: p. 141.

(52) Ho, J., K. Ervin, and W.C. Lineberger, *Photoelectron spectroscopy of metal cluster anionsL Cun-, Agn- and Aun-.* J. Chem. Phys 1990. **93**(10): p. 6987.

(53) Hild, U., et al., *Time-resolved photofragmentation of stored silver clusters Agn+ (n=8-21).* Phys. Rev. A 1998. **57**(4): p. 2786.

(54) Spasov, V., et al., *Measurement of the dissociation energies of anionic silver clusters (Agn-, n= 2-11) by collision-induced dissociation.* J. Chem. Phys. 1999. **110**(11): p. 5208.

(55) Tiggesbaumker, J., et al., *Giant Resonances in Silver-Cluster Photofragmentation.* Chem. Phys. Lett. 1992. **190**(1,2): p. 42.

(56) Loudon, R., *The Quantum Theory of Light*. 2nd ed. 1983, Oxford: Clarendon.

(57) Ward, D., *A cursory review of Raman spectroscopy.* www.mit.edu/people/dwward/papers/raman.pdf.

(58) Cotton, F., *Chemical Applications of Group Theory*. 1963, New York: Wiley Interscience.

(59) Balasubramanian, K. and M.Z. Liao, *Electronic states and potential energy surfaces of gold and silver trimers.* Chem, Phys. 1988. **127**(1-3): p. 313.

(60) Peyser, L.A., T.H. Lee, and R.M. Dickson. *Harnessing Single Particle Dynamics in Silver Nanomaterials*. in *SPIE : International Society of Optical Engineers.* 2002. San Jose, CA.

(61) Ikezawa, Y., et al., *A study of the competitive adsorption of pyridine and monosubstituted pyridines on a silver electrode by the SERS method.* Surf. Sci. 1986. **176**(3): p. 603.

(62) Nikoobakht, B. and M. El-Sayed, *Surface-enhanced Raman scattering studies on aggregated gold nanorods.* J. Phys. Chem. A. 2003. **107**(18): p. 3372.

(63) Lopez-Tocon, I., et al., *Selection rules for the charge transfer enhancement mechanism in SERS: dependence of the intensities on the L-matrix.* J. Molec. Struc. 2001. **565-566**: p. 369.

(64) Mal'shukov, A.G., *The role of surface electronic states in surface enhanced Raman scattering.* Sol. St. Commun. 1985. **54**(11): p. 969.

(65) Kneipp, K., et al., *Population pumping of excited vibrational states by spontaneous surface-enhanced Raman scattering.* Phys. Rev. Lett. 1996. **76**(14): p. 2444.

(66) Niaura, G. and A. Malinauskas, *Surface-enhanced Raman scattering from cholide on copper electrodes.* Chem. Phys. Lett 1993. **207**(4-6): p. 455.

(67) Kneipp, K., H. Kneipp, and F. Seifert, *Near-infrared excitation profile study of surface-enhanced hyper-Raman scattering and surface-enhanced Raman scattering by means of tunable mode-locked Ti:Sapphire laser excitation.* Chem. Phys. Lett. 1995. **233**(5,6): p. 519.

(68) Zhang, H.-T. and Z.-Y. Xu, *Stimulated Raman scattering in nanorod silicon carbide films.* Semicond. Phot. Tech. 2002. **8**(1): p. 32.

(69) Behrouz, A. and F.F. Chen, *The stimulated Raman threshold. I. Experiment.* Phys. Fluid. 1986. **29**(11): p. 3864.

(70) Zhang, H.-t. and Z.-Y. Xu, *Stimulated Raman scattering in nanorod silicon carbide films.* Semicond. Photon. Tech. 2002. **8**(1): p. 32.

(71) Corni, S. and J. Tomasi, *Surface enhanced Raman scattering from a single molecule adsorbed on a metal particle aggregate: A theoretical approach.* J. Chem. Phys. 2002. **116**(3): p. 1156.

(72) Eggeling, C., et al., *Photobleaching of fluorescent dyes under conditions used for single-molecule detection: Evidence of two-step photolysis.* Anal. Chem. 1998. **70**(13): p. 2651.

(73) Bosnick, K.A., J. Jiang, and L.E. Brus, *Fluctuations and local symmetry in single-molecule rhodamine 6G Raman scattering on silver nanocrystal aggregates.* J. Phys. Chem.B. 2002. **106**: p. 8096.

(74) Wang, Z., et al., *The structural basis for giant enhancement enabling single-molecule Raman scattering.* PNAS 2003. **100**(15): p. 8638.

(75) Dickson, R.M., et al., *Blinking and switching behavior of individual green fluorescent protein molecules.* Nature 1997. **388**: p. 355.

(76) Harbich, W., et al., *Deposition of mass selected silver clusters in rare gas matrices.* J. Chem. Phys. 1990. **93**: p. 8535.

(77) Rabin, I., W. Schulze, and G. Ertl, *Light emission during the agglomeration of silver clusters in noble gas matrices.* J. Chem. Phys. 1998. **108**(12): p. 5137.

(78) Mihalcea, C., et al., *Intrinsic fluorescence and quenching effects in photoactivated reactively sputtered silver oxide layers.* J. Am. Chem. Soc. 2001. **123**(29): p. 7172.

LIST OF PUBLICATIONS

(1) L.P. Capadona, J. Zheng, and R.M. Dickson. “Nanoparticle-Free Single Molecule Antistokes Raman Spectroscopy. Submitted, *Science*, (2004).

(2) P. Kumar, A. Mehta, M.D. Dadmun, J. Zheng L.A. Peyser, A.P. Bartko, R.M. Dickson, T. Thundat, B. Sumpter, D. Noid, and M. D. Barnes, “Narrow bandwidth spontaneous luminescence from oriented semiconducting polymer nanostructures” J. Phys. Chem. B. **107** 6252-6257 (2003).

(3) L.A. Peyser, T-H. Lee, and R.M. Dickson “Harnessing Single Particle Dynamics in Silver Nanomaterials”. PROC PAP SPIE –Int. Soc. Opt. Eng. **4636** 81-87 (2002).

(4) L.A. Peyser, T-H. Lee, and R.M. Dickson, “Mechanism of Ag_n Nanocluster Photoproduction from Silver Oxide Films”. J. Phys. Chem. B. **106** 7725-7728 (2002).

(5) A.P. Bartko, L.A. Peyser, R.M. Dickson, A. Mehta, T. Thundat, R. Bhargava, and M.D. Barnes. “Emission patterns from single Eu_3^+:Y_2O_3 doped nanocrystals”. Chem. Phys. Lett. **358** 459 (2002).

(6) L.A. Peyser, A.E. Vinson, A.P. Bartko and R.M. Dickson. “Photoactivated Fluorescence from Individual Silver Nanoclusters”. Science **291**103-106 (2001).

(7) R.A. Farrer, M.J.R. Previte, C. E. Olson, L. A. Peyser, J. T. Fourkas, and Peter T.C. So. “Single Molecule Detection using a Two-Photon Fluorescence Microscope with Fast-Scanning Capabilities and Polarization Sensitivity”. Optics Letters **24** 1832-1834 (1999).

VITA

Lynn Anne (Peyser) Capadona was born in 1977 in Boston, Massachusetts. She graduated from Boston College in Chestnut Hill, MA after completing a B.S. in Chemistry. During her undergraduate years, Lynn was exposed to many different areas of chemistry including single molecule studies and polymer chemistry while studying abroad in Australia. An interest in small molecules and their interactions with intense laser fields drew her to graduate school in August of 1999 where she has since been studying the photophysical properties of silver nanoclusters for her Ph.D. dissertation research. Lynn also has significant interests in science technology transfer and earned two certificates from the Management of Technology program in the School of Business at Georgia Tech while working toward her doctorate. She will continue work as a Chemical Engineer for NASA in the area of nanocomposite materials in Cleveland, OH.